

Manh Cuong Do Piezoelectric Transformer Integration Possibility in High Power Density Applications

Manh Cuong Do

Piezoelectric Transformer Integration Possibility in High Power Density Applications

ISBN 978-3-940046-85-7

TUD*press*

TUD*press*

TUD*press*

Do Manh Cuong
Piezoelectric Transformer Integration Possibility in High Power
Density Applications

Do Manh Cuong

**Piezoelectric Transformer
Integration Possibility in High
Power Density Applications**

TUD*press*

2008

Bibliografische Information der Deutschen Bibliothek

Die Deutsche Bibliothek verzeichnet diese Publikation in der Deutschen Nationalbibliografie; detaillierte bibliografische Daten sind im Internet unter <http://dnb.ddb.de> abrufbar.

Bibliographic information published by Die Deutsche Bibliothek

Die Deutsche Bibliothek lists this publication in the Deutsche Nationalbibliografie; detailed bibliographic data is available in the Internet at <http://dnb.ddb.de>

Zugl.: Dresden, Techn. Univ., Diss., 2008

ISBN 978-3-940046-85-7

© TUDpress

Verlag der Wissenschaften GmbH

Bergstr. 70 | D-01069 Dresden

Tel.: 0351/47 96 97 20 | Fax: 0351/47 96 08 19

<http://www.tudpress.de>

Alle Rechte vorbehalten. All rights reserved.

Gesetzt vom Autor.

Druck und Bindung: Sächsisches Digitaldruck Zentrum GmbH.

Made in Germany.

TECHNISCHE UNIVERSITÄT DRESDEN

Piezoelectric Transformer Integration Possibility in High Power Density Applications

M. Sc. Do Manh Cuong

von der Fakultät Elektrotechnik und Informationstechnik der
TECHNISCHEN UNIVERSITÄT DRESDEN

zur Erlangung des akademischen Grades eines

Doktoringenieurs

(Dr.-Ing.)

genehmigte Dissertation

Vorsitzender:	Prof. Dr.-Ing. habil. Schreiber
Gutachter 1:	Prof. Dr.-Ing. habil. Güldner
Gutachter 2:	Prof. Dr.-Ing. habil. Ng.Ph.Quang
Gutachter 3:	Prof. Dr.-Ing. Hoffmann

Tag der Einreichung: 22.12.2007

Tag der Verteidigung: 02.06.2008

For my Parents

Acknowledgements

The research work is a part of project "*Lokale Innovative Energiesysteme - Local Innovative Energy Systems - LIES*" supported by the Deutsche Forschungsgemeinschaft - German Research Foundation at the Dresden University of Technology (TU Dresden).

First of all, I would like to express my sincerest appreciation and gratitude to my academic supervisor, Prof. Dr.-Ing. habil. Henry Güldner, for his invaluable guidance, encouragement, and continued support during the course of this research work.

I would like to express my thanks to Prof. Dr.-Ing. habil. Nguyen Phung Quang from Hanoi University of Technology for his suggestions and incessantly encouragement, and I want to express my gratitude to Prof. Dr.-Ing. Hoffmann from Helmut-Schmidt-Universität Hamburg for his supports and evaluations

I would like to thank Dr.-Ing. Thomas Hanisch for his guidance on the beginning days of the work and his encouragement, opinions during carrying out this research. My thanks also go to Dr.-Ing. Bernhard Siessegger from OSRAM Company for his supports and discussions during the time when I was at OSRAM for testing the ignition circuit. I am grateful to Dr. Igor Kartashev from EPCOS Company for his instructions and information about piezoelectric material.

I also wish to send my thanks to Mr. Yuan Mingbo from Konghong Company - China, Mr. Clement Chou from ELECERAM TECHNOLOGY Company for supplying the sample for my experiments and applications. Thanks also go to Dr. Vázquez Carazo Alfredo from FACE Company for his support.

My special thanks to all staffs and colleges especially Dr.-Ing.habil Witte, Dr.-Ing. Frank Benecke, Dipl-Ing. Sven Wendt at Chair of Power Electronic, Faculty of Electrical Engineering and Informatics, Dresden University of Technology for their help in the past years.

From the view point of language, this dissertation was read through and corrected by Mr. David Walker - Director of Training Center of Yokogawa Australia. I would like to express my thanks to him for his helps and supports.

Finally, I would like to send my deepest gratitude to my parents and my family for their love, support, incessantly encouragement and waiting hours from my distant home country - Vietnam.

M. Sc. Manh Cuong Do
Dresden, 05st, June, 2008

Contents

Acknowledgements	v
Abstract	xv
1 Introduction	1
1.1 Overview	1
1.2 Motivation	2
1.3 Research Goals and Organization	2
2 Fundamentals of Piezoelectric Transformer	5
2.1 Introduction	5
2.2 Physical Basics	6
2.2.1 Piezoelectric Materials	6
2.2.2 Depolarization	8
2.2.3 Piezoelectric Constants	9
2.2.4 Piezoelectric Transformer: Structure and Classification	11
2.3 Piezoelectric Transformer Generic Operational Characteristics	14
2.3.1 Physics Based Equivalent Circuit	14
2.3.2 Voltage Transfer Function of Piezoelectric Transformer	15
2.3.3 Output Power of Piezoelectric Transformer	18
2.3.4 Efficiency of Piezoelectric Transformer	19
2.4 Summary	20
3 Limitations to Throughput Power of Piezoelectric Transformer	25
3.1 Introduction	25
3.2 Effect of Temperature on Power Density	25
3.3 Electromechanical Limitations	34
3.4 Effect of the Output Rectifier	38
3.4.1 Operation of PT with voltage doubler	38
3.4.2 Operation of PT with current doubler	41
3.4.3 Voltage doubler and current doubler in comparison	43

3.5	Summary and Discussion	45
4	Converter Topologies and Control Considerations	49
4.1	Introduction	49
4.2	Class D Resonant Converter using PT	50
4.2.1	Operational Principle of Class D Converter	50
4.2.2	Inductor-less Class D PT Converter	52
4.2.3	Class D PT Converter with Impedance Matching	56
4.3	Class E Resonant Converter using PT	61
4.4	Resonant Frequency Tracking	65
4.4.1	Purpose of Frequency Tracking for PT	65
4.4.2	Series and Parallel Resonant Frequency of a PT	66
4.5	Discontinuous Working Mode of PT	67
4.6	Summary and Discussion	72
5	High Power Density Applications	75
5.1	Introduction	75
5.2	Igniter for HID Lamp	75
5.2.1	Ignition Concepts for HID Lamp	75
5.2.2	PT based Igniter for HID Lamp	76
5.3	High Output Voltage DC/DC Converter	79
5.4	PT based Electronics Ballasts for LED	82
5.5	Stand Alone Ionizer for Food Sterilizer	84
6	Conclusions and Future Work	87
A	Specifications of PT samples	91
A.1	Sample PT#1: MPT3608A70L0	92
A.2	Sample PT#2: ELM610	93
A.3	Sample PT#3	94
B	Determination of Parameters of Equivalent Circuit	95
B.1	Introduction to Admittance Circle Method	95
B.2	Parameters of Equivalent Circuit of PT	97
B.2.1	Admittance circle of PT#1	97
B.2.2	Admittance circle of PT#2	99
B.2.3	Admittance circle of PT#3	101
C	Program to Determine the Operational Characteristics of PT	103

List of Figures

2.1	Piezoelectric elementary cell	7
2.2	Electric dipole moments in Weiss domains	8
2.3	Designation of the axes and direction of deformation	11
2.4	Vibration mode of piezoelectric element	12
2.5	Three common types of piezoelectric transformer	13
2.6	Typical equivalent circuit of a PT in multi-resonant mode	15
2.7	Physical based equivalent circuit of PT	16
2.8	Models of equivalent PT with load	17
2.9	Output to input voltage boost ratio of PT	19
2.10	Dependence of PT's output power on load and operating frequency	21
2.11	Efficiency of PT versus load	22
2.12	Generic operational characteristics of PT	23
3.1	Output Power of PT#1 - Simulation and measurement results	27
3.2	Scheme for determining the output power and surface temperature of PT	28
3.3	Dependencies of piezoelectric material constants on temperature	31
3.4	Temperature of PT during operation with different input voltage	32
3.5	Distribution of surface temperature of PT	33
3.6	Distribution displacement and stress of PT in λ mode	34
3.7	Operating cycle of a PT	35
3.8	Several output rectifier stage and their relations of load	39
3.9	Voltage doubler fed by PT	40
3.10	Current doubler fed by PT	42
3.11	Operational wave form of voltage and current doubler	44
3.12	Comparison of power handling of PT with current and voltage doubler	45
4.1	PT based class D converter	50
4.2	The key waveforms of PT based class D converter	51
4.3	Phase relation between resonant current i_{rL} and input voltage V_{Cin}	53
4.4	Simulation of class D converter with PT#1	54

4.5	Inductor-less PT based class D converter	55
4.6	Temperature of PT in inductor-less class D inverter	56
4.7	Class D resonant converter using PT with series inductor	56
4.8	Class D converter for PT operating with input impedance matching	58
4.9	Class D converter for PT operating with input filter $L_f = 42\mu H$	59
4.10	Temperature rising of PT based class D converter with series inductor	60
4.11	PT based class E resonant inverter	61
4.12	Basic operation wave form of PT based class E converter	62
4.13	Simulation results of PT based class E converter	63
4.14	Experimental results of PT based class E converter	64
4.15	Temperature rising of PT based class E converter	65
4.16	Series and parallel resonant frequency of PT#2 when output short circuit	67
4.17	Excitation scheme for PT in discontinuous working mode	68
4.18	Dynamic response of PT's output voltage	69
4.19	Experiment setup for PT in discontinuous working mode	70
4.20	Performance of discontinuous operation mode PT	70
4.21	Output voltage of discontinuous operation mode PT with different V_{DCbus}	71
5.1	Resistance of metal halide lamp with different operating period	76
5.2	Design of HID lamp igniter using discontinuous working mode of PT	77
5.3	Prototype of HID lamp igniter using discontinuous working mode of PT	78
5.4	Behavior of igniter for HID lam using discontinuous working mode PT	78
5.5	Design of high DC voltage power supply	79
5.6	Prototype of high DC voltage power supply	80
5.7	Measurement results of high output voltage power supply	81
5.8	Feedback signals: voltage and current phase	81
5.9	A single LED: 3W - 350 mA	82
5.10	Applications of light emitting diode	82
5.11	Proposal design for LED ballasts using PT	83
5.12	Prototype of LED ballasts using PT	83
5.13	Wave-form of ballasts for LEDs	84
5.14	Principle circuit of stand alone ionizer for food sterilizer	85
5.15	Stand alone ionizer	86
A.1	The outlook of PT sample #1	92
A.2	The outlook of PT sample #2	93
A.3	The outlook of PT sample #3	94

B.1	Equivalent circuit of PT operating closed to resonant frequency	95
B.2	Admittance circle	95
B.3	PT#1: Admittance Circle - Input short circuit	97
B.4	PT#1: Admittance Circle - Output short circuit	97
B.5	PT#1: Admittance and phase characteristics	98
B.6	PT#2: Admittance Circle - Input short circuit	99
B.7	PT#2: Admittance Circle - Output short circuit	99
B.8	PT#2: Admittance and phase characteristics	100
B.9	PT#3: Admittance Circle: Input short circuit	101
B.10	PT#3: Admittance Circle: Output short circuit	101
B.11	PT#3: Admittance and phase characteristics	102

List of Tables

1.1	Prospective applications of Piezoelectric Transformer	4
2.1	Achievable Voltage Boost Ratio of Piezoelectric Transformer	20
2.2	Practical parameters of PT	24
3.1	Characteristics of piezoelectric transformer samples	26
3.2	Resonant frequency shift versus temperature rise	29
3.3	Comparison of heat conductivity of piezoelectric material with others . .	30
3.4	Material constants of PT samples	36
4.1	The parameters of PT's equivalent circuit in λ vibration mode	53
A.1	Fundamental materials characteristics of sample PT#1	92
A.2	Fundamental materials characteristics of sample PT#2	93
A.3	Fundamental materials characteristics of sample PT#3	94
B.1	Parameters of equivalent circuit of PT samples	96

Abstract

It has been more than 50 years since the initial concept of a piezoelectric transformer (PT) was proposed by C.A. Rosen, K. Fish, and H.C. Rothenberg and was described in the U.S. Patent 2,830,274, applied in 1954. Nowadays, this technology has become one of the most promising alternatives for replacing magnetic transformers in a wide range of applications. Piezoelectric transformers convert electrical energy into electrical energy by using acoustic energy. These devices are typically manufactured using piezoelectric ceramic materials that vibrate in resonance. The requirements of minimizing the size and weight of electronic devices have awoken the high potential of piezoelectric transformer in small power range applications.

The contents of this work investigates the capability of integrating the PT in applications by invoking the ratio of the throughput power to volume represented by the term: **power density**. The fundamentals of the PT are introduced in chapter two. In chapter three, the fundamental limitations of the PT's capability of transferring power to the load are studied. There are three major limitations: temperature rise due to losses during operation, electromechanical limits of material, and interactions with output rectifier. The analysis and estimation are then verified by experiments and calculations implemented on three different PT samples fabricated from three different manufacturers. The subject of chapter four is the behavior of the PT's power amplifier. This chapter concentrates on two main amplifier topologies, optimized based on the simplicity of structure and minimization of components (passive and active): class D and class E amplifiers. The operational characteristics of these amplifiers with the PT are then comparison. Methods to track the optimum frequency and discontinuous working mode of the PT are proposed as the approaches to improve the energy transfer of the PT. In chapter five, prototypes of four devices using a PT are developed and introduced as illustrations of the integration of PTs into practical applications: an igniter for high intensity discharge (HID) lamps, high DC voltage power supplies, electronic ballasts for LEDs, and stand-alone ionizers for food sterilizers. Some concluding statements and ideas for future works are located in the last chapter - chapter six.

Nomenclature

Symbols

Symbol	Description	Unit
c_{ijkl}, c_{pq}	Elasticity Module	$\frac{N}{m^2}$
C	Capacitor	F
C_{in}, C_o	Input and Output Capacitor of Equivalent Circuit	F
L_r	Series inductor of PT's equivalent circuit	H
C_r	Series capacitor of PT's equivalent circuit	F
\vec{D}	Charge density	C/m ²
\vec{E}	Electrical strength	V/m
\vec{S}	Strain	-
\vec{T}	Stress	N/m ²
R_m	Mechanical losses of PT	Ω
R_L	Load resistor	Ω
d_{ijk}, d_{ip}	Piezoelectric Constant	$\frac{m}{V} = \frac{C}{N}$
g_{ijk}, g_{ip}	Piezoelectric Constant	$\frac{Vm}{N} = \frac{m^2}{C}$
f_s	Series Resonant Frequency, $2\pi f_s = \frac{1}{\sqrt{L_r C_r}}$	Hz
f_p	Parallel Resonant Frequency	Hz
f_m	Frequency at Minimum Impedance @ Y_{max}	Hz
f_n	Frequency at Maximum Impedance @ Y_{min}	Hz
f_r	Resonant frequency	Hz
f_a	Anti-resonant frequency	Hz
n_{21}	Output to input voltage boost ratio	-
Q_m	Mechanical quality factor, $Q_m = \frac{2\pi f_s L_r}{R_m}$	-
V_{in}, V_{out}	Input and output voltage of PT	V
\underline{Y}	Admittance	S
\underline{Z}	Impedance	Ω

Greek symbols

Greek symbol	Description	Unit
λ	Wave length	<i>m</i>
ω	Angular frequency	<i>rad/s</i>
μ	Efficiency	
ε	Permittivity	<i>F/m</i>
ρ	Density	<i>g/cm³</i>
θ	Conducting angle of diode	<i>rad</i>
φ	Phase angle (u,i)	<i>rad</i>

Subscripts and Superscripts

Subscripts & Superscripts	Description	Unit
<i>D</i>	At constant electric displacement	
<i>E</i>	At constant electrical field	
<i>S</i>	At constant strain	
<i>T</i>	At constant stress	

Abbreviations

Abbreviations	Description
V_{GS}	Control signal at gate of power switch
PLL	Phase locked loop
HVPT	High voltage or step up PT
LVPT	Low voltage or step down PT
MLPT	Multi-layer PT
SLPT	Single-layer PT
PT	Piezoelectric Transformer
ZVS	Zero voltage switching
ZCS	Zero current switching
EMI	Electromagnetic interference
CCFL	Cold cathode fluorescent lamp
LED	Light emitting diode
HID	High intensity discharge
PEF	Pulsed electric field

Chapter 1

Introduction

1.1 Overview

The piezoelectric effect was discovered by brothers Curie when they researched the behavior of some crystal materials. In the family of these materials, piezoelectric ceramics are the most important group and they have already been widely used in the area of actuators and transducers during the first and second World War. Until 1956, the new piezoelectric effect based component, which is regarded as a power transferring device, was first introduced by C.A.Rosen [14, 15] and it was named the Piezoelectric Transformer (PT). PT's operational principle is the combination of a piezoelectric actuator and a piezoelectric transducer and energy is transferred from electrical form to electrical form via electro-mechanical coupling. In comparison to a conventional magnetic transformer, on one hand, PTs have many advantages, such as:

- High power density
- High efficiency
- High galvanic isolation
- Without winding part so have no EMI
- Low size and weight, and not flammable

on the other hand, PTs still have some disadvantages listed as following:

- Resonant device
- Low applicable power range
- High cost

1.2 Motivation

After the first introduction, due to the difficulties in material quality, design and manufacturing, control and driving technique, PTs had not been utilized in practical applications, further more, its operational characteristics could not compare with the advantages of magnetic transformers at that time. But in the last 20 years, with so many achievements in materials field [1, 95, 106] and demands for minimizing the size and weight of electrical devices, there has been a strong interest in PT as the most promising alternatives for replacing the bulky and heavy magnetic transformers within a small power range (up to hundreds of watts) devices[23].

Simultaneously with successes in the materials area, many applications using PTs have been proposed by researchers and developers over the world. Some remarkable applications which have been developed and commercialized are: electronics ballasts for CCFLs [17, 18, 120, 121, 122], DC/DC converters [40, 70, 82], battery chargers [58], power supplies for various loads [8, 36, 48] ... The prospective applications of piezoelectric transformers are listed in table 1.1 below.

However, in most of the literature mentioned above, the operation of a PT is only considered as results of linear interactions between electrical and mechanical parts and some nonlinear causes such as temperature rise, depolarization, aging, and structure that affect the stability, capability of transferring power of PT are not mentioned or only briefly discussed [16]. In order to guarantee the applicability and integration of PTs in power electronics devices, these nonlinear effects must be fully studied and then the solutions that diminish or eliminate these problems will be proposed.

Power density is an important parameter to confirm the integration possibility of a PT in practical applications. This parameter is expressed in the equation 1.1 as below:

$$P_D = \frac{P_{out}}{Vol} \quad [W/cm^3] \quad (1.1)$$

The equation 1.1 shows that in practical applications with a specific requested power level, the higher the power density it gets, the smaller the profile (size and weight) and hence cheaper it is.

1.3 Research Goals and Organization

Within the content of this research work, following issues will be taken into consideration:

- The fundamentals of Piezoelectric Transformer are located in chapter 2. In this chapter, the material properties and the electrical operational characteristics of a PT based on its equivalent circuit are introduced.

- Chapter 3 studies the most important effects that influence the PTs capability of transferring power:
 - Temperature rise due to losses during operation
 - Electro-mechanical limitations
 - Effect of operating conditions such as: load, matching network, output rectifier, excitation method (continuous and discontinuous)[75, 76]
- The consideration for circuit, driver topologies and control methods for Piezoelectric Transformer are represented in Chapter 4. In this chapter, two common power amplifier topologies (class D and class E) for PT will be compared. Further, the control methods for PT are also discussed.
- In Chapter 5, four typical applications:
 - Igniters for HID lamps based on discontinuous working mode of PT
 - High output voltage DC/DC converters
 - Stand alone ignition device using for ionizer machine in fertilizer
 - PT based electronic ballasts for Light Emitting Diodes (LEDs)

will be introduced as the demonstrations of PT's integration possibility in power electronics devices.

- Some concluding statements and ideas for future works are located in the last chapter - chapter six.

Application	Power range	PT design	Market needs (mil.pcs)
Lighting system <ul style="list-style-type: none"> • Ignition • HID ballast • Fluorescent ballast • LED lamp ballast • Special lamp 	<ul style="list-style-type: none"> < 10W < 50W 5-50W < 50W < 50W 	<ul style="list-style-type: none"> multi/mono multi multi/mono multi/mono multi/mono 	
Power supply <ul style="list-style-type: none"> • Copy machine • Electrostatic filter • Power laser • X-ray tube 	<ul style="list-style-type: none"> < 10W < 20W < 30W < 500W 	<ul style="list-style-type: none"> multi/mono multi/mono multi/mono multi/mono 	
Ionizers <ul style="list-style-type: none"> • O_3 machine • for medical purposes • for household devices 	<ul style="list-style-type: none"> < 20W < 20W < 20W 	<ul style="list-style-type: none"> multi/mono multi/mono multi/mono 	
Other Applications <ul style="list-style-type: none"> • Semiconductor gate driver 	<ul style="list-style-type: none"> < 10W 	<ul style="list-style-type: none"> multi/mono 	

Table 1.1: Prospective applications of Piezoelectric Transformer

Chapter 2

Fundamentals of Piezoelectric Transformer

2.1 Introduction

In 1880's Jacques and Pierre Curie discovered two interesting effects that happened in some certain crystal materials:

- **Direct piezoelectric effect:** With these crystal materials, when a mechanical strain is applied, they will be electrically polarized and the level of polarization is proportional to the applied strain but not exceeding their withstanding limitation. This phenomena is so called the piezoelectric effect and the devices operating based on this effect are known as piezoelectric actuators.
- **Inverse piezoelectric effect:** The Curies also discovered that these same materials deformed when they were exposed to an electric field. This has been known as the inverse piezoelectric effect and the devices derived from this effect are named as piezoelectric transducers.

From the time of its discovery, a few practical uses had been developed during World War I and II based on either direct or inverse piezoelectric effect [59]. These applications were found in laboratory devices for measuring pressure or electric charge.

In 1956, a new device derived from piezoelectric material regarded as a power transforming equipment was firstly introduced by C.A.Rosen [14] and the device was named Piezoelectric Transformer(PT). A piezoelectric transformer is composed by the combination of a piezoelectric actuator as an input (or primary side) and one or several piezoelectric transducers [23, 26, 88] as outputs (or secondary side). But after the first introduction, this device did not receive much interest due to difficulties in material quality, controlling and driving technics. Until the years of 70s of last century, thanks

to the incessant exertions of Japanese researchers in concentration on developing new processes, applications, and opening new commercial markets for piezoelectric devices including Piezoelectric Transformer, this device has been regarded as the new and most potential component in power electronics area. In the last decade of the 20th century, with the combination of advanced technics and the demands for minimizing the size and weight and hence the price of electrical devices, PT has been paid attention to by researchers and developers all over the world especially from USA and Japan in purpose to replace the traditional, heavy and bulky magnetic transformer in small power range applications (up to hundreds of watts).

The next parts of this chapter are introductions to the fundamentals of PT including the physical and electrical properties.

2.2 Physical Basics

2.2.1 Piezoelectric Materials

In a piezoelectric transformer, both sides are made of piezoelectric ceramics such as barium titanate (BaTiO₃), lead zirconate titanate (PZT) because of handling the highest piezoelectric constant $(100 - 149) \cdot 10^{12} m/V$, and $(250 - 365) \cdot 10^{12} m/V$ respectively. These are poly-crystalline ferroelectric materials with the perovskite crystal structure - a tetragonal/rhombahedral structure very close to cubic. They have the general formula $A^2 + B^1 + O_3^{2-}$, in which A presents a large bivalent metal ion such as barium or lead, and B expresses a tetravalent metal ion such as titanium or zirconium.

With these piezoelectric ceramics, temperature is one of very important parameters that effect their performance. The structure and properties of the materials will be partially or completely changed when their temperature are under or above a special point, the so called Curie point , this phenomenon is depicted in the figure 2.1:

- **Above Curie point:** these crystallites exhibit simple cubic symmetry, the elementary cell of which is shown in figure 2.1a This structure is centrosymmetric with positive and negative charge sites coinciding, so there are no dipoles present in the material (which is said to exhibit para-electric behavior).
- **Below Curie point:** the crystallites take on tetragonal symmetry in which the positive and negative charge sites no longer coincide as shown in figure 2.1b so each elementary cell then has a built-in electric dipole which may be reversed, and also switched to certain allowed directions by the application of an electric

field. The dipoles are not randomly oriented throughout the material. Neighboring dipoles align with each other to form regions of local alignment known as Weiss domains. Within a Weiss domain, therefore, all the dipoles are aligned, giving a net dipole moment to the domain, and hence a net polarization (dipole moment per unit volume).

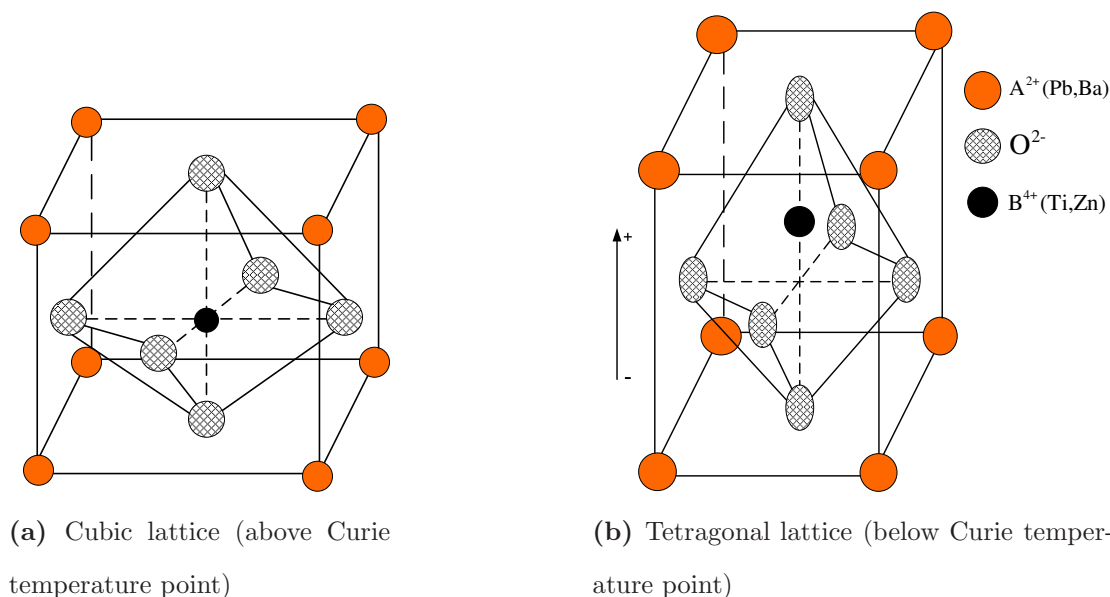


Figure 2.1: Piezoelectric elementary cell

In general, all the piezoelectric based devices including piezoelectric transformers can not work until they are polarized because the piezoelectric effect is only exhibited after the polarizing process has been carried out. The distribution of electric dipole moments in piezoelectric materials before polarization is expressed in the Fig 2.2a. The polarization can be made in any given direction by poling treatment by means of exposing piezoelectric material to a strong electric field at a temperature slightly below the Curie point as presented in the figure 2.2b. The electric field will be removed after a specific time which guarantees that the dipoles remain locked in approximately alignment as seen in figure 2.2c after removal of this field. Thanks to the poling treatment, a remanent polarization and permanent deformation are set up in the materials. The poling treatment is the final process in manufacturing piezoelectric based components and devices.

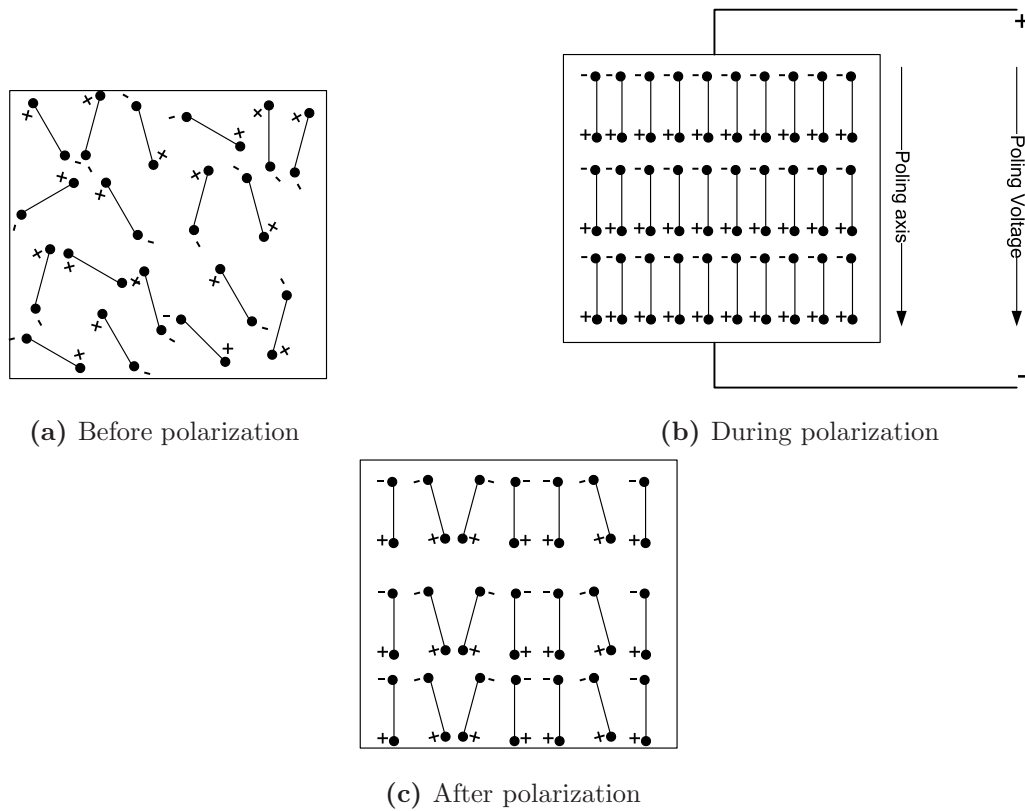


Figure 2.2: Electric dipole moments in Weiss domains

2.2.2 Depolarization

As mentioned above, after poling treatment phase a piezoelectric ceramic will be permanently polarized and there fore maintenance must be taken in all subsequent handling to guarantee that the ceramic will never be depolarized, because this will lead to partial or even total loss of its piezoelectric properties. The ceramic can be depolarized by some of the following causes:

- **Mechanical depolarization:**

Mechanical depolarization occurs when the mechanical stress on a piezoelectric element becomes high enough to disturb the orientation of the domains and hence destroy the alignment of the dipoles. The safety limits for mechanical stress vary considerably with material grade.

- **Electrical depolarization:**

Exposure to a strong electric field of opposite polarity to the poling field will depolarize a piezoelectric element. The field strength required for marked depolarization depends, among other things, on the material grade, the time the material

is subjected to the depolarizing field and the temperature. For static fields, it's typically between 200 and 500 V/mm.

- **Thermal depolarization:**

If a piezoelectric element is heated to its Curie point, the domains become disordered and the element becomes completely depolarized. A piezoelectric element can therefore function for long period without marked depolarization only at temperatures well below the Curie point. A safe operating temperature would normally be about half way between 0°C and the Curie point.

2.2.3 Piezoelectric Constants

Since piezoelectric ceramics are anisotropic, their physical constants (elasticity, permittivity etc.) are tensor quantities and relate to both the direction of the applied stress, electric field etc., and to the directions perpendicular to these. For this reason the constants are generally given two subscript indices which refer to the direction of the two related quantities (e.g. stress and strain for elasticity, displacement and electric field for permittivity).

The direction of positive polarization is usually chosen to coincide with the Z-axis of a rectangular system of crystallographic axes X, Y, Z. If the directions of X, Y and Z are represented by 1, 2 and 3 respectively, and the shear about these axes by 4, 5 and 6 respectively, the various constants may be written with subscripts referring to these (figure 2.3). The physical behaviors of piezoelectric elements are described by linear relationships shown in equations 2.1 and 2.2:

$$\vec{S} = \mathbf{s}^E \cdot \vec{T} + \mathbf{d} \cdot \vec{E} \quad (2.1)$$

$$\vec{D} = \mathbf{d} \cdot \vec{T} + \boldsymbol{\epsilon}^T \cdot \vec{E} \quad (2.2)$$

where \vec{S} , \vec{T} , \vec{E} , \vec{D} are strain, stress, electrical strength and charge density vectors, respectively. \mathbf{s}^E , \mathbf{d} , $\boldsymbol{\epsilon}^T$ are matrices of piezoelectric material properties. Equation 2.1 means that the mechanical strain, \vec{S} , derived from the applied mechanical stress, \vec{T} , and/or the electrical field, \vec{E} , on piezoelectric element. In other words, only an applied electrical field on piezoelectric element leads to the mechanical strain, \vec{S} , in the piezoelectric element.

Equation 2.2 informs that the electric displacement, D, results from the applied mechanical stress and/or applied electric field in a piezoelectric element. Without applying the electric field, E, an applied mechanical stress, T, on a piezoelectric element results in an electric displacement induced on the electric plates of the piezoelectric element, which

functions as a transducer.

Some important piezoelectric constants will be listed as follows:

Permittivity ϵ :

The (absolute) permittivity (or dielectric constant) is defined as the dielectric displacement per unit electric field. The first subscript gives the direction of the dielectric displacement, the second gives the direction of the electric field. For example:

ϵ_{11}^T : is the permittivity for the dielectric displacement and electric field in direction 1 under conditions of constant stress.

ϵ_{33}^S : is the permittivity for the dielectric displacement and electric field in direction 3 under condition of constant strain.

Compliance s :

The compliance s of a material is defined as the strain produced per unit stress. It's the reciprocal of the modulus of elasticity. The first subscript refers to the direction of strain, the second to direction of stress. For example: s_{11}^E : is the compliance for stress and accompanying strain in direction 1 under condition of a constant electric field.

s_{36}^E : is the compliance for a shear stress about axis 3 and accompanying strain in direction 3 under condition of constant electric displacement.

Piezoelectric charge constants d :

The piezoelectric charge constant is defined as the electric polarization generated in a material per unit mechanical stress applied to it. Alternatively, it is the mechanical strain experienced by the material per unit electric field applied to it. The first subscript refers to the direction of polarization generated in the material (at $E = 0$) or to the applied field strength, the second refers respectively to the direction of the applied stress or to the direction of the induced strain. For example:

d_{33} : is induced polarization per unit applied stress in direction 3. Alternatively, it is the induced strain per unit electric field in direction 3.

d_{31} : is the induced polarization in direction 3 per unit stress applied in direction 1. Alternatively, it is the mechanical strain induced in the material in direction 1 per unit electric field applied in direction 3.

Piezoelectric voltage constant g :

The piezoelectric voltage constant is defined as the electric field generated in a material per unit mechanical stress applied to it. Alternatively, it is the mechanical strain experienced by the material per unit electric displacement applied to it. The first subscript refers to the direction of the electric field generated in the material or to the applied electric displacement, the second refers respectively to the direction of the applied stress or to the direction of the induced strain. For example:

g_{31} : is the induced electric field in direction 3 per unit stress applied direction 1. Alternatively, it is the mechanical strain induced in the material in direction 1 per unit electric displacement applied in direction 3.

g_{15} : is the induced electric field in direction 1 per unit shear stress applied about axis direction 2. Alternatively, it is the shear strain induced in the material about axis 2 per unit electric displacement applied in direction 1.

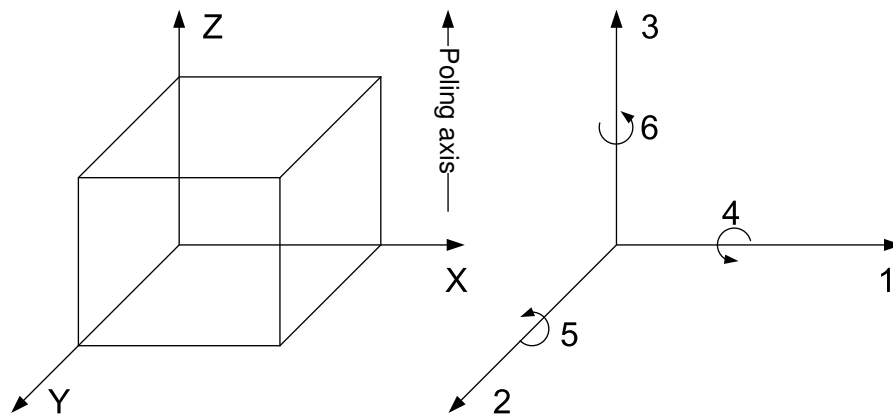


Figure 2.3: Designation of the axes and direction of deformation

2.2.4 Piezoelectric Transformer: Structure and Classification

A piezoelectric element can operate in either longitudinal mode or transverse mode (figure 2.4). When a piezoelectric element operates in longitudinal mode, as depicted in figure 2.4a, at one of its corresponding operating frequencies related to the wavelength in the direction of operating stress (T), the direction of T is parallel to the polarization direction (P).

Figure 2.4b describes the operation of piezoelectric element in transverse mode with one of corresponding operating frequency related to the wavelength in the direction of the operating stress, T , the direction of the operating stress, T , is perpendicular to the polarization direction, P . The most simple Piezoelectric Transformer is composed by

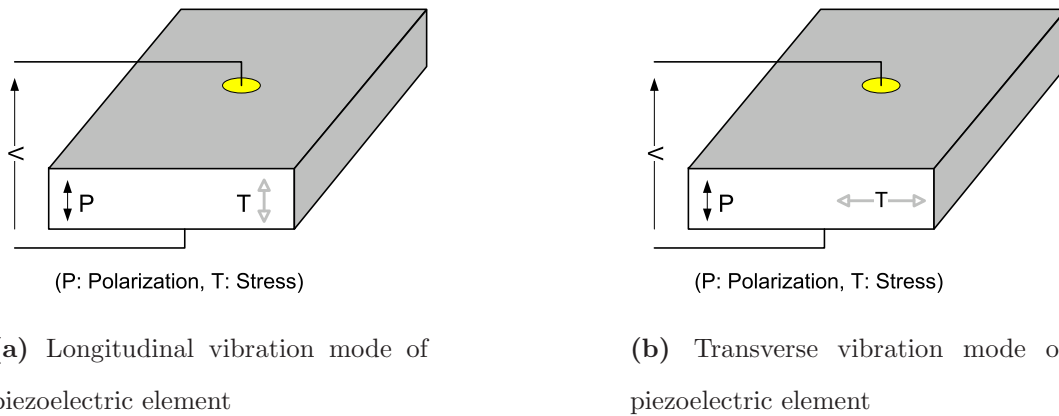


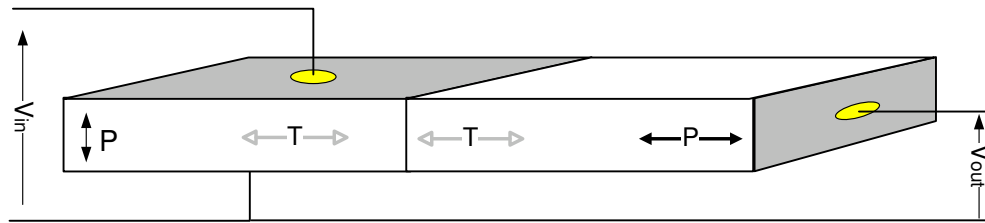
Figure 2.4: Vibration mode of piezoelectric element

combination of a piezoelectric element as an input (primary side) and another one as an output (secondary side), corresponding with 2 typical vibration modes of piezoelectric element mentioned above. There are 3 types of Piezoelectric Transformer: Rosen-type PT, thickness vibration mode PT and radial vibration mode PT, are shown in the figure 2.5.

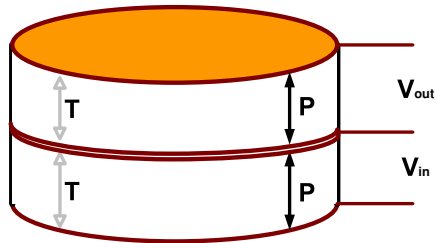
- **Rosen type Piezoelectric Transformer:**

Rosen type piezoelectric transformer, introduced in figure 2.5a, is composed by combination of two piezoelectric elements: a transverse mode piezoelectric element (actuator) as an input (primary side) and a longitudinal mode piezoelectric element (transducer) as an output (secondary side). When an input voltage, V_{in} , is applied to the primary side, i.e., the transverse mode piezoelectric actuator, the material becomes polarized in the direction parallel to that of the material thickness. The greatest vibration strain occurs in the planar direction perpendicular to the polarization direction. The planar vibration of the transverse mode piezoelectric actuator transmits to the longitudinal mode piezoelectric transducer. With the transmitting vibration from the primary side, the longitudinal mode piezoelectric transducer induces an electric charge on the electrode plates of the piezoelectric transducer to generate the output voltage, V_{out} . The vibration direction of the secondary side is parallel to the direction of the induced polarization, P . Rosen type PT is also regarded as HVPT¹ because of its inherent high voltage gain [16, 75].

¹HVPT: High Voltage Piezoelectric Transformer

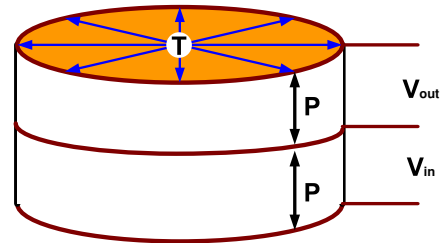


(a) Rosen-type piezoelectric transformer



P: Polarization, **T:** Stress

(b) Thickness vibration mode piezoelectric transformer



P: Polarization, **T:** Stress

(c) Radial vibration mode piezoelectric transformer

Figure 2.5: Three common types of piezoelectric transformer

This type of PT is compatible with high input impedance load and currently its applications are electronics ballast for CCFL² [16, 17, 33, 39] and high voltage source [75].

- **Thickness Vibration Mode Piezoelectric Transformer:**

Thickness vibration mode PT, shown in figure 2.5b, is the combination of two piezoelectric elements and both of them are longitudinal mode piezoelectric elements. With the applied voltage, V_{in} , on the primary side, i.e., the piezoelectric actuator, the material becomes polarized in the direction parallel to that of the material thickness. The greatest vibration strain occurs in the thickness direction parallel to the polarization direction. The thickness vibration of the primary side, the piezoelectric actuator, transmits to the secondary side, the piezoelectric transducer. With the transmitting vibration from the primary side, the piezoelectric transducer induces an electric charge on the electrode plates of the piezoelectric transducer in order to generate the output voltage, V_{out} . The vibration direction of the secondary side, the transverse mode piezoelectric transducer, is also parallel to the direction of the induced polarization. This type of PT is also known as LVPT

²CCFL: Cold Cathode Fluorescent Lamp

³ because of its inherent low voltage gain [16]. Its present applications include use in converters and adapters.

- **Radial Vibration Mode Piezoelectric Transformer:**

Radial vibration mode PT, as depicted in figure 2.5c, is composed by the combination of two piezoelectric elements and both of them operate in transverse mode. With the applied voltage, V_{in} , on the primary side, i.e., the piezoelectric actuator, the material becomes polarized in the direction parallel to that of the material thickness. In this case, the greatest vibration strain occurs in the planar direction perpendicular to the polarization direction. The planar vibration of the piezoelectric actuator transmits to the piezoelectric transducer. The vibration transmits from the primary side, inducing an electric charge on the electrode plates of the piezoelectric transducer in order to generate the output voltage, V_{out} . The vibration direction of the transverse mode piezoelectric transducer is perpendicular to the direction of the induced polarization. At first, this type of PT has square shape but due to the distances from the center to the every point in edges of electrode are unequal leading to its wavelengths of planar vibration are not the same, which causes the undesired additional vibration frequencies. The round shape radial vibration mode PT (figure 2.5c) was invented in order to eliminate these undesired frequencies. Currently radial vibration mode PT is used in electronic ballast for LED ⁴ [88], power converters and adapters [58]

2.3 Piezoelectric Transformer Generic Operational Characteristics

2.3.1 Physics Based Equivalent Circuit

In practice, a Piezoelectric Transformer is able to operate at 3 frequency ranges close to three resonant frequencies that are referred to as three vibration modes: Half lambda ($\frac{\lambda}{2}$), lambda (λ) and three second lambda ($\frac{3}{2}\lambda$) respectively. The equivalent circuit of Piezoelectric Transformer, corresponding to three resonant frequencies, is expressed in the figure 2.6 as below. In the study work, in order to simplify the model of a PT and guarantee its generic properties still remain, its model is considered for one resonant

³LVPT: Low Voltage Piezoelectric Transformer

⁴LED: Light Emitting Diode

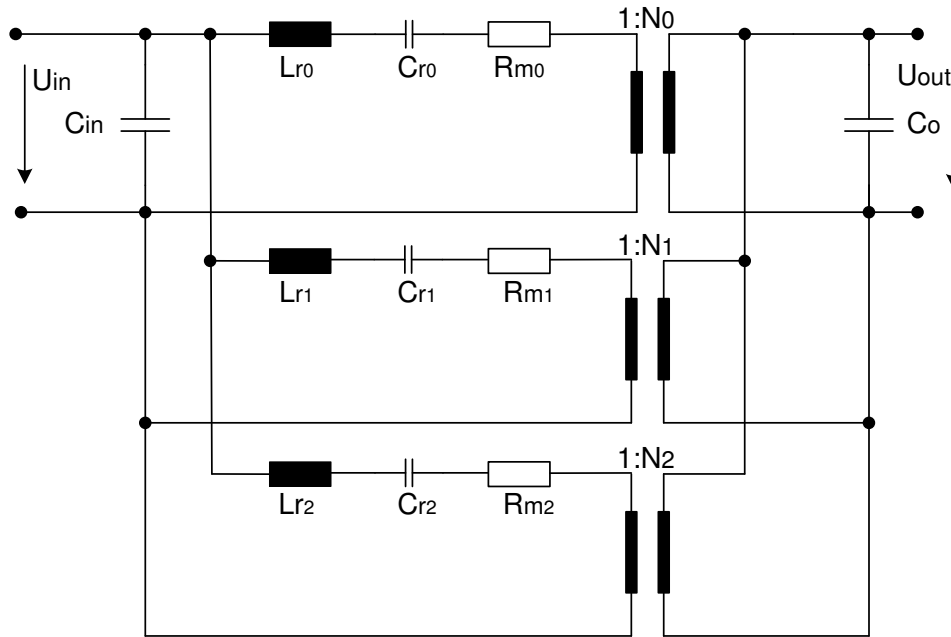


Figure 2.6: Typical equivalent circuit of a PT in multi-resonant mode

mode which is close to a specific resonant frequency. Two common equivalent circuit of a PT at one of its resonant frequencies are described in the figure 2.7: In the two common equivalent circuits, the second one (figure 2.7b) is preferred in simulation [7], in this model the ideal transformer of the first model (figure 2.7a) is replaced by dependent voltage and current source. From the electronics point of view, these are the same. In simulation, however, it will get into trouble if the first model is applied. The reason is, in the simulation, the ideal transformer will be expressed by putting two large inductances and the output inductance is a short circuit if it is connected to a DC source, voltage doubler for example. From now on in this research work, the second equivalent circuit (figure 2.7b) of PT is officially used.

2.3.2 Voltage Transfer Function of Piezoelectric Transformer

One of the most important parameters of a transformer is the voltage transfer coefficient. Generally speaking, with a specific conventional magnetic transformer, its voltage ratio between output and input is determined by ratio of turns of secondary and primary and this ratio is an independent parameter with load. In contrast, because of being a

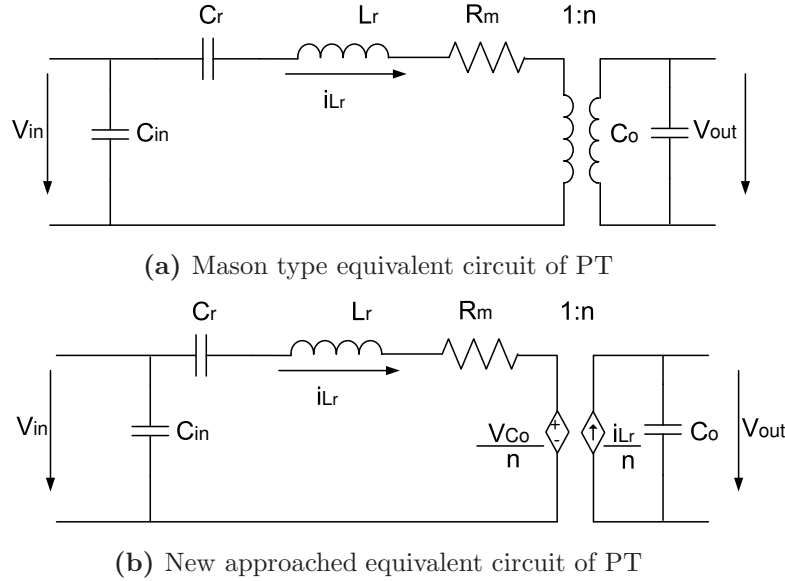


Figure 2.7: Physical based equivalent circuit of PT

resonant device this parameter of PT is strongly dependent on load [7, 73]. In order to study the generic electrical characteristics of PT, an equivalent circuit of PT with resistive load is set up as introduced in the figure 2.8. Base on the view about power transfer, the loaded equivalent circuit (figure 2.8a) can be simplified by reflecting the output capacitance (C_{out}) and load (R_o) from secondary side to primary side as shown in the figure 2.8b in which the input capacitance (C_{in}) is ignored since it does not effect the capability of transferring power to the load of PT. The value of primary side - reflected parameters are calculated:

$$R'_o = \frac{R_o}{n^2} \quad (2.3)$$

$$C'_o = n^2 \cdot C_o \quad (2.4)$$

$$V'_{out} = \frac{V_{out}}{n} \quad (2.5)$$

With the simplifications mentioned above, the equivalent of PT is regarded as a series-parallel resonant tank [73]. The further simplification can be carried out by converting the parallel network $R'_o \parallel C'_o$ to series network. Following [51, 73], the series resistance R'_{os} and series capacitance C'_{os} are defined:

$$R'_{os} = \frac{R'_o}{1 + (\omega C'_o R'_o)^2} \quad (2.6)$$

$$C'_{os} = C'_o \frac{1 + (\omega C'_o R'_o)^2}{(\omega C'_o R'_o)^2} \quad (2.7)$$

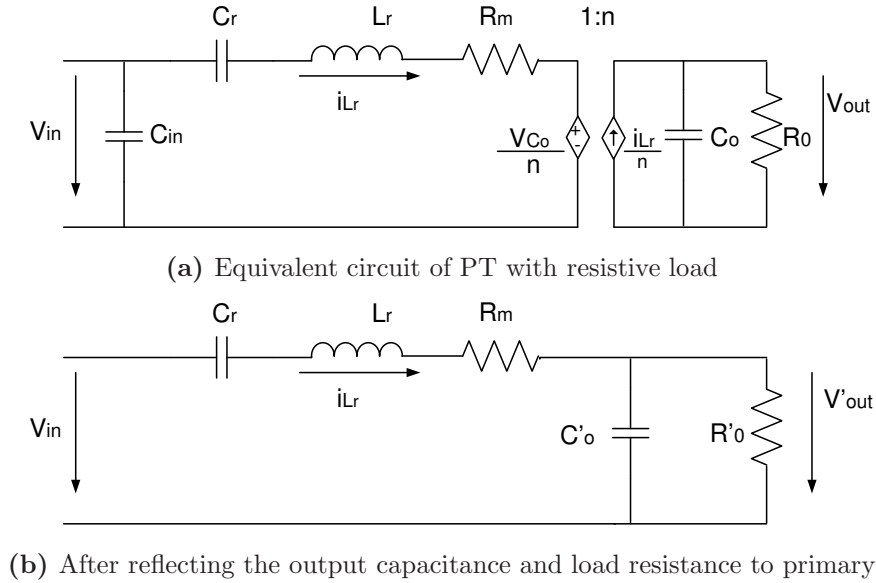


Figure 2.8: Models of equivalent PT with load

For easier analysis and calculation, some following parameters of PTs equivalent circuit are normalized:

- The ratio of capacitances:

$$A = \frac{C'_o}{C_r} \quad (2.8)$$

- The corner frequency (output open circuit):

$$\omega_{r0} = \sqrt{\frac{C'_o + C_r}{L_r C_r C'_o}} \quad (2.9)$$

- Series resonant frequency (output short circuit):

$$\omega_{rs} = \frac{1}{\sqrt{L_r C_r}} \quad (2.10)$$

- Equivalent capacitance of series value of C_r and C'_{os} :

$$C_{eq} = \frac{C_r C'_{os}}{C_r + C'_{os}} \quad (2.11)$$

- Resonant frequency of PT:

$$\omega_r = \frac{1}{\sqrt{L_r C_{eq}}} = \sqrt{\frac{C_r + C'_{os}}{L_r C_r C'_{os}}} \quad (2.12)$$

- Electrical quality factor:

$$Q = \omega_{rs} C_0 R_0 \quad (2.13)$$

- Mechanical quality factor:

$$Q_m = \frac{1}{\omega_{rs} C_r R_m} \quad (2.14)$$

With normalized parameters declared above, the output to input voltage ratio of a PT 2.8b can be calculated:

$$n_{21} = \frac{V'_{out}}{V_{in}} = \frac{1}{\sqrt{Y}} \quad (2.15)$$

where:

$$Y = \left\{ 1 - A \cdot \left[\left(\frac{\omega}{\omega_{rs}} \right)^2 - 1 \right] + \frac{R_m}{R'_o} \right\}^2 + \left\{ \frac{\omega_{rs}}{\omega} \cdot \frac{A}{Q} \cdot \left[\left(\frac{\omega}{\omega_{rs}} \right)^2 - 1 \right] + \frac{\omega}{\omega_{rs}} \cdot \frac{A}{Q_m} \right\}^2 \quad (2.16)$$

The equation 2.16 informs that, with a specific PT, its output to input voltage boost ratio depends on two parameters: operating frequency ω and volume of load R_o . With a PT, for any given load R_o , its output voltage is dependent upon operating frequency and gets maximum value n_{21m} at resonant frequency ω_r introduced in the equation 2.12, in other words, the output voltage of PT can be control by shifting the operating frequency around resonant frequency ω_r in the range of: $\omega_{rs} \leq \omega \leq \omega_{r0}$ where ω_{r0} and ω_{rs} are expressed in the equation 2.9 and 2.10 respectively. The dependence of PTs output to input voltage boost ratio is depicted in the figure 2.9.

Currently, following the estimation [114] the achievable voltage boost ratio of PT is introduced in the Table 2.1

2.3.3 Output Power of Piezoelectric Transformer

Derivation from the figure 2.8b and normalized parameters that are calculated in previous parts, the output power of a PT can be defined in equation 2.17:

$$P_o = \frac{(V'_{out})^2}{R'_o} = \frac{(n_{21} \cdot V_{in})^2}{R'_o} \quad (2.17)$$

With a PT, for any given load, the output power at the resonant frequency will depend on the fraction of R'_{os} and R_m . Equation 2.6 addressed that R'_{os} is convex, it means that there are two values of R'_{os} (therefore two R_o) satisfy that the maximum output power condition [51]. The equation 2.17 also informs that PT's output power is dependent on load and operating frequency. This relationship is depicted in the figure 2.10

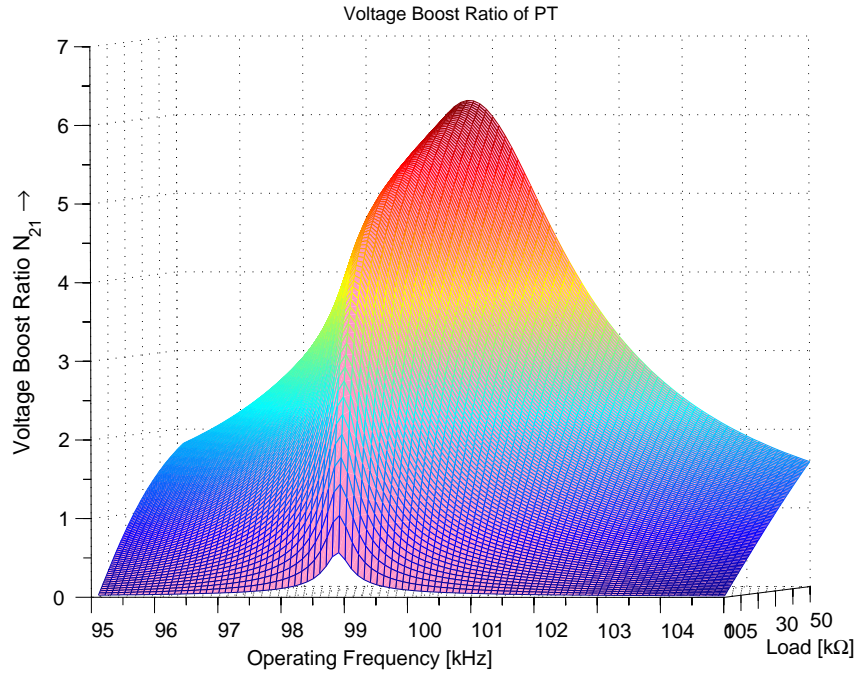


Figure 2.9: Output to input voltage boost ratio of PT

2.3.4 Efficiency of Piezoelectric Transformer

From the figure 2.8b, the primary-side reflected equivalent circuit of PT is considered as a two port model. After taking the conversion to series from parallel network (equation 2.6, 2.7), calculations and analysis in [51, 93] the efficiency η of a PT can be found in the equation 2.18.

$$\eta = \frac{R'_{os}}{R'_{os} + R_m} \quad (2.18)$$

The equation 2.18 denotes that, the efficiency of PT is getting more and more significant when $R'_{os} \gg R_m$ and it reaches to maximum value when R'_{os} increases to its peak point. Considering equation 2.6, it expresses the dependence of R'_{os} on R'_o . When R'_o is increasing from 0 to ∞ , R'_{os} is changing from 0 back to 0 with maximum value R'_{osm} at:

$$R'_{osm} = \frac{1}{\omega_r \cdot C'_o} \quad (2.19)$$

Applying the equations 2.3 and 2.4 to 2.19, we obtain the relationship between optimal load R_{opt} and output capacitance of a PT as shown in equation 2.20:

$$R_{opt} = \frac{1}{\omega_r \cdot C_o} \quad (2.20)$$

Voltage boost ratio of:	Value
Single-layer PT	
With load	$n_{21}=0.02 \dots 50$
Without load	$n_{21}=0.1 \dots 2500$
Multi-layer PT	
With load	$n_{21}=0.001 \dots 1000$
Without load	$n_{21}=0.05 \dots 50000$

Table 2.1: Achievable Voltage Boost Ratio of Piezoelectric Transformer

The dependence of PT's efficiency on load is represented in the figure 2.11.

Equation 2.20 also shows that, with a specific application, if PT operates at highest efficiency ($R_o = R_{opt}$) then R'_o achieves its maximum value leading to a local minimum output power P_o with a given input excitation. On a supposition that, a PT is always operated in one of its resonant frequency, the generic operational characteristics including output power P_o , output to input voltage boost ratio n_{21} and efficiency η are functions of load R_o . These relationships are illustrated in the figure 2.12: The relationships shown in figure 2.12 really match with applications which have negative impedance performance such as fluorescent lamps, gas discharge lamps, etc. First of all, at the moment of switch on, these lamps are considered as an opened circuit since their impedance is very high (at level of $M\Omega$) and of course they need very high ignition voltage (from several hundreds of volts [18, 66] to more than 10 kV [10]). After ignition phase, these lamps go to steady state via short time so-called warm up phase. In steady state operation, their impedance is low (some hundreds Ω) and the optimum operating point of PT will be matched with the impedance, in case the optimum point of PT does not match with this impedance, there are some approaches of impedance matching to overcome this issue. The other PTs parameters used in practice are listed in the Table 2.2 [114]:

2.4 Summary

This chapter introduces the fundamentals of piezoelectric transformers in both physical-material view and electrical view. Piezoelectric transformer is created by the combination of two or more piezoelectric elements made from piezoceramic materials which have high power density. Derivation from this combination, there are three main type

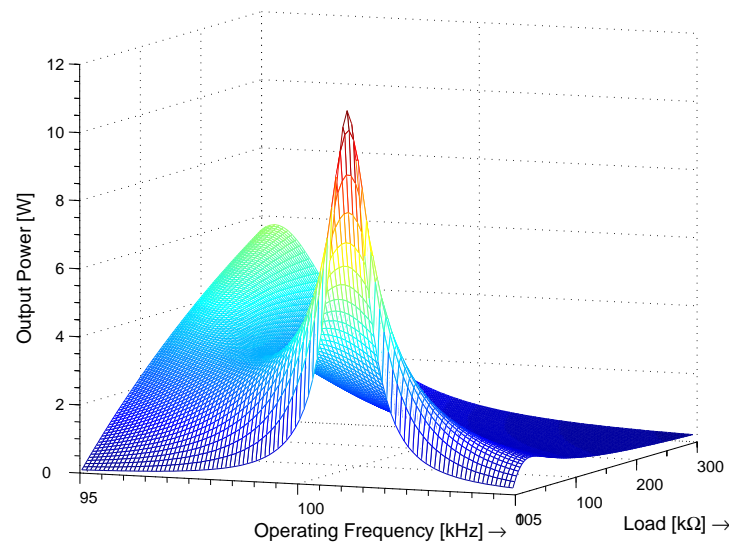


Figure 2.10: Dependence of PT's output power on load and operating frequency

of piezoelectric transformer:

- Longitudinal vibration mode (Rosen-type) PT,
- Radial vibration mode PT and
- Thickness vibration mode PT

The operation of PT is based on direct and inverse piezoelectric effect via electro-mechanic coupling. In order to guarantee the safety operation of PT, there are some strict requirements to prevent depolarization from taking place. If depolarization appears then PT's functionalities are no longer valid. There are three main causes of depolarization: Mechanical stress; electrical strength and temperature. A PT is considered to be in correct operation condition if and only if excited by a signal having frequency close to its individual mechanical vibration frequency. In practise, each PT has three different applicable frequencies and they are referred to as three vibration modes expressed by the wavelength: first order or half wavelength ($\lambda/2$ mode); second order or full wavelength (λ mode) and third order or one and a half wavelength ($\frac{3}{2}\lambda$ mode).

From electrical point of view, the operation of PT is represented by the electrical equivalent circuit where all the physical and mechanical quantities are replaced by electrical counterparts as following:

- The mass m is replaced by inductor L

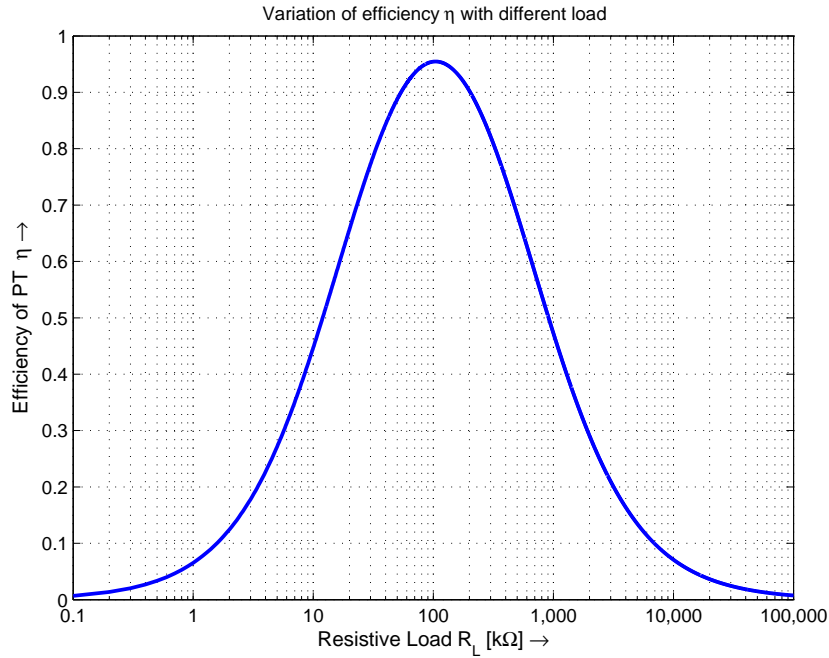


Figure 2.11: Efficiency of PT versus load

- Compliance c is replaced by capacitor C
- Mechanical losses are replaced by resistor R
- Mechanical transmissions are represented as transformers
- Velocities v are marked as currents i , forces F as voltages v , and sources of forces as generators

Then the generic operational characteristics of PT are studied and analyzed based on its modified model where the conventional transformer is replaced by two dependent sources. The equivalent circuit of PT is considered a series - parallel resonant tank with input and output capacitors to describe the high galvanic isolability. Because of being a resonant device, the behavior of PT is strongly dependent on two variables: operating frequency and load. The effect of frequency and load on the performance of PT are studied from the view of:

- Output to input voltage boost ratio,
- The overall power transmission and
- The efficiency

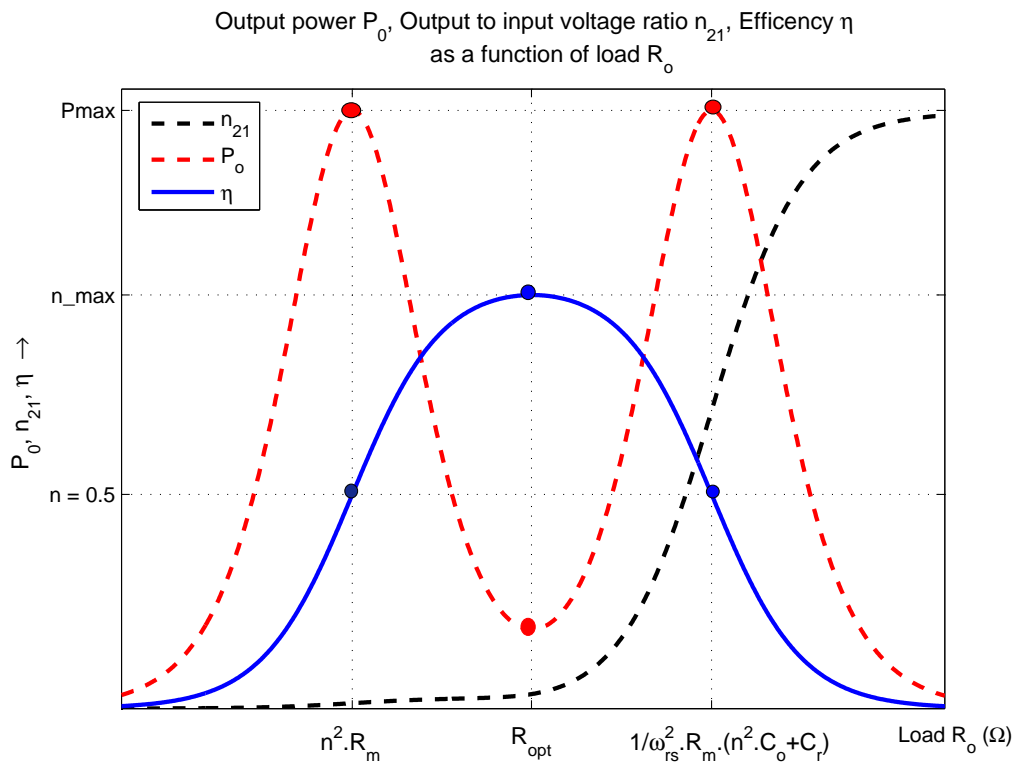


Figure 2.12: Generic operational characteristics of PT

In order to operate PT effectively, PT should be driven in a frequency range around one of its resonant frequencies corresponding with a specific vibration mode. Within the operation frequency range, the load variation will influence to the performance of PT as depicted in the figure 2.12. Derivation from figure 2.12, the operation of PT can be divided into three operating regimes:

- Low voltage boost ratio area is defined when the load resistance $R_O < n^2 R_m$ is applied.
- High efficiency priority area is specified when the load resistance $n^2 R_m < R_O < \frac{1}{\omega_{rs}^2 R_m (n^2 C_o + C_r)}$ is connected at the PT's output.
- High voltage boost ration area is taken if the load resistance $R_O > \frac{1}{\omega_{rs}^2 R_m (n^2 C_o + C_r)}$

Based on the generic operational characteristics and requirements of application (range of load, power, output voltage...), the PT is then designed to overcome these demands.

Parameters of PT	Value
Output Power	$P_o = 10\mu W \dots 80W$
Power Density	$P_D = 10 \dots 100W/cm^3$
Efficiency	
PT:	$\eta = 80\% \dots 99\%$
System:	$\eta \leq 95\%$
Operating Frequency	$f_R = 50Hz \dots 3MHz$

Table 2.2: Practical parameters of PT

Chapter 3

Limitations to Throughput Power of Piezoelectric Transformer

3.1 Introduction

In this Chapter, some facts that effect the capability of transferring power to the load, referred to by power density P_D , of a PT will be taken into consideration. The most important causes must be mentioned and dealt with in the area of the research work are:

- Effect of temperature rise during operation.
- Effect of electromechanical limitations on transferred energy of a PT.
- Effect of working conditions.

In the content of the research work, several types of PT from different manufacturers were used to study the major causes that effect to the inherent high power density P_D of a PT.

3.2 Effect of Temperature on Power Density

As mentioned in previous section (2.2.2), temperature rising inside the body of piezoelectric transformer is one of main reasons that leads to the destruction of the device. When a piezoelectric transformer is applied in power applications as a power transferring device, it will generate heat because of energy losses including the mechanical and electrical loss. These losses will be converted into heat by physical processes and it will raise the temperature of the PT's body. The excessive temperature influences the PT's

operation due to the changes of piezoelectric material properties. From electrical engineering point of view, the consequences are low efficiency, poor reliability, and short life time. The operation temperature of PT depends on internal losses, ambient temperature, structure, and heat conductivity coefficient [44, 101]. In the research project, some PT samples were used for studying their operational temperature characteristics. The information about structure, material properties, and electrical operating conditions of the PT samples are shown in the Table 3.1 and all of them are Rosen-type MLPT ¹. The detailed information of PT samples can be found in the Appendix A.

PT sample	PT#1	PT#2	PT#3
Dimension: $l_L \times l_W \times l_T [mm^3]$	$36 \times 8.2 \times 3.0$	$30 \times 7.4 \times 2.5$	$34 \times 10 \times 4$
Density $\rho [\times 10^3 kg/m^3]$	8	7.9	7.85
Curie point $T_C [^{\circ}C]$	320	290	325
Electromechanical Coupling Coefficient [%]			
K_p	60	62	56
K_{33}	68	70	67
K_{31}	35	37	31
Piezoelectric Constant ($\times 10^{-12} [m/V]$)			
d_{33}	280	290	265
d_{31}	-122	-140	-120
Vibration mode	$\lambda/2$	$\lambda/2$	λ
f_r (kHz)	47 ± 2	55 ± 2	100 ± 2
$C_o(pF)$	20 ± 2	22 ± 2	15 ± 1
Structure of PT	Rosen MLPT	Rosen MLPT	Rosen MLPT
Output Power [W]	8.5	6.5	10
Origin of Product:	KONGHONG	ELECERAM	EPCOS

Table 3.1: Characteristics of piezoelectric transformer samples

¹MLPT: Multi-layer Piezoelectric Transformer

In this section, all the PT samples are operated in the highest efficiency regime [44], that means the load resistance will be chosen according to the equation 2.20. With the optimum load R_{opt} , the output power per square of input voltage unit (P_o/V_{in}^2) will be minimum as depicted in figure 2.12 but the output power can be increased by increasing the input voltage. The output power of PT#1 was simulated (based on the equivalent circuit) and measured with different input voltages under optimum load conditions. The simulation and measurement results are shown in the figure 3.1:

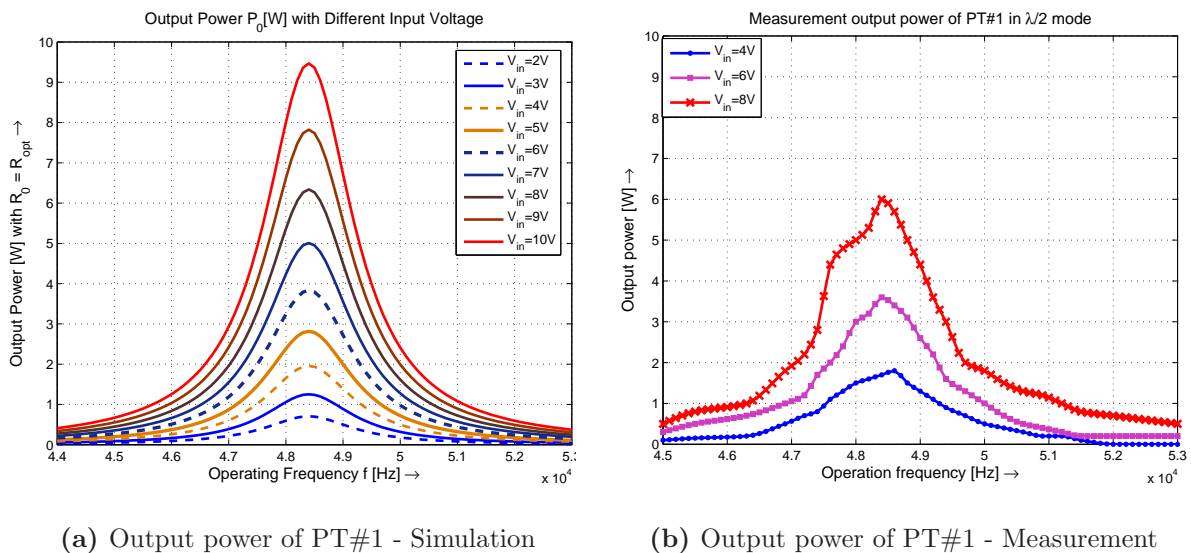


Figure 3.1: Output Power of PT#1 - Simulation and measurement results

The experiment for determining the output power and surface temperature of PT is set up as shown in figure 3.2. In the measurements, PT is fed by a function generator through a power amplifier and the surface temperature of PT is supervised continuously by IR² thermometer. The excitation signal to PT can be controlled in fields of amplitude, frequency and wave-form. During the experiment, to guarantee the safety for PT, its temperature is kept below the half of Curie point. For all PT samples listed in the Table 3.1 above, the temperature limit is 120^oC. The simulation results in figure 3.1a are carried out with PT#1 based on its parameters of equivalent circuit then they were verified by experiment as illustrated in figure 3.1b. In the experiment, PT was excited by a regulated frequency square wave signal and the maximum input voltage was 8 volts, in this case, the output power was around 6 watts and the saturation temperature on the surface of PT was about 100^oC. As discussed in the [80], with a given geometry, the power density P_D of PT is proportional to resonant frequency f_r , permittivity ϵ , the

²IR: Infra-red

square of electromechanical coupling coefficient K^2 , the square of electrical field strength E and mechanical quality factor Q_m as expressed in the equation 3.1 following:

$$P_D = \frac{\text{Output Power}}{\text{Volume}} = 2\pi \cdot f_r \cdot \varepsilon_{33}^T \cdot K^2 \cdot E^2 \cdot Q_m \quad (3.1)$$

From theory point of view, the relationship above informs that, the power density P_D of a PT can be improved by means of optimizing the electromechanical coupling coefficient K_r [58] because others quantities are regarded as constants. In fact, however, most of the quantities in the equation 3.1, except electrical field strength E , are dependent on PT's operational temperature, furthermore, the mechanical quality factor Q_m strongly depends on number of layers, vibration velocity and temperature [101]. The temperature characteristics of these quantities of PT#1 are shown in the figure 3.3³. In order to

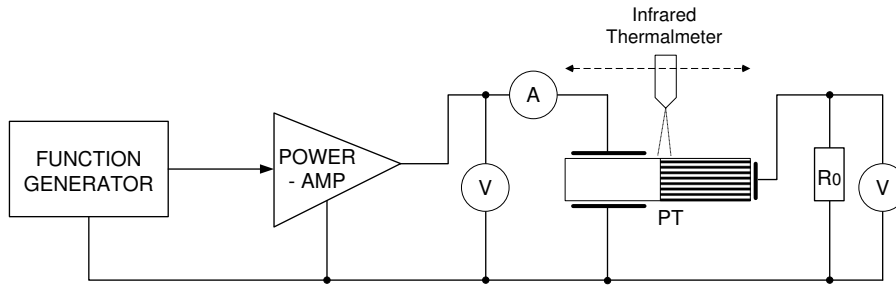


Figure 3.2: Scheme for determining the output power and surface temperature of PT

increase the power density P_D of a given PT operating in a specific condition (load, ambient temperature, operation mode ...), the common way is by increasing the input voltage V_{in} , but it will reach V_{inmax} which is limited by boundary conditions to ensure the safety for the device and one of them is limitation of temperature. The operating temperature of a PT in the given condition is described in the equation 3.2 below:

$$\vartheta_{PT} = \vartheta_0 + K_{VS} \cdot E \cdot t_{sat} \cdot \frac{f_r}{Q_{eff}} \quad (3.2)$$

where:

- ϑ_{PT} : Current temperature on the surface of PT
- ϑ_0 : Temperature of PT at beginning time of operation (Surrounding environment temperature)
- K_{VS} : Overall heat transfer coefficient (including volume and surface properties)

³These data are supplied by XI'AN KONGHONG Ltd - PT#1 Manufacturer

- E : Electrical field strength [V/mm]
- t_{sat} : Saturation time [s] (after this point of time, PT's temperature stops rising)
- f_r : Resonant frequency [Hz]
- Q_{eff} : Effective quality factor (concerned to load, impedance matching)

First of all, the effect of temperature on resonant frequency of given PT operating with specific load must be fully studied because this is one of the most important parameters for PT's operation as analyzed in the second chapter. Combining the analysis in [42, 58, 101] and measurement results, the resonant frequency of a given PT will be reduced as its operation temperature rises. The reduction of PT's resonant frequency versus its surface temperature is illustrated in the figure 3.3a and table 3.2. The reduction of

PT Sample PT Temperature	PT#1	PT#2	PT#3
60°C	$\Delta f_r=120$ Hz	$\Delta f_r = 80$ Hz	$\Delta f_r = 100$ Hz
70°C	$\Delta f_r=200$ Hz	$\Delta f_r = 170$ Hz	$\Delta f_r = 180$ Hz
80°C	$\Delta f_r=400$ Hz	$\Delta f_r = 390$ Hz	$\Delta f_r = 390$ Hz
90°C	$\Delta f_r=620$ Hz	$\Delta f_r = 600$ Hz	$\Delta f_r = 610$ Hz
100°C	$\Delta f_r=870$ Hz	$\Delta f_r = 830$ Hz	$\Delta f_r = 860$ Hz
110°C	$\Delta f_r=1110$ Hz	$\Delta f_r = 1070$ Hz	$\Delta f_r = 1100$ Hz
120°C	$\Delta f_r=1400$ Hz	$\Delta f_r = 1340$ Hz	$\Delta f_r = 1370$ Hz

Table 3.2: Resonant frequency shift versus temperature rise

resonant frequency of a given PT when its temperature is rising because of following main reasons:

- The extension of its dimensions while temperature rising, this is the common phenomenon of solid materials
- Reduction of vibration velocity of piezoelectric materials when operation temperature rises
- Others physical effects

The measurement results shown in table 3.2 inform that the reduction of resonant frequency is significant when the surface temperature exceeds 60°C and will be more and more serious when PT's temperature is rising higher and higher. The temperature characteristics of PT#1 with different input voltage is shown in figure 3.4, in this case the PT is excited with frequency regulated square wave signal. From electrical point of view, PT behaves as a bandpass filter so its capability to transfer power to load will be improved if the excitation signal is of a sinusoidal form instead of a square one. This issue will be discussed and analyzed in detail in the next chapter. In addition, there was an interesting phenomenon appearing during the experiments, as mentioned earlier, the thermal meter (figure 3.2) was being moved along PT compatible with the main vibration direction and PT's temperature field was unequal for every part of PT. The distribution of the temperature field of PT#1 and PT#2 in two cases high and low output power are introduced in the figure 3.5 where the position 0 indicates the beginning point of the input (primary) side corresponding with main vibration direction. The measurement results shown in figure 3.5 can be expressed by a concept called thermal stress distribution. For the PT, the thermal stress at the primary part is bigger than that one at the secondary part and it is highest at the center area of the primary part. Thanks to this discovery, from now on the thermal meter to collect PT's temperature should be located in the center section of primary part. However, because of inherent poor heat conductivity of piezoelectric materials, the comparison of heat conductivity of piezoelectric material with others is shown in table 3.3, over-heating may take place in the core of PT.

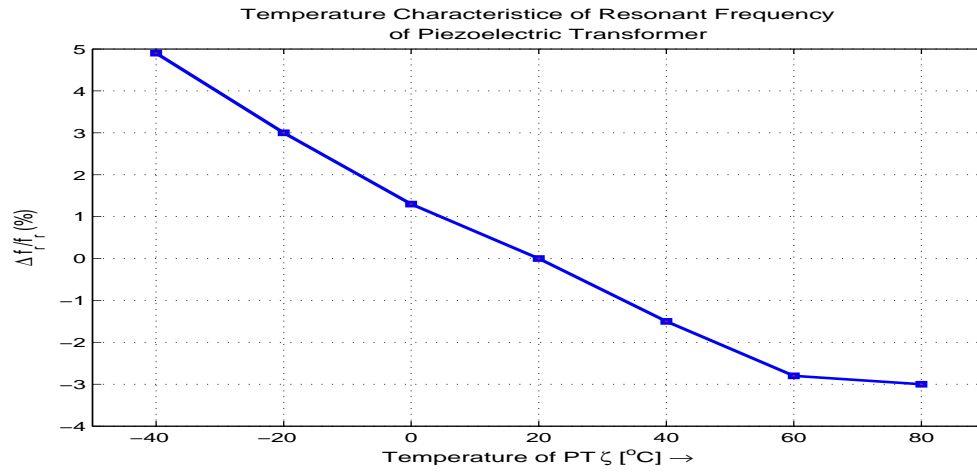
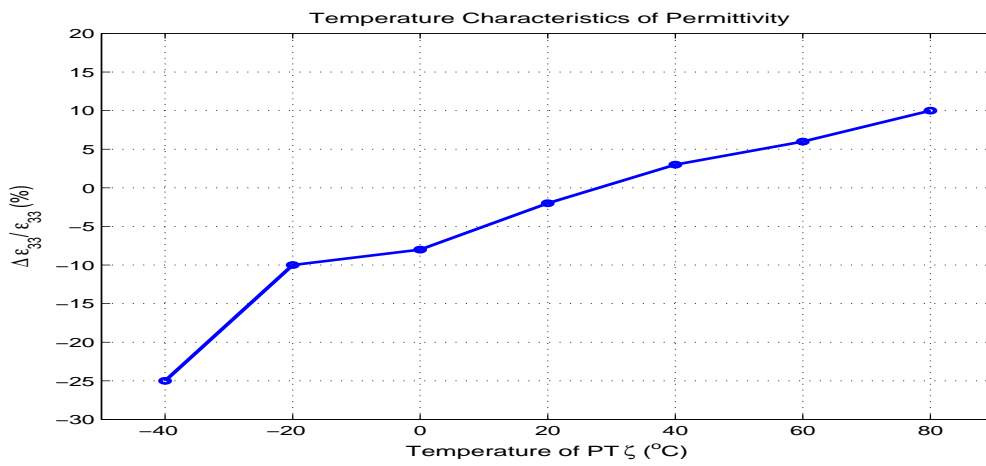
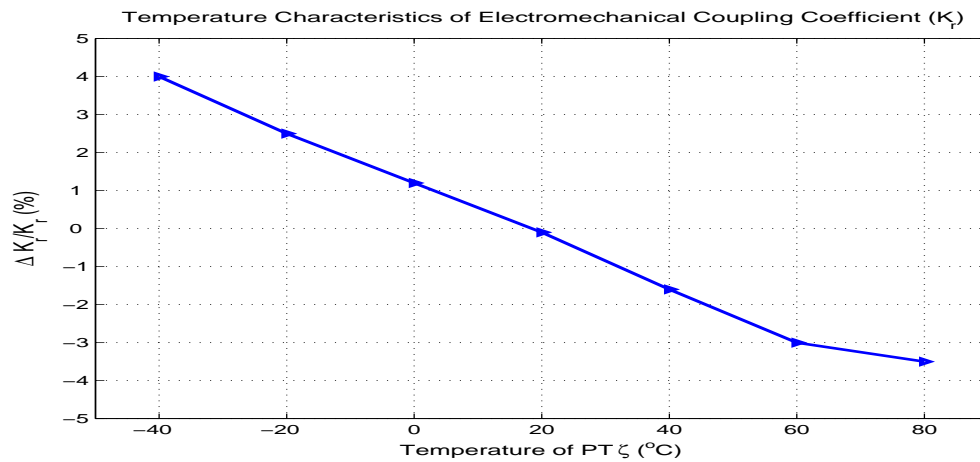
	Morgan Electro Ceramics: PZT	Philips PXE	Copper	Silver	Lead
Heat Conductivity [$W.m^{-1}.K^{-1}$]	1.25	1.2	402	430	34.8
Source	[22]	[93]	Internet	Internet	Internet

Table 3.3: Comparison of heat conductivity of piezoelectric material with others

In order to improve the capability of transferring heat from core to surface of PT, the MLPT⁴ with number of inner metal electrodes was introduced to replace the bulk SLPT⁵ and in comparison with bulk SLPT, the surface temperature of MLPT can be reduced

⁴MLPT: Multi-layers Piezoelectric Transformer

⁵SLPT: Single-layer Piezoelectric Transformer

(a) Temperature characteristics of resonant frequency f_r (b) Temperature characteristics of permittivity ϵ_{33} (c) Temperature characteristics of electromechanical coupling coefficient K_T **Figure 3.3:** Dependencies of piezoelectric material constants on temperature

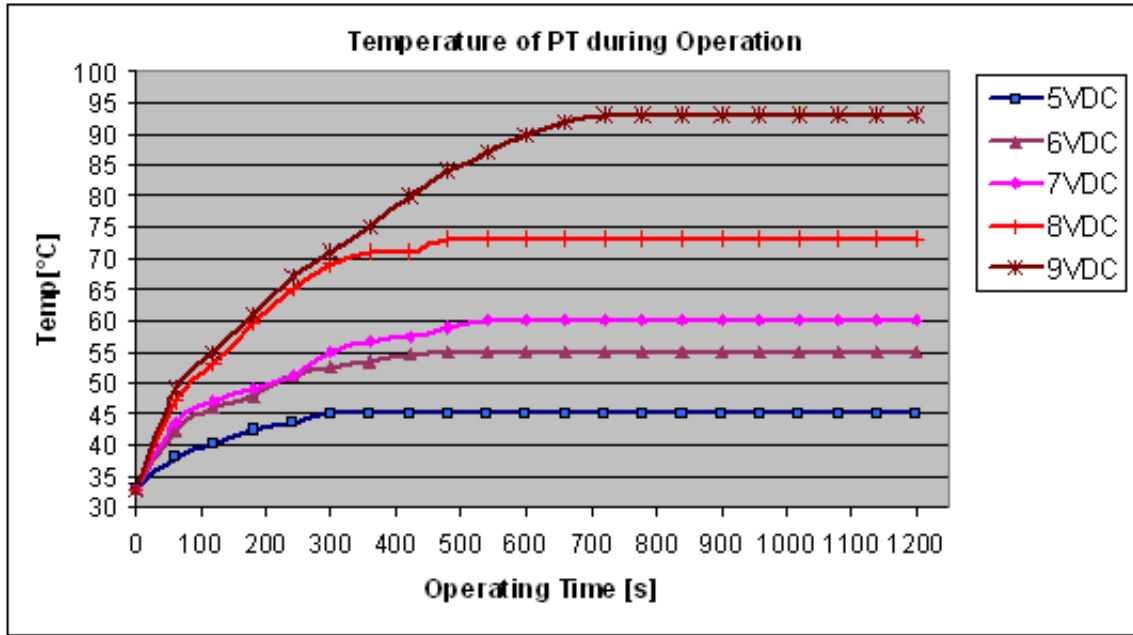


Figure 3.4: Temperature of PT during operation with different input voltage

significantly if the number of layers are more than ten [44]. However, the mechanical quality factor Q_m will be reduced as the number of piezoelectric layers is increased which raises the equivalent resistance [101]. Hence this is an issue which should be taken into consideration while designing PT for every application. The temperature rise of PT affects not only resonant frequency but also two other parameters: permittivity ε and electromechanical coupling coefficient K . The effects of temperature rise on permittivity ε and electromechanical coupling coefficient K of PT#1 are shown in the figure 3.3b and 3.3c, respectively. As illustrated in the figure 3.3b, the permittivity ε of piezoelectric material ε will increase whilst temperature rising. In this case, the permittivity ε of PT#1 will increase 10% as the temperature changes from 20°C to 80°C . In contrast, the rising temperature is the cause of decreasing the electromechanical coupling coefficient K . The relationship between K and temperature ϑ_{PT} of PT#1 is introduced in the figure 3.3c. In this example, the electromechanical coupling coefficient K of PT#1 will decrease 3.5% when its temperature reaches 80°C .

In combination the analysis in previous parts and the equation 3.1, with a given PT and input excitation, the power density of PT is the first order equation of resonant frequency f_r and permittivity ε , and the second-order one of electromechanical coupling K^2 . As temperature rises, the permittivity ε will increase but the resonant frequency f_r and electromechanical coupling K will decrease. In fact, the decreases of these two parameters are larger than the increase of permittivity ε , and hence the power density

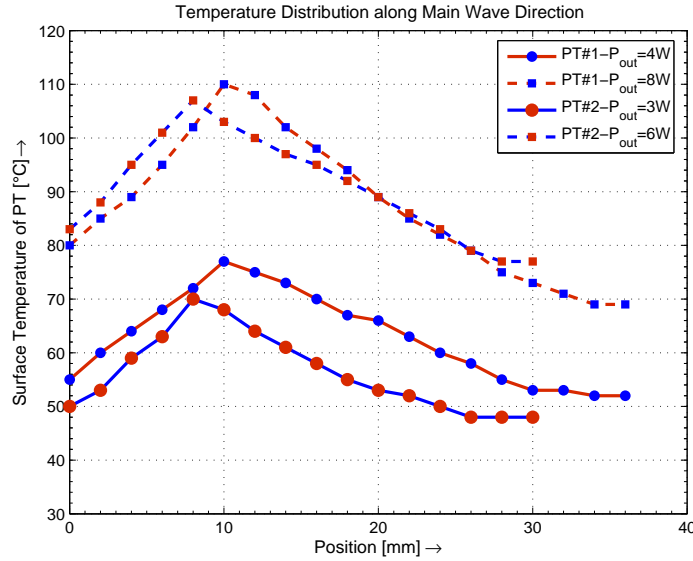


Figure 3.5: Distribution of surface temperature of PT

Point of position 0 indicates the beginning of primary side of PT along the vibration direction

P_D will be reduced. To illustrate this intuitive analysis, the PT#1 will be taken into consideration. The power density of this PT sample will be compared in two cases:

- **Temperature at beginning phase:** In this case, PT#1 operates with the room temperature ($\vartheta_{PT} = 20^\circ C$). Apply the equation 3.1 with the materials parameters at $20^\circ C$ as defined in the figure 3.3, the power density of the PT will be calculated: $P_D^* = 2\pi \cdot f_r^* \cdot \varepsilon_{33}^{T*} \cdot K^{*2} \cdot E^2 \cdot Q_m^*$
- **Temperature at saturation phase:** After being excited with specific vibration mode (λ mode for instance) and given input voltage, temperature of PT reaches saturation point (for this measurement $\vartheta_{PT_{sat}} = 80^\circ C$). The corresponding power density for this case will be defined: $P_D^{**} = 2\pi \cdot f_r^{**} \cdot \varepsilon_{33}^{T^{**}} \cdot K^{**2} \cdot E^2 \cdot Q_m^{**}$

The absolute difference of power density because of temperature rise during operation demonstrated above can be calculated as follows:

$$\Delta P_D = \frac{P_D^{**} - P_D^*}{P_D^*} = -2.8\% \quad (3.3)$$

The example above proves the effect of temperature not only on power density but also on operating characteristics of PT. The combination of this effect with other changes of operating conditions such as the variation of load will be a more complicated process being handled in order to keep output power of PT constant.

3.3 Electromechanical Limitations

In this part, the limitations of PT's material such as maximum electric field strength E_{max} , maximum electric displacement⁶ D_{max} , maximum stress T_{max} and maximum strain S_{max} which effect directly its capability of transferring power to the load will be concentrated. The effect of these limitations on power density of PT can be fully studied through its operating cycle [77]. If a given PT is excited by a signal having frequency equal or close to one of its resonant frequencies, in steady state, it will create a standing wave distributions of large amplitude of stress and displacement along main vibration direction as illustrated in figure 3.6. All the PT samples in the research work are Rosen-type or HVPT [16], following the analysis in [16, 98], the operation of the PT can be described:

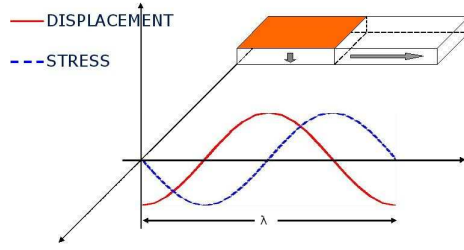


Figure 3.6: Distribution displacement and stress of PT in λ mode

- **At primary side:** At this part, PT operates as an actuator in the transverse mode where an applied electrical field will be converted into strain in the body of PT. For the Rosen-type PT, this transformation is expressed by a one dimension relation following the axes convention in part 2.2 (figure 2.3):

$$\begin{bmatrix} S_1 \\ 0 \\ 0 \end{bmatrix} = \begin{bmatrix} s_{11}^E & s_{12}^E & s_{13}^E \\ s_{12}^E & s_{11}^E & s_{13}^E \\ s_{13}^E & s_{13}^E & s_{33}^E \end{bmatrix} \cdot \begin{bmatrix} T_1 \\ 0 \\ 0 \end{bmatrix} + \begin{bmatrix} 0 & 0 & d_{31} \\ 0 & 0 & d_{31} \\ 0 & 0 & d_{33} \end{bmatrix} \cdot \begin{bmatrix} 0 \\ 0 \\ E_3 \end{bmatrix} \quad (3.4)$$

- **At secondary side:** In contrast, this part operates as a transducer in the longitudinal mode. The vibration is transmitted from primary side resulting in a potential between electrodes of PT's output part, in other words, the energy is converted from mechanical form to electrical form via reverse mechanic-electrical coupling. This process is described by the one dimension equation 3.5 below:

$$\begin{bmatrix} 0 \\ 0 \\ D_3 \end{bmatrix} = \begin{bmatrix} 0 & 0 & 0 \\ 0 & 0 & 0 \\ d_{31} & d_{31} & d_{33} \end{bmatrix} \cdot \begin{bmatrix} 0 \\ 0 \\ T_3 \end{bmatrix} + \begin{bmatrix} \varepsilon_{11}^T & 0 & 0 \\ 0 & \varepsilon_{22}^T & 0 \\ 0 & 0 & \varepsilon_{33}^T \end{bmatrix} \cdot \begin{bmatrix} 0 \\ 0 \\ E_3 \end{bmatrix} \quad (3.5)$$

⁶Electric displacement: In some other literatures is named as surface charge density or electric induction

Finally, the operations of these PT samples are represented by minimizing the equations 3.4 and 3.5, and the results are:

$$S_1 = s_{11}^E \cdot T_1 + d_{31} \cdot E_3 \quad (3.6)$$

$$D_3 = d_{33} \cdot T_3 + \varepsilon_{33}^T \cdot E_3 \quad (3.7)$$

The maximum transferred power of a given PT will be investigated via an operating cycle defined as the period that a standing wave transmitted from the beginning point of the primary side to the end of the secondary side along the main vibration direction. For example, in the λ mode, one cycle of standing wave PT is expressed in the figure 3.6.

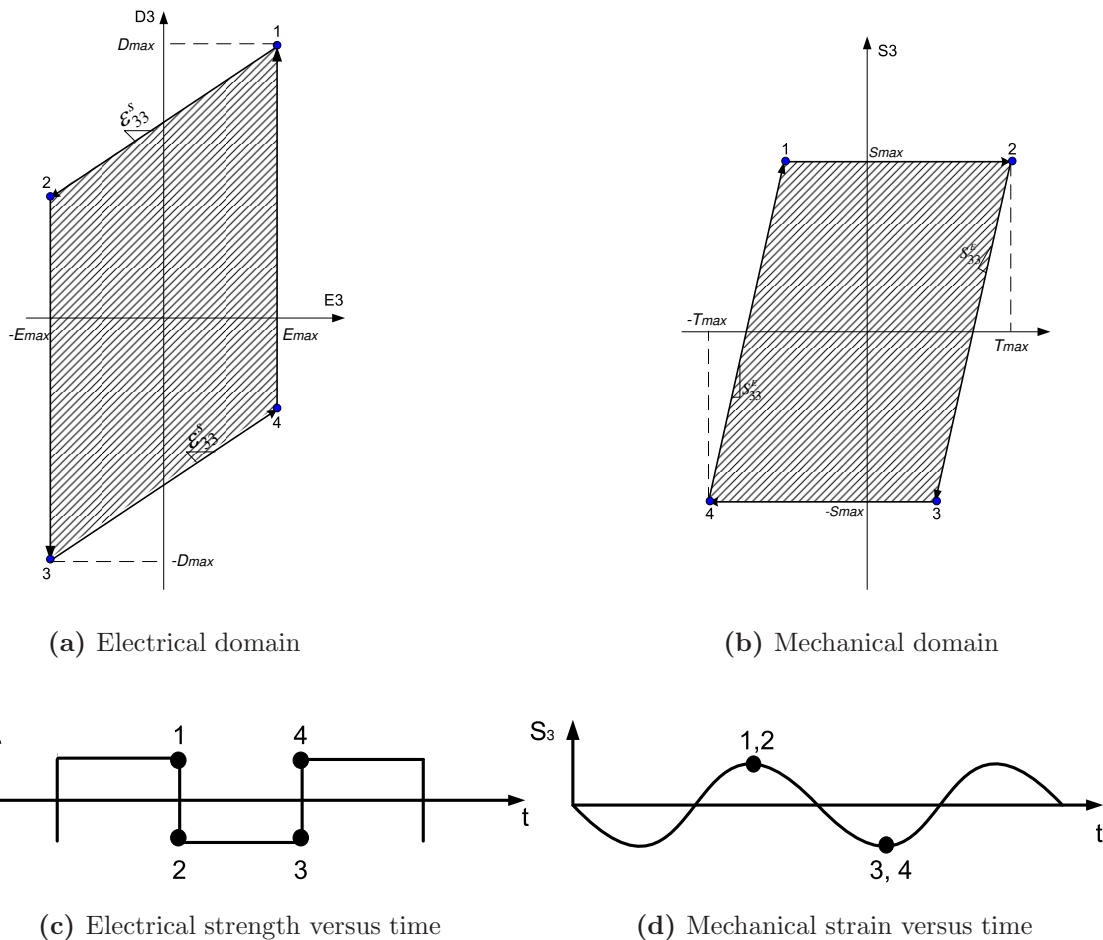


Figure 3.7: Operating cycle of a PT

On the supposition that PT is a lossless device (that means the effect of temperature rise, which is mentioned in the previous part, will be ignored), in one operation cycle, when input of PT is connected to an electrical source has operating frequency close

to one of the resonant frequencies of PT, it will convert the electrical energy of the source into mechanical energy (mechanical vibration). This amount of energy (expressed by mechanical vibration) transmits to the secondary side. In contrast, the vibration creates a polarization at the output part of PT, in another word, the mechanical energy mentioned above is converted back into electrical energy. It informs that during every operating cycle of PT, the energy is transformed by the following means:

Electrical form (source) \Rightarrow Mechanical form \Rightarrow Electrical form (load)

So the transferred energy of a given PT is limited by some important parameters such as maximum electrical strength E_{max} , maximum electric displacement D_{max} , maximum stress T_{max} and maximum strain S_{max} which are determined by quality and the characteristics of piezoelectric ceramics and geometric dimensions of PT [38]. Therefore, the throughput power in each operating cycle must be investigated in both electrical and mechanical domains. The operating cycle of a given PT in the electrical domain and mechanical domain are demonstrated in the figure 3.7.

Symbol	Meaning	Unit	PT#1	PT#2
K_3^T	Relative dielectric constant		1300	1200
ϵ_{33}^T	Dielectric at constant stress	$10^{-8}F/m$	1.15	1.06
d_{33}	Piezoelectric strain coefficient	$10^{-12}m/V$	280	290
c_{33}^E	Elastic modulus at constant E	$10^{10}N/m^2$	7.73	7.0
s_{33}^E	Elastic compliance at constant E	$10^{-12}m^2/N$	12.9	14.3
ρ	Density	$10^3kg/m^3$	8.0	7.9
E_{max}	Maximum electric strength	kV/mm	5.8	2.5
S_{max}	Maximum strain	10^{-3}	1.8	1.5
D_{max}	Maximum electric displacement	C/m^2	0.5	0.4
T_{max}	Maximum stress	$10^7N/m^2$	1.7	1.6

Table 3.4: Material constants of PT samples

In most designs of PT, they have symmetric geometrical form (dimensions of input and output are similar) so the limitation of throughput power in each part is the same. The maximum transferable energy (electrical energy) of the input part is defined by the

hatch area illustrated in figure 3.7a, in this case, the correlative value of charge density D with maximum electrical strength E_{max} is regarded as D_{max} . Hence, the maximum electrical energy $W_{E_{max}}$ can be transferred through the input part is:

$$W_{E_{max}} = 2E_{max}2D_{max} - 2 \left(\frac{1}{2} 2E_{max} 2E_{max} \varepsilon_{33}^s \right) = 4E_{max} (D_{max} - E_{max} \varepsilon_{33}^s) \quad (3.8)$$

In a similar approach, the maximum transferred energy of the output part (mechanical energy) is presented by the area in figure 3.7b, in this case, the correlative value of strain S with maximum stress T_{max} is considered as maximum strain S_{max} . With the analysis, the maximum mechanical energy $W_{M_{max}}$ can be transferred through the output part is:

$$W_{M_{max}} = 2S_{max}2T_{max} - 2 \left(\frac{1}{2} 2S_{max} 2S_{max} / s_{33}^E \right) = 4S_{max} (T_{max} - S_{max} / s_{33}^E) \quad (3.9)$$

By substitution the material constants in table 3.4 into the equation 3.8 and 3.9 confirms that $W_{M_{max}} \ll W_{E_{max}}$, therefore in order to prevent the PT from being broken by over stress, during its operation the total amount of transferred energy should be smaller than $W_{M_{max}}$. From the stress limit T_{max} , the area depicted in the figure 3.7b correlative with transferred power is a function of strain S and this function achieves maximum with optimum value of strain S_{opt} :

$$S_{opt} = \frac{1}{2} (s_{33}^E T_{max}) \quad (3.10)$$

The value of S_{opt} is first calculated by applying the material constant in table 3.4 into 3.10, then compared to the S_{max} , this value is usable if and only if not exceeding the maximum strain. The optimum strain S_{opt} of PT#1 and PT#2 are $10.97 \cdot 10^{-5}$ and $11.44 \cdot 10^{-5}$ respectively. These value are much smaller than their maximum strain value listed in the table 3.4 above. Substitution of 3.10 into 3.9, the maximum energy density of a given PT is:

$$W_{max} = s_{33}^E T_{max}^2 [J/m^3] \quad (3.11)$$

and hence, the maximum power density corresponds to maximum energy density per unit time will be:

$$P_{D_{max}} = \frac{W_{max}}{T} = f s_{33}^E T_{max} [W/m^3] \quad (3.12)$$

where f is operating frequency.

The maximum energy density W_{max} of piezoelectric material of sample PT#1 and PT#2 calculated according to equation 3.11 are $3728.1 [J/m^3]$ and $3660.8 [J/m^3]$ respectively. According to 3.12, the power density P_D also depends on the vibration mode of PT, if the

operating frequency is 100kHz then the power density of sample PT#1 and PT#2 are $372.8 [W/cm^3]$ and $366 [W/cm^3]$ respectively. The results here confirm the high potential of PT in transferring power, of course under the lossless operation. In comparison, the PT in this case can handle an amount of power density much higher than that one the PT can transfer in practise where the thermal limitation is considered, which is addressed in previous section. Last but not least, this approach is applicable not only for the symmetric square-wave excitation generated by class D full-bridge converter but also for asymmetric square-wave signal created by class D amplifier and other types of excitation like sinusoidal or triangular wave form⁷.

3.4 Effect of the Output Rectifier

The DC/DC converter is one of the remarkable potentials of PT in practice, it can be found in various applications such as battery chargers [58], electronics ballast for LED [97, 25], DC power supply [123, 88] and so on... In these applications, a rectifier is interposed between the output of PT and the load, it accompanies with others passive element (capacitor and/or inductor) to form the output matching network [16]. There are several output rectifier topologies, which are shown in the figure 3.8 below, interfacing with the output of PT and their interactions with the PT's throughput power will be studied in this section. The object is to calculate the equivalent load R_{Eq} , for the rectifier stage and load R_L then the matching network can be built to match the equivalent load R_{Eq} to the optimal load as defined by equation 2.20. Among output rectifier topologies represented in the figure 3.8, the voltage doubler [49] and current doubler [123] are most preferred because of simplicity and ease of use. In this part, the operation of PT with voltage doubler and current doubler will be analyzed and compared from a power transferring point of view.

3.4.1 Operation of PT with voltage doubler

As mentioned in previous sections, PTs have some advantages over magnetic transformers. One of the important characteristics is high voltage isolation of material used to manufacture PT. This is especially useful when integrating into high voltage applications [75, 76]. In high voltage applications the output filter seems to be impossible if it contains an inductive element because of the size and weight of the inductor when operating under high voltage condition [49]. The use of a capacitive filter is regarded as

⁷Discussion via email with Prof. Seth Sanders - at EECS - University of California Berkeley

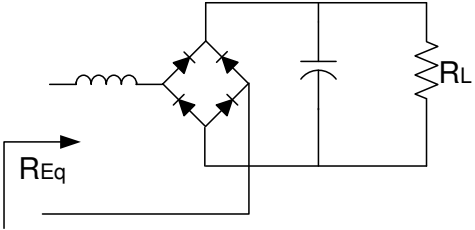
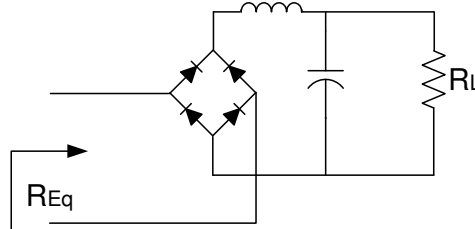
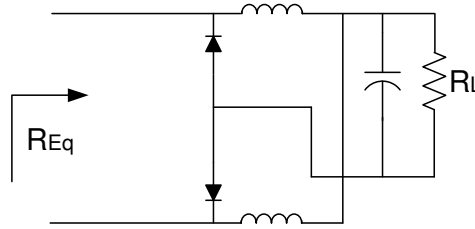
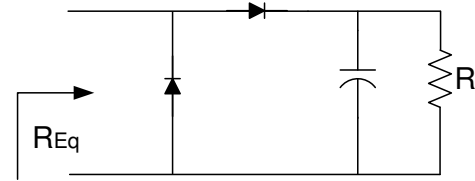
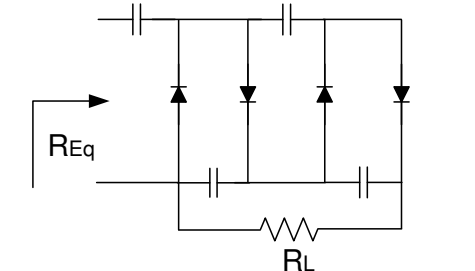
Full-bridge with Voltage Load		$R_{Eq} = \frac{8}{\pi^2} R_L$
Full-bridge with Current Load		$R_{Eq} = \frac{\pi^2}{8} R_L$
Current Doubler		$R_{Eq} = \frac{\pi^2}{2} R_L$
Voltage Doubler		$R_{Eq} = \frac{2}{\pi^2} R_L$
Voltage Multiplier		$R_{Eq} = \frac{1}{32} R_L$

Figure 3.8: Several output rectifier stage and their relations of load

a practical alternative in high voltage - low current applications. The target of a high voltage PT based converter is generating a high output voltage and the voltage doubler is the best choice.

The simplest voltage doubler with output filter is created by the combination of two diodes and one high voltage capacitor. The operational analysis and modeling of the voltage doubler fed by a PT was introduced in the [49]. This part investigates only the effect of this rectifier topology on PT's capability of transferring power to the load. With the purpose of creating a relatively high output voltage, the output of PT is always connected with a high load. Normally the load should be: $R_L \geq R_{opt}$ with R_{opt} defined in equation 2.20 leading to PT operating with a high electrical quality factor Q [51]. Because of this reason, the output current is a sinusoidal wave form. So every operation cycle of a voltage doubler fed by PT can be separated into two periods:

- Positive half cycle $i_o > 0$
- Negative half cycle $i_o < 0$

and they are depicted in the figure 3.9. In the figure 3.9b and 3.9c, two diodes D_1 and D_2 in the figure 3.9a are replaced by the large signal model represented by a battery in series with a resistance. With the analysis before, the input current of the voltage doubler can be written as:

$$i_o = I_{om} \sin \omega t \quad (3.13)$$

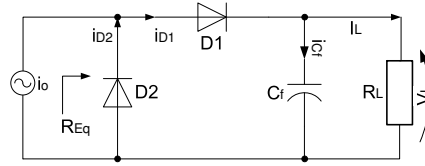
where I_{om} is the amplitude of i_o , then the current through the diode D_1 is:

$$i_{D1} = \begin{cases} I_{om} \sin \omega t, & \text{for } 0 < \omega t \leq \pi \\ 0, & \text{for } \pi < \omega t \leq 2\pi, \end{cases} \quad (3.14)$$

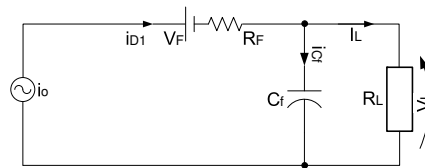
so the DC current on load can be calculated as follows:

$$I_L = \frac{1}{2\pi} \int_0^{2\pi} i_{D1} d(\omega t) = \frac{I_{om}}{2\pi} \int_0^{\pi} d(\omega t) = \frac{I_{om}}{\pi} \quad (3.15)$$

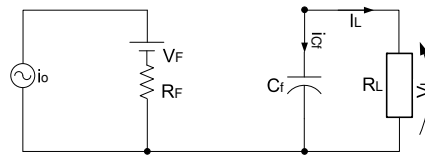
Equation 3.15 shows that the DC current on load I_L is directly proportional to the amplitude of PT's output current I_{om} , the relation between AC and DC current can be



(a) Circuit of voltage doubler fed by a current source



(b) When $i_o > 0$



(c) When $i_o < 0$

Figure 3.9: Voltage doubler fed by PT

expressed by the current transfer factor K_I which is introduced in the equation 3.16:

$$K_I = \frac{I_L}{I_{orms}} = \frac{\sqrt{2}I_L}{I_{om}} = \frac{\sqrt{2}}{\pi} \simeq 0.45 \quad (3.16)$$

Since the output current of PT is sinusoidal, so the input power of voltage doubler is equal to the power of the fundamental component. Hence, on the one hand, the output power of PT is:

$$P_o = \frac{I_{om}^2 R_{Eq}^{VD}}{2} = \frac{\pi^2 I_o^2 R_{Eq}^{VD}}{2} \quad (3.17)$$

where R_{Eq}^{VD} is the equivalent load looked from the output of PT. On the other hand, the DC power on the load can be expressed as:

$$P_L = I_L^2 R_L \quad (3.18)$$

With the assumption that the rectifier is a loss-less system or in other words, the output power of PT will be transferred and dissipated completely on the load, then:

$$P_o = P_L \quad (3.19)$$

substitution of equation 3.17 and 3.18 into equation 3.19, the equivalent resistance will be:

$$\frac{\pi^2 I_o^2 R_{Eq}^{VD}}{2} = I_o^2 R_L \Rightarrow R_{Eq}^{VD} = \frac{2}{\pi^2} R_L \quad (3.20)$$

The equation 3.20 addresses that, the voltage doubler can be regarded as a load expansion device with the step up ratio is $\pi^2/2$.

3.4.2 Operation of PT with current doubler

In contrast with the rectifier introduced in the §3.4.1, a current doubler is a full wave rectifier circuit created by the combination of two diodes and two inductors as shown in figure 3.10a. Because of the interaction of the inductors L_f , the input source of the rectifier is regarded as a voltage source with sinusoidal wave form and defined as follows:

$$u_o = U_{om} \sin \omega t \quad (3.21)$$

where U_{om} is the amplitude of u_o . The operation of current doubler is divided into two periods:

- Positive half cycle $u_o > 0$

- Negative half cycle $u_o < 0$

During the positive half cycle of u_o , the output current i_o of PT flows through L_{f1} and supplies power to the load as shown in the figure 3.10b and the energy stored at L_{f2} is also released to the load simultaneously. In turn, in the negative half cycle, shown in the figure 3.10c, the output current i_o of PT supplies power to the load via L_{f2} at the same time L_{f1} releases its stored energy on load. As a result, the amplitude of output current I_o of the PT is $I_L/2$, where I_L is the DC current on the load.

With the assumption that all elements are ideal and current doubler is lossless system, the voltage at the output of rectifier v_{AB} can be written as:

$$v_{AB} = \begin{cases} U_{om} \sin \omega t, & \text{for } 0 < \omega t \leq \pi \\ 0, & \text{for } \pi < \omega t \leq 2\pi, \end{cases} \quad (3.22)$$

Because the average voltage on the filter inductor is zero, so the DC voltage on the load is the same as the average value of v_{AB} , which is defined:

$$\begin{aligned} V_L &= \frac{1}{2\pi} \int_0^{2\pi} v_{AB} d(\omega t) \\ &= \frac{1}{2\pi} \int_0^{\pi} V_{om} d(\omega t) = \frac{V_{om}}{\pi} \end{aligned} \quad (3.23)$$

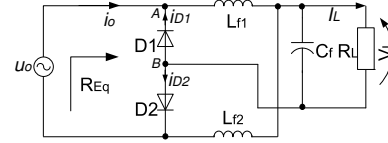
Equation 3.23 shows that the DC voltage on the load is directly proportional to the amplitude of the output voltage of PT V_{om} . Consequently, the voltage on the load V_L can be regulated by controlling the input voltage of PT (PWM method [118, 56]) or shifting the operating frequency of the PT [53, 87].

The output current of PT fed to the rectifier is a square wave and given by:

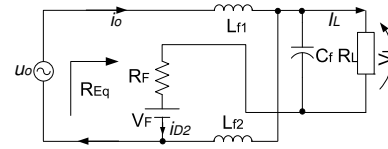
$$i_o = \begin{cases} I_L/2, & \text{for } 0 < \omega t \leq \pi \\ -I_L/2, & \text{for } \pi < \omega t \leq 2\pi, \end{cases} \quad (3.24)$$

The wave form of i_o exhibits an odd function with respect to ωt , so $i_o(-\omega t) = -i_o(\omega t)$. With this analysis, the amplitude of the fundamental of PT's output current i_o is calculated as:

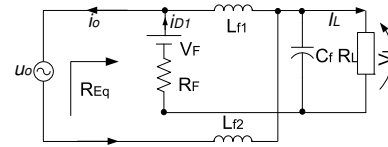
$$I_{o1m} = \frac{2}{\pi} \int_0^{\pi} i_o \sin \omega t d(\omega t) = \frac{I_L}{\pi} \int_0^{\pi} \sin \omega t d(\omega t) = \frac{2I_L}{\pi} \quad (3.25)$$



(a) Circuit of current doubler fed by a voltage source



(b) When $u_o > 0$



(c) When $u_o < 0$

Figure 3.10: Current doubler fed by PT

Because the output voltage of PT is sinusoidal form, on one hand, the PT's output power contains only the power of the fundamental component:

$$P_o = I_{o1}^2 R_{Eq}^{CD} = \frac{I_{o1}^2}{2} R_{Eq}^{CD} = \frac{2I_L^2}{\pi^2} R_{Eq}^{CD} \quad (3.26)$$

where I_{o1} is the average value of the fundamental of PT's output current and R_{Eq}^{CD} is the equivalent resistance viewed from output of PT. On the other hand, the power that dissipated on the load R_L is determined in equation 3.18. With the assumption before, the losses on the elements of the rectifier are ignored, so the relation of output power of PT P_o and dissipated power on the load P_L is introduced in equation 3.19. Substituting equations 3.18 and 3.26 into 3.19, the equivalent resistance can be found as follows:

$$P_o = \frac{2I_L^2}{\pi^2} R_{Eq}^{CD} = P_L = I_L^2 R_L \Rightarrow R_{Eq}^{CD} = \frac{\pi^2}{2} R_L \quad (3.27)$$

Derivation from equation 3.27, the current doubler operates like a load "compressor" with the ratio $2/\pi^2$. For instance, if the PT is driven at the high efficiency area, and the load is determined by equation 2.20, with the current doubler, in fact, the load should be chosen: $R_L = (2/\pi^2)R_{opt}$.

3.4.3 Voltage doubler and current doubler in comparison

In sections (3.4.1) and (3.4.2), two common rectifier topologies and their functionalities for PT were studied. In this part, their effects on the PT's capability of transferring power while load is changing will be investigated and compared. The typical operational wave forms of voltage doubler and current doubler are introduced in figures 3.11a and 3.11b respectively where θ is the conducting angle of the diode of the voltage doubler and ν is the conducting angle of the diode of the current doubler.

In order to simplify the calculation and analysis on the effect of these rectifiers on the throughput power of PT, some following normalized parameters [48, 49, 51] will be defined based on parameters of PT's equivalent circuit:

- Normalized load factor K_{PT} :

$$K_{PT} = R_L/n^2 R_m \quad (3.28)$$

- Normalized PT factor A_{PT} :

$$A_{PT} = \omega_r C_o n^2 R_m \quad (3.29)$$

- Mechanical quality factor of PT Q_m : which is defined in the equation 2.14

Through the equivalent circuit, from an electrical point of view, PT operates as a band-pass filter and the output voltage contains high harmonic components. Thanks to the high quality factor of the resonant circuit (L_r - C_r) the transferred power on the load is only affected by the first harmonic component. Because of this reason, both rectifiers will be examined under the first harmonic approximation.

In both cases, the output capacitor C_o and filter capacitor C_f are combined and considered as output equivalent capacitor C_{Eq} . The DC load R_L is also converted by the rectifier conversion factor as specified in the equation 3.20 and 3.27. Consequently, PT will transfer power to parallel network: $C_{Eq} - R_{Eq}$.

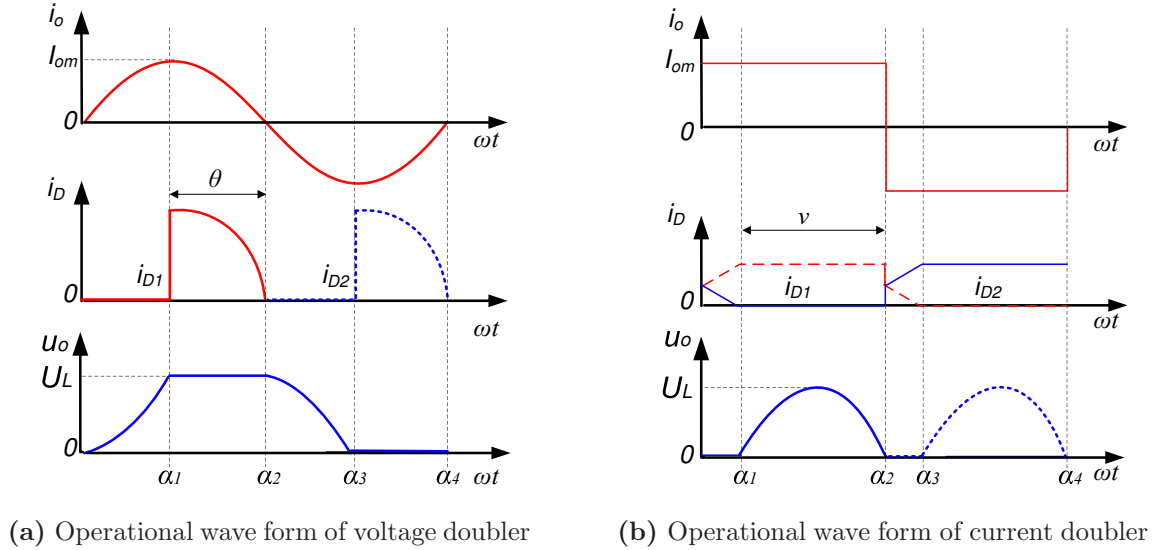


Figure 3.11: Operational wave form of voltage and current doubler

If all the losses of the rectifier's elements are ignored, the power dissipated on the DC load R_L will be directly specified:

$$P_L = \frac{V_L^2}{R_L} = \frac{V_{om}^2}{2R_{Eq}} \quad (3.30)$$

where V_{om} is the amplitude of the PT'S output voltage, and the equivalent capacitor C_{Eq} is:

$$C_{Eq} = \frac{\tan|\varphi|}{\omega R_{Eq}} \quad (3.31)$$

where φ is the phase angle between the output voltage $v_o(t)$ and output current $i_o(t)$ while PT is applied with the equivalent parallel network $C_{Eq} - R_{Eq}$ [49, 50].

After that, the parallel network $R_{Eq}||C_{Eq}$ is reflected to the primary side following the calculation in previous part (part 2.3), the new parallel network with $R'_{Eq}||C'_{Eq}$ and $C'_{Eq} = C_{Eq} \cdot n^2$; $R'_{Eq} = R_{Eq}/n^2$. This parallel network is then converted into a serial network $R''_{Eq} - C''_{Eq}$ and the parameters of serial network are defined by:

$$\begin{cases} R''_{Eq} = R'_{Eq} \cos^2 \varphi \\ C''_{Eq} = C'_{Eq} / \sin^2 \varphi \end{cases} \quad (3.32)$$

By applying the equations 2.15 to 2.18 in the part 2.3.2 to determine the ratio of output power P_o to the dissipated power on the PT P_{PD} for both VD and CD:

$$\Delta_{PT} = \frac{P_o}{P_{PD}} = \frac{P_o}{P_{in} - P_o} = \frac{\eta_{PT}}{1 - \eta_{PT}} \quad (3.33)$$

Using equation 2.18 for this case, the PT's efficiency η_{PT} is:

$$\eta_{PT} = \frac{R''_{Eq}}{R''_{Eq} + R_m} = \frac{K_{PT} R_{Eq} \cos \varphi}{K_{PT} R_{Eq} \cos \varphi + R_L} \quad (3.34)$$

substituting the equation 3.34 into equation 3.33, finally, the ratio of output power P_o and power dissipated on PT P_{PD} is:

$$\Delta_{PT} = \frac{R_{Eq}}{R_L} K_{PT} \cos \varphi \quad (3.35)$$

This ratio is depicted in the figure 3.12 above. The Δ_{PT} presents the PT's capability of transferring power to the load with two different output rectifiers. This result can be applied in choosing the model of the output rectifier for specific DC/DC applications. The voltage doubler offers the high output voltage (because of having large voltage step up ratio) and it is suitable for applications needing high load. In contrast, the current doubler is preferred in the applications demanding a high level of current (because of having a large current step up ratio) and low load.

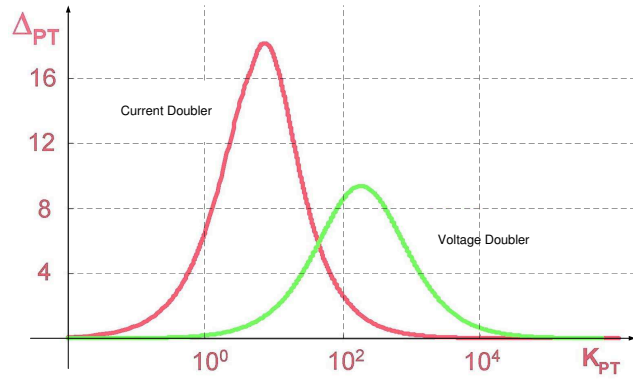


Figure 3.12: Comparison of power handling of PT with current and voltage doubler

3.5 Summary and Discussion

The contents of this chapter concentrated on the fundamental causes that effect the PT's capability of transferring power to the load. This is expressed by the term: **power**

density P_D which is defined by the ratio between the amount of transferred power per volume unit. Obviously, with a specific PT, the higher the power density P_D it is, the higher the output power it gets. From materials and electrical points of view, there are three main causes affecting power density P_D of a PT: Effect of temperature rise, electromechanical limits and the circuit topology especially in the output rectifier.

The equation 3.1 expresses that power density P_D is dependent on both material properties $\varepsilon; K; Q_m$ and electrical parameters ($f_r; E$). During operation, the PT'S losses will be converted into heat and make the temperature increase. If the losses are too large this will lead to the PT overheating, and it's body temperature will reach Curie point, consequently the piezoelectric effect is no longer valid because of depolarization. In other words, the PT is completely damaged. In fact, the depolarization appears when the temperature of PT exceeds half the Curie point and more and more serious if temperature does not stop increasing. In practice, the Curie point of PT varies from $280^{\circ C}$ to $330^{\circ C}$ so the safety temperature range for PT is from room temperature to $120^{\circ C}$. The experimental results implemented on some different PT samples in this chapter confirm that, the increasing temperature of PT during the operation makes the PT's material quality and operation parameter f_r decrease and the temperature of PT in operation depends on input voltage, vibration mode, and environment temperature also. Hence, the proposals to reduce the temperature rise of PT should be focused on.

Next, the second major limitation to the power density P_D of PT is taken into consideration: electromechanical limitation. The operation of PT is studied based on the piezoelectric linear equations and the transferred energy is supervised via electro-mechanical conversion in one operating cycle. The critical transferred energy is determined by either maximum mechanical energy (regarded as mechanical domain) or electrical energy (regarded as electrical domain) expressed by the coupling parameters: $S_{max} - T_{max}$ and $E_{max} - D_{max}$ respectively. The calculation results based on the material parameters of the PT samples inform that the maximum transferred energy on the electrical domain is much larger than that one on the mechanical domain. Hence, to guarantee the safety conditions for PT's operation, the transferred energy must be smaller than the maximum mechanical energy otherwise the PT will be broken down because of over stress. After that, the maximum power density P_D will be investigated on the $S - T$ domain under the lossless assumption. To optimize the transferred energy in the mechanical domain, the second order function of the strain S with critical stress T_{max} is assumed, and maximum is achieved at optimum value of strain S_{opt} . Derivation from the result of maximum transferred energy, the maximum power density P_{Dmax} is calculated as a

function of operation frequency and material parameters. The maximum power density P_{Dmax} from material constants of two PT samples provides the evidence to prove the high power density of PT (more than $300W/cm^3$). However, when being applied into a specific application, the temperature rise within PT must be taken into consideration and the power density P_D is in the range $20W/cm^3$ more or less. The experiment results showed the high potential to ameliorate the throughput power of PT significant if there are some effective methods to cool down PT during operation.

Finally, the effect of the output rectifier to output power of PT was studied. The interaction of output rectifier and PT in the load variation condition is investigated via two typical rectifiers: Voltage doubler and current doubler. In the PT based DC/DC converter, the combination of an output rectifier with passive elements forms the impedance matching - a important part to guarantee high efficiency, hence the high output power. The output rectifier itself can be regarded as a load conditioner expressed by a rectifier factor. This factor is changing from such topology to such topology. When operating with PT, voltage doubler behaves like a load extender and it should be used in applications requiring high load, high voltage and low current, the rectifier factor of voltage doubler is $\pi^2/2$. In contrast, the current doubler operates as a load compressor and it is preferred in applications with light load, low voltage and high current. The comparison of transferred power/dissipated power ratio of voltage doubler and current doubler was also implemented and the results show that the transferred power/dissipated power ratio of current doubler in the low load area is higher than that one of voltage doubler in the high load area.

Derivation from the analysis and calculations in this chapter, some conclusions are established:

- A frequency closed loop as a major controller should be used in the PT based applications not only to saturate the variation of load but also to overcome or diminish the shift of resonant frequency because of temperature rise.
- The power density P_D of PT will be much higher if PT's heat is scattered as fast as possible by new PT design (like increasing the number of layer) or obligatory cooling methods.
- In DC/DC applications, the output rectifier should be chosen based on the requirements of load dimension, voltage and current level...
- Consideration for the amplifier topology, control and operation mode to minimize the losses and temperature rising

Chapter 4

Converter Topologies and Control Considerations

4.1 Introduction

From a power electronics point of view, a typical power converter functions as a part in the system to increase the amplitude of a signal to a higher power level. In this chapter, some typical converter topologies, which are very popular for applicability of PT in power electronics area, will be taken into consideration. PT can be applied in either DC/AC with sinusoidal waveform at output or DC/DC with power rectifier interposed between PT's output and load.

This chapter will concentrate on all the possible interactions between PT and converter topologies then the comparisons will be performed. In this chapter, three PT samples with their equivalent parameters as studied in the previous chapters will be chosen for simulation then verified by experiments and measurement results. In the simulation results, all PT samples are driven with fixed frequency signal close to one of the resonant frequencies corresponding to a specific vibration mode. In the experimental results, all PT samples will be excited with a variable frequency in order to eliminate or minimize the effects that are mentioned in chapter three.

Because PTs are regarded as low power, low cost, and high efficiency devices, the targets of the converter circuit design for PT in applications are simple structure, minimum number of passive elements, and switches. Two common converter topologies for PT are:

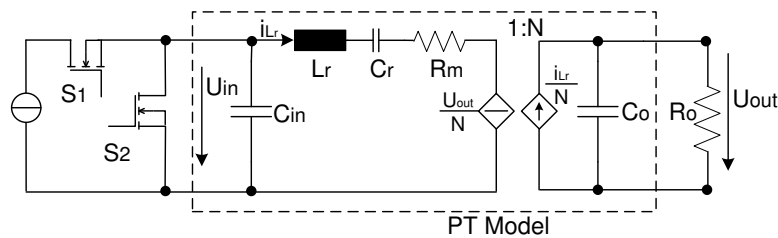
- Class D Converter
- Class E Single Ended Converter

In order to increase the efficiency of PT based applications, the converter will be designed and driven to achieve either ZCS¹ or ZVS² operating-condition, but in fact ZVS is preferred and widely used [12, 40, 56, 67, 122]. In the experiments, all the PT samples are operated in a specific vibration mode ($\lambda/2$ or λ mode) with corresponding optimized load determined in equation 2.20.

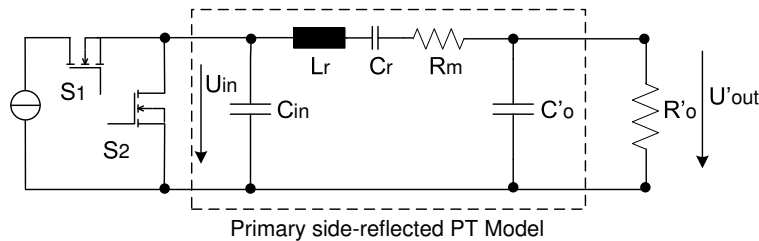
4.2 Class D Resonant Converter using PT

4.2.1 Operational Principle of Class D Converter

The class D converter is regarded as square wave source and composed of two bidirectional two quadrant switches driven in a way that they are switched ON and OFF alternatively. The class D converter with equivalent circuit and primary side reflected circuit of PT are represented in figure 4.1a and figure 4.1b respectively.



(a) PT based class D converter circuit diagram



(b) PT based class D converter with primary side reflected equivalent circuit

Figure 4.1: PT based class D converter

It is much easier for analysis and simulation with the PT's model as illustrated in

¹ZCS: Zero Current Switching

²ZVS: Zero Voltage Switching

figure 4.1b. In this case, the primary side reflected equivalent circuit of PT functions as a series-parallel resonant tank and the whole system becomes a class D series-parallel resonant converter [73] with its key waveforms are shown in figure 4.2 below. In figure

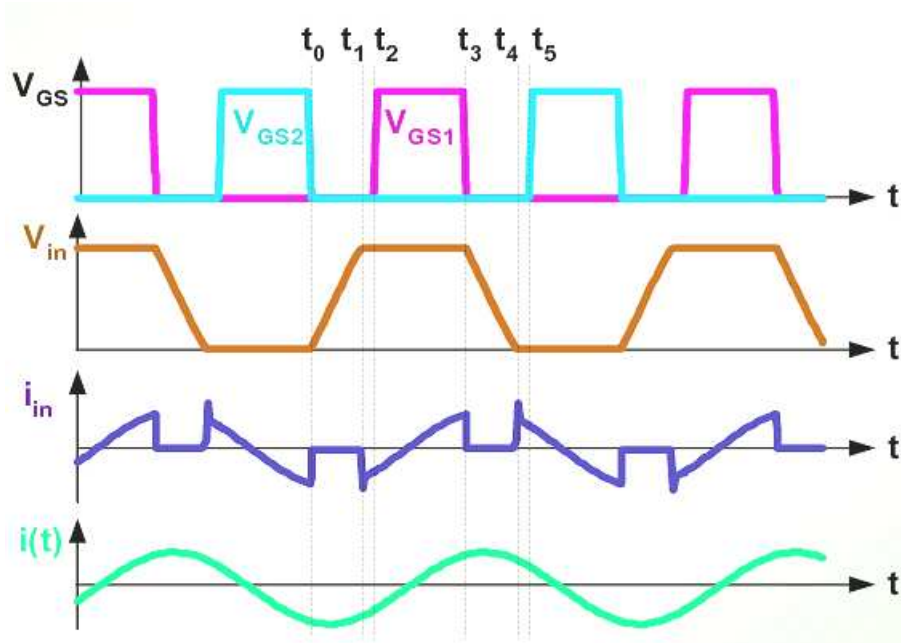


Figure 4.2: The key waveforms of PT based class D converter

4.2 above, V_{GS1} , V_{GS2} , V_{in} , i_{in} and $i(t)$ are the gate signal of the switches S_1 and S_2 , PT's input voltage, input current and resonant current flowing through PT respectively. The operating cycle of this topology for PT is divided into following periods:

- $t_o - t_1$: C_{in} charging time
- $t_o - t_2$: dead time
- $t_2 - t_3$: S_1 ON
- $t_3 - t_4$: C_{in} discharging time
- $t_3 - t_5$: dead time

With assumption that the parameters of PT's equivalent circuit as depicted in figure 4.1b are suitable (this assumption will be verified in the experiment in the next parts) to guarantee the high quality factor Q of the network leading to the sinusoidal wave form of the current flowing through the resonant branch ($L_r - C_r - R_m$). This current is expressed in figure 4.2 and written in equation 4.1:

$$i(t) = I_m \sin(\omega t - \psi) \quad (4.1)$$

where I_m and ψ are amplitude and initial phase of the resonant current $i(t)$ respectively. After the $S - 2$ is switched OFF at t_o , this current is reversed from S_2 to the input capacitor C_{in} and the input capacitor C_{in} is charged by with period $t_o - t_1$, hence the charging current for C_{in} in this period is:

$$i_C(t) = -i(t) = -I_m \sin(\omega t - \psi) \quad (4.2)$$

and the input voltage v_{in} on the C_{in} (across S_2 also) is increasing until reaching DC bus voltage at t_1 , immediately the anti-paralleled diode of S_1 starts to conduct leading to the voltage across S_1 to go to zero. The anti-paralleled diode of S_1 conducts in the interval $t_1 - t_2$. At t_2 , the input voltage v_{in} is equal to V_{DC} and S_1 is switched ON during period $t_2 - t_3$ then it is turned OFF at t_3 . Within interval $t_3 - t_4$, both switches S_1 and S_2 still remain OFF, so the input capacitor is discharged by resonant current. Consequently, the input voltage v_{in} or V_{DS2} decreases leading to V_{DS1} increases. When the input voltage v_{in} reaches to zero at t_4 as soon as the anti-paralleled diode of S_2 starts to conduct causing the voltage across S_2 to go to zero. The charge/discharge processes of the input capacitor take place one after another and repeatedly to ensure the converter operates under ZVS condition - an important operating mode to improve the efficiency of the converter [12, 66].

4.2.2 Inductor-less Class D PT Converter

In this section the operation of PT with a class D amplifier without input impedance matching is analyzed, and simulated based on parameters of the equivalent circuit. The operation of the system is then calculated to satisfy the ZVS operation in order to minimize the losses and EMI³ suppression hence improve the capability of transferring power of PT.

The simulation of PT based inductor-less class D converter with the equivalent circuit's parameters taken from the Appendix B are shown in the table 4.1 and all PT samples in the research work are operated in full-wave vibration mode with resonant frequency around 100kHz. As mentioned before, the equivalent circuit of PT is replaced by a serial-parallel resonant network and within an overall load range ($R_L = 0 \rightarrow \infty$: output is short and open circuit, respectively) the network performs like an inductive load which was improved in [73] and confirmed in Appendix B (admittance circle of PT). In consequence, in order to operate PT based class D converter under ZVS mode, the operating frequency must be slightly larger than the series resonant frequency of PT [13, 82].

³EMI: Electromagnetic interference

PT Sample	C_{in}	L_r	C_r	R_m	N	C_o
PT#1	230nF	0.41mH	6.7nF	0.22 Ω	107	20pF
PT#2	96nF	0.6mH	3.4nF	0.55 Ω	37	22pF
PT#3	55.56nF	0.52mH	3.0nF	1 Ω	70	14.8pF

Table 4.1: The parameters of PT's equivalent circuit in λ vibration mode

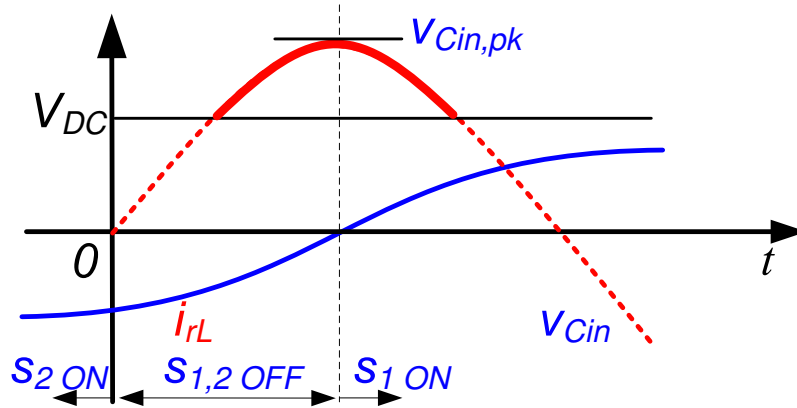
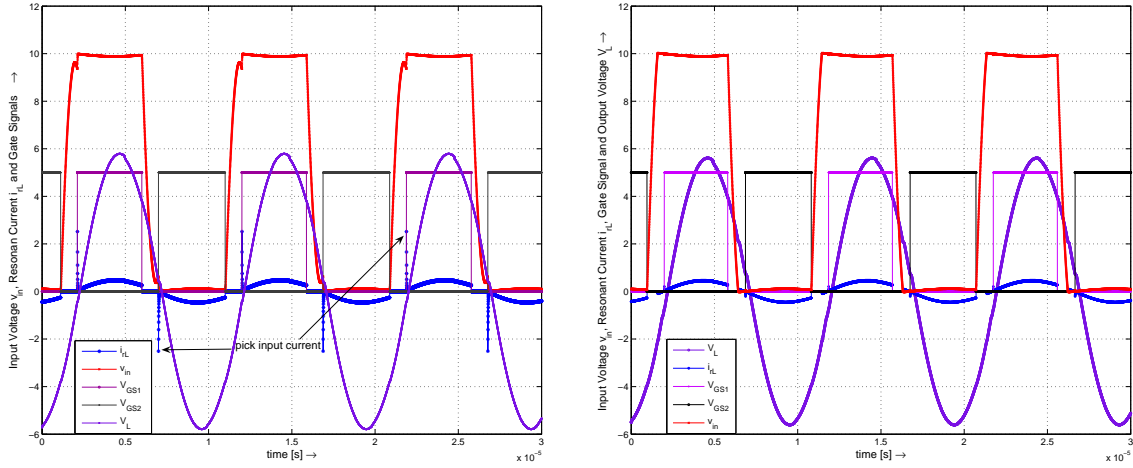


Figure 4.3: Phase relation between resonant current i_{rL} and input voltage V_{Cin}

To guarantee the ZVS operation of PT based class D converter, following two conditions must be satisfied [12, 66]:

- Threshold voltage of input capacitor C_{in} : When the inductor L_r charges the input capacitor C_{in} , as shown in Figure 4.3, the electric charge of input capacitor C_{in} , charged/discharged by the resonant current i_{rL} can be expressed as: $dQ = C_{in}dV = i_{rL}dt$ where: dV is the voltage difference of the input capacitor C_{in} and dt is the charged/discharged time duration. In order to achieve the ZVS condition, the pick value of the input capacitor voltage V_{Cin} must be: $V_{Cin,pk} \geq V_{DC}$ [13] and for every operating cycle of the converter, the input capacitor C_{in} must be charged/discharged completely.
- Critical dead time between S_1 and S_2 : In order to provide the sufficient time for inductor L_r charge/discharge the input capacitor C_{in} , the dead time t_d between S_1 and S_2 should be equal or greater than the charge/discharge time, in this case, the input capacitor C_{in} operates as a turn-off snubber for S_1 and S_2 . In order to

operate the class D converter under the ZVS condition, the dead time t_d must be: $t_d \geq \frac{1}{4}T$ [12, 66] where T is the operating cycle ($T = 1/f$)



(a) PT based class D converter operating under f_r (b) PT based class D converter operating above f_r .

Figure 4.4: Simulation of class D converter with PT#1

Following the strategy analyzed above, the operation of a PT based inductor-less class D converter was studied firstly with a simulation model by using Matlab-Simulink with embedded PLECS. The simulation was implemented based on parameters of an equivalent circuit of PT#1 operating in full wave vibration mode. During simulation, the operating frequency was varied around the resonant frequency of PT and the duty cycle D is kept below 40% as addressed in the second critical of dead-time above.

The simulation results are shown in figure 4.4 with two different operating frequencies. In the first case, the class D amplifier was driven by signal smaller than the resonant frequency of PT#1, the operation of the converter is presented in figure 4.4a: the red and blue line are PT's input voltage and current, respectively, the violet line is the output voltage, the black and pink lines are the gate signal of S_1 and S_2 . Figure 4.4a shows that the input current contains a high peak element at the point when S_1 and S_2 switch ON. The high peak current will increase the losses in both: commutation loss of switches and electromechanical loss of PT leading to higher temperature rise.

In the second case, the excitation frequency of the class D converter was increased slightly above the resonant frequency, the simulation result is introduced in figure 4.4b. In this case, the peak element of input current is much smaller than that one of the first case. This will minimize the commutation and electromechanical losses. Thanks to this,

the throughput power of PT can be increased by raising the DC bus voltage.

The simulation model of PT based class D converter is then verified by experiments. The measurements are carried out with PT#1, optimum load and frequency adjustable gate signal for S_1 , S_2 which are power MOSFET. The experimental result is depicted in figure 4.5: In the measurement result above, the yellow line is input voltage of PT,

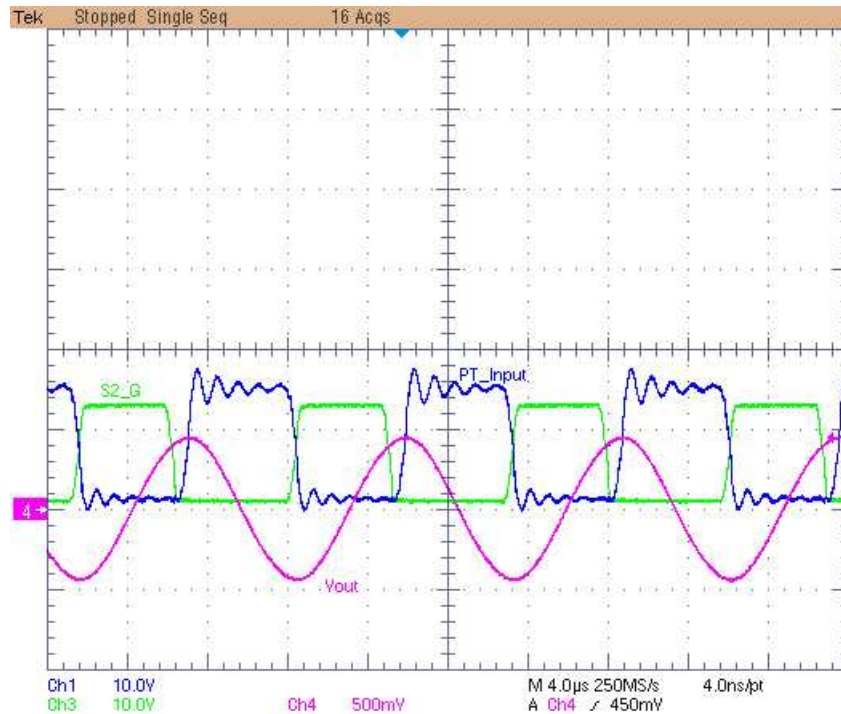


Figure 4.5: Inductor-less PT based class D converter

the pink line is the gate signal of low side MOSFET and the green line is the voltage on the load (PT's output) measured via a high voltage probe with scale 1:1000. From measurement result, it informs that the input voltage of PT still contains high harmonic components which will increase the losses of the PT, hence increase the temperature. The operating temperature of inductor-less PT based class D converter with different input voltage is shown in figure 4.6. In the experiment depicted in figure 4.5, the load was chosen equal to the optimal load corresponded with the full wave vibration (λ mode $R_L \simeq 70k\Omega$). Because the pulse width of gate signals are kept constant (in this case $D = 40\%$), the transferred power to the load depends on the level of DC bus voltage V_{DCbus} and expressed as P_L/V_{DCbus}^2 . The maximum power in this case is the amount of power dissipated on load corresponding with V_{DCbus} which ensures the PT's temperature does not exceed the critical value (normally, this value is $120^\circ C$). From the temperature measurement in figure 4.6, the maximum DC bus can be estimated as $V_{DCbus} = 10V$,

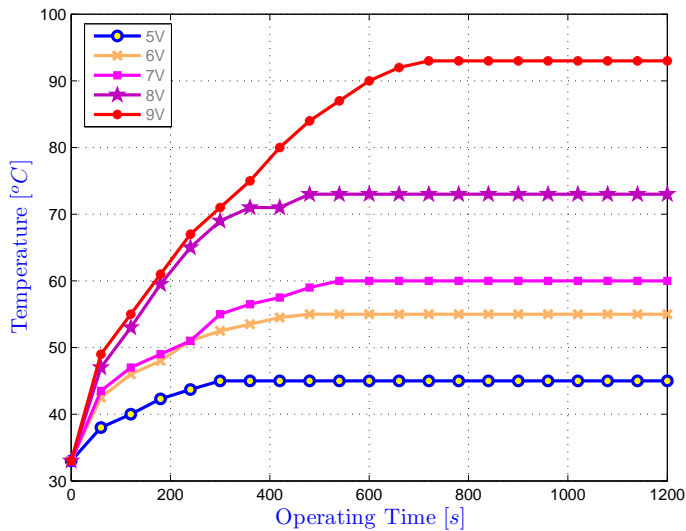


Figure 4.6: Temperature of PT in inductor-less class D inverter

and the power on the load is about $P_L \simeq 3.5[W]$. This result is relatively small when compared to the rated power of PT#1 (6W⁴).

4.2.3 Class D PT Converter with Impedance Matching

As shown in figure 4.5 in (4.2.2) above, the output signal of class D converter contains high order harmonic components which are the main cause to increase the losses in the PT which limits its throughput power. Furthermore, in the inductor-less PT based class D converter, the frequency range for ZVS operation of the switches will be narrowed if we want to increase the efficiency and vice versa [12]. In order to overcome these problems, a low-pass filter regarded as an input impedance matching circuit should be added at the input of PT [16]. For this topology of PT based power converter, the input impedance matching circuit is interposed between output of class D amplifier and PT's input to satisfy:

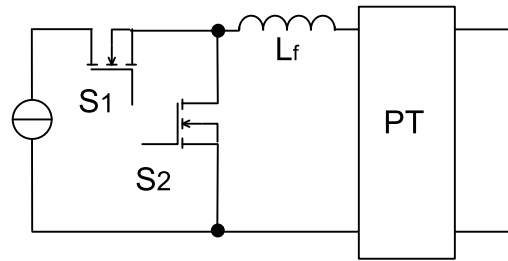


Figure 4.7: Class D resonant converter using PT with series inductor

⁴This value is official announced by the sample manufacture

- Preventing the harmonic contents from entering into PT
- Extend the ZVS operation range of the converter against the variation of the load

There are many structures of input impedance matching for PT reported in [7, 32, 53, 84], all of them are composed by either an inductive element or combination of inductive and capacitive elements. The comparison among these filters were fully carried out in the literature, so in the content of this research work, the choice of an impedance matching network was based on its simplicity and feasibility in order to reduce the profile of the whole system hence the price of the product. Finally, the impedance matching structure with a series inductor was chosen because of its simplicity in both simulation and experiment. The class D resonant converter using PT with series connected inductor is shown in figure 4.7.

With the structure depicted above, PT will be driven sinusoidally leading to minimization of the PT's losses hence optimizing its efficiency [7, 84]. Thanks to these results, the output power of PT is improved, in other words, the power density of PT is increased. The combination of a series inductor L_f and the input capacitance C_{in} of PT's equivalent circuit constitutes a low pass filter with the aim of:

- Operating the PT under less stress.
- Eliminating the circulating current hence improve the efficiency of whole converter.
- Realizing the achievement of ZVS operation in the power MOSFETs S1, S2.
- Reduce common mode noise, therefore reducing conducted EMI [37]. This is possible because the noise path impedance for high frequency components is much lower than that of the fundamental frequency component. Operating the PT with sinusoidal excitation will eliminate these high frequency components.

By adding a series inductor at the input of PT, the input impedance (Z_{in}), seen by the class D converter, is modified and this is an important parameter to design the converter properly. The input impedance is expressed by two key components:

- Input impedance phase θ_{in} - introduces an stronger inductive behavior than that one of an inductor-less PT based class D converter.
- Input conductance G_{in} - the real part of input admittance, expresses the capability of transferring power to load for a given input voltage [100].

With a series inductor L_f , the square-wave source shown across L_f can be approximated by its first order harmonics and the input signal of PT will be:

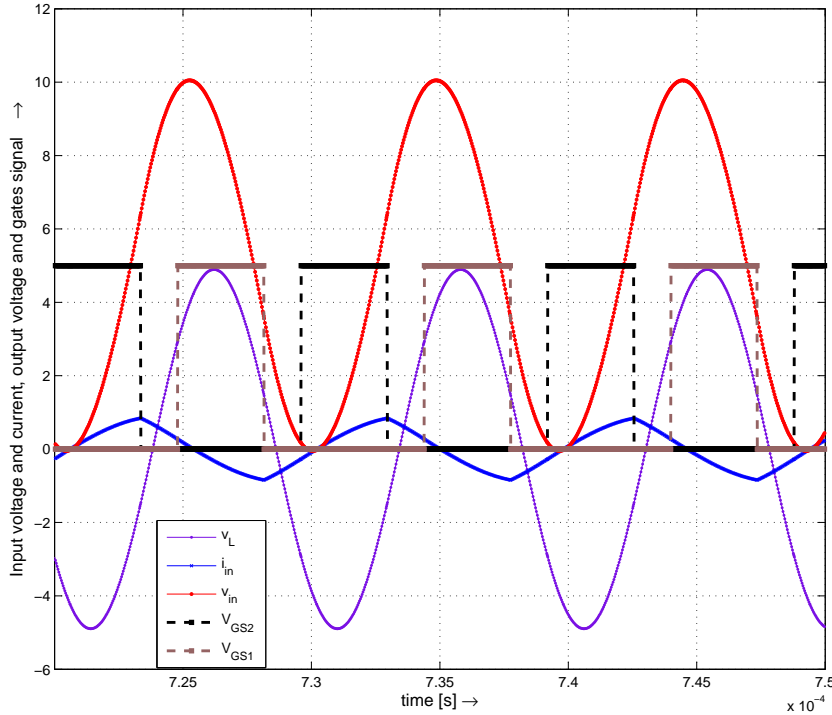


Figure 4.8: Class D converter for PT operating with input impedance matching

$$|V_{in}| = \frac{2}{\pi} V_{DCbus} \sqrt{1 - \cos(2\pi D)} \quad (4.3)$$

where D is the duty cycle of the class D converter and is less than 50%. In fact, in order to give enough dead-time for two switches S_1 , S_2 and enhance transient response performance, the maximum duty cycle is chosen from 35% to 40%.

In practice, the series inductor L_f is calculated to assure that its peak stored energy is always larger than the total energy needed to discharge the parasitic capacitor of S_1 and S_2 . With assumption is that the duty cycle $D = 50\%$, the series inductor L_f can be chosen to satisfy the relation 4.4:

$$\frac{1}{2} L_f i_{inmax}^2 \geq \frac{1}{2} C_{\Sigma} V_{DCbus}^2 \quad (4.4)$$

where C_{Σ} is the total capacitance of a shorted and a fully charged parasitic capacitance of S_1 , S_2 and can be found in the data sheet of the switch. The peak current of L_f , i_{inmax} , is one half of the current charged by $V_{DCbus}/2$ when S_1 is turned on:

$$i_{inmax} = \frac{V_{DCbus}}{8L_f f} \quad (4.5)$$

where f is the operating frequency of the class D converter. With substitution equation 4.5 into 4.4, the series inductor can be determined as:

$$L_f \leq \frac{1}{64C_\Sigma f^2} \quad (4.6)$$

The series inductor L_f combines with input capacitor C_{in} to form a low pass filter, so the inductor must be calculated to allow the fundamental of the class D converter to pass through. In addition, the series inductor should be chosen carefully to minimize the circulating current because of interaction between the class D converter and PT.

The operation of PT based class D converter with series input inductor is modeled and simulated by embedded PLECS in the environment of Matlab-Simulink with the parameters of PT#1's equivalent circuit. The series input inductor L_f is calculated in the range from $20\text{-}30\mu\text{H}$ and the duty cycle $D = 35\%$. The simulation results are represented in figure 4.8 above, where the red and blue lines are the PT's input voltage and current, the violet line is the voltage on the load R_L and the square-broken lines are the gate signals of S_1 and S_2 , respectively.

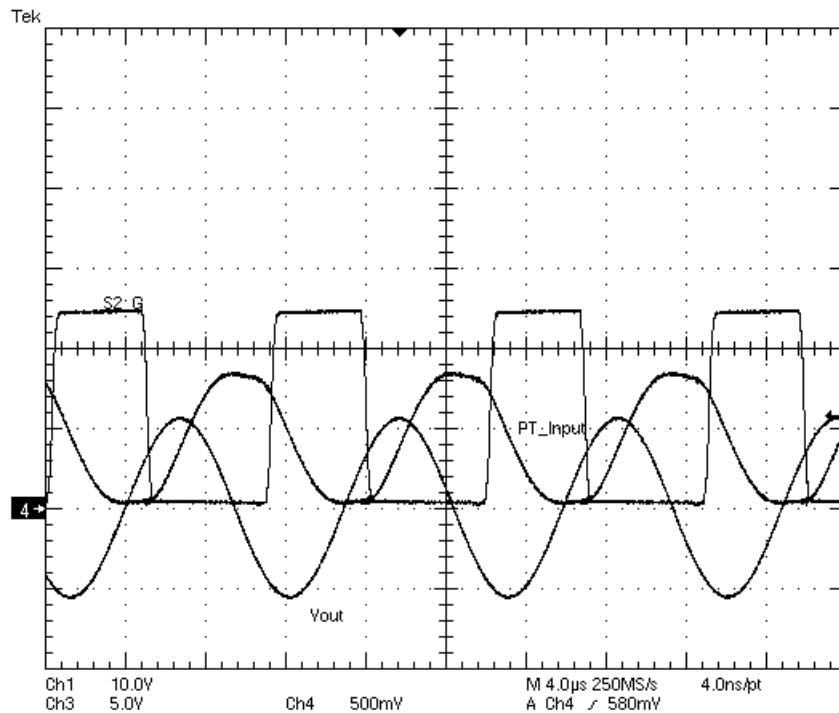


Figure 4.9: Class D converter for PT operating with input filter $L_f = 42\mu\text{H}$

Derivation from the simulation results, with a small additional series inductor at the input, the PT is operated with a sinusoidal wave form and the input current does not

contains high order harmonic components (the blue line in figure 4.8). In this case, the PT's input signals will be improved significantly compared to that one of inductor-less class D converter. Thanks to sinusoidal operation, the PT's losses will be minimized leading to reduction of temperature rise, hence the throughput power of PT can be improved by increasing the DC bus voltage V_{DCbus} of the converter.

The simulation above is then verified by the experiment where the DC bus is a voltage adjustable power supply and the class D is created by a couple of IRF740. The experimental results are shown in figure 4.9 with following parameters:

- DC bus voltage: $V_{DCbus} = 10V$
- Input series inductor: $L_f = 42\mu H$
- Resistance load: $R_L = 65k\Omega$

In the measurement results introduced in figure 4.9, the yellow line, blue line and pink line are PT's input voltage, voltage on load and S_2 gate signal respectively. The voltage on the load was measured via a high voltage probe with step down scale: 1:1000. The measurement results confirm the response of PT with sinusoidal excitation. The

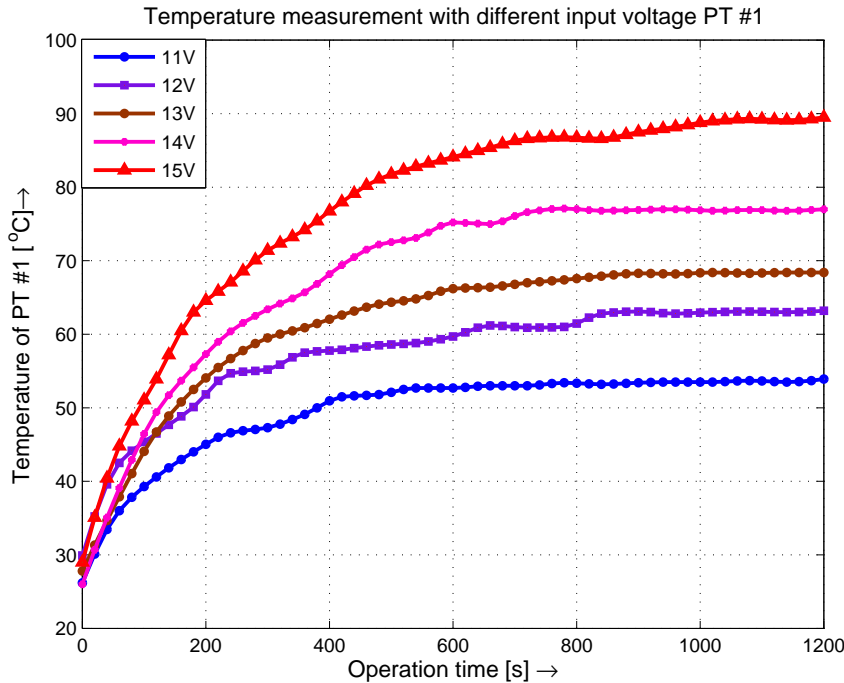


Figure 4.10: Temperature rising of PT based class D converter with series inductor

experiment was repeated with different DC bus and PT's temperature was monitored

uninterruptedly. The temperature rises of PT with different DC bus voltage are illustrated in figure 4.10 above. These measurement results are compared with these ones in figure 4.6 in the previous part (4.2.2): in the former case PT's temperature reached more than 90°C after ~ 700 seconds and being constant when the DC bus was 9V. In the latter case, PT's temperature increased to 90°C and being constant in this level after ~ 1000 seconds while the DC bus was 15V. This means that the PT's throughput power is improved significantly or in other words, the power density P_D of PT is increased by adding a small inductor as an input filter.

4.3 Class E Resonant Converter using PT

In this section, the operation of PT based class E⁵ will be studied. A class E converter as defined in [16] is a circuit composed of a bidirectional switch and a load network and it is capable of not only delivering a sinusoidal voltage to the output but also achieving the ZVS operation for the main switch. The principle circuit of PT based class E converter [69, 89, 97, 122] is introduced in figure 4.11 below: Derivation from the scheme of PT

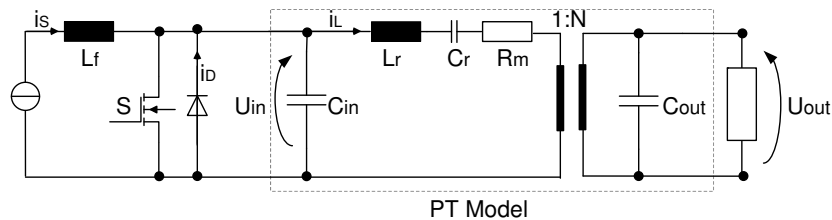


Figure 4.11: PT based class E resonant inverter

based class E converter in figure 4.11, the input inductor L_f is always large to suppress the AC input current peak and the resonant flows through the resonant circuit(or PT) is sinusoidal form. The critical issue of class E converter is the input voltage evolution, it is also the voltage across the input capacitor C_{in} , after the switch S is turned OFF. The evolution is a complicated process because the current flowing through input capacitor C_{in} contains a constant component due to the current I_S and a sinusoidal component as the resonant current i_L .

The key wave form of a class E converter are shown in figure 4.12. Once the input capacitor is completely discharged the current starts flowing through anti-parallel diode, such that the voltage across the switch S drops to zero. To minimize the switching losses,

⁵class E is also referred to single ended power converter

the switch must be turned ON within the conduction period of the diode, hence the ZVS operation is warranted. From the equivalent circuit of PT based class E converter when

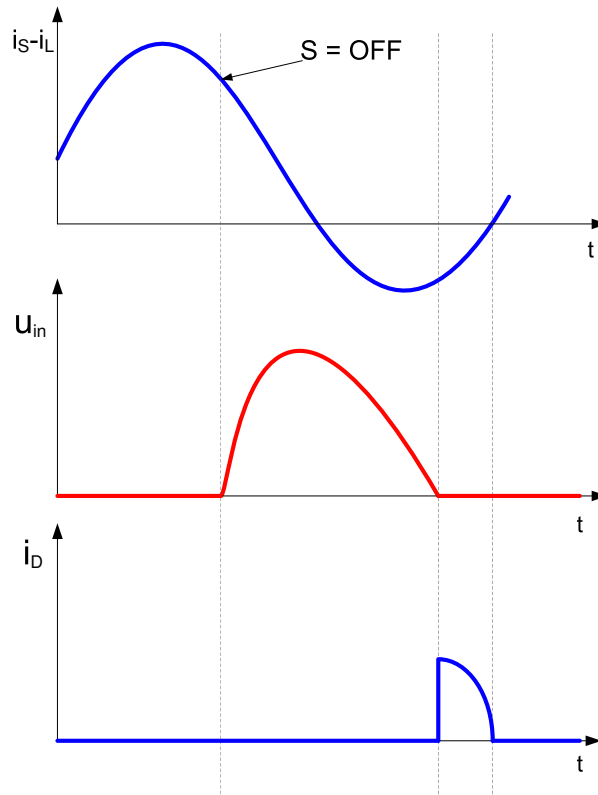


Figure 4.12: Basic operation wave form of PT based class E converter

operating close to one of resonant frequencies of PT depicted in figure 4.11, theoretically, the dissipative component is only the series resistor R_m . So, in order to minimize the losses, the resonant current should be minimized. In fact, the dielectric loss due to the circulating current flowing through input capacitor C_{in} will be taken into account [51]. In most applications using PT, the load has to be calculated within the maximum efficiency operation condition, mentioned in the part 2.3.4 or the matching network should be added to satisfy this condition. In [16] the method to calculate the impedance matching network was introduced in details.

However, an estimation of the maximum efficiency operating point for a resistive load can be calculated using the simplified model as shown in figure 4.11. Based on this model, the maximum efficiency can be warranted if the phase shift between the input voltage of PT v_{in} and the current flowing through the resonant branch i_{rL} is zero. In other words, the operating point of class E is dependent upon the change of load.

According to the analysis in [16, 73], the input inductor can be calculated by equation

4.7 in the case of a constant frequency controlled PT based class E converter:

$$L_f = \frac{1}{C_{in} \left(\frac{\omega_s^2}{f_n^2} + \frac{1}{4R_{in}^2 C_{in}^2} \right)} \quad (4.7)$$

where:

- f_n is the normalized operating frequency $f_n = \frac{f_s}{f} = \frac{\omega_s}{\omega}$
- R_{in} is the real part of the impedance looking from the input of PT including volume of load R_L

Derivation from calculations above, the model and operation of PT based class E converter was built and simulated in the environment of Matlab-Simulink with embedded PLECS. The simulation results are shown in figure 4.13: The model of PT based class

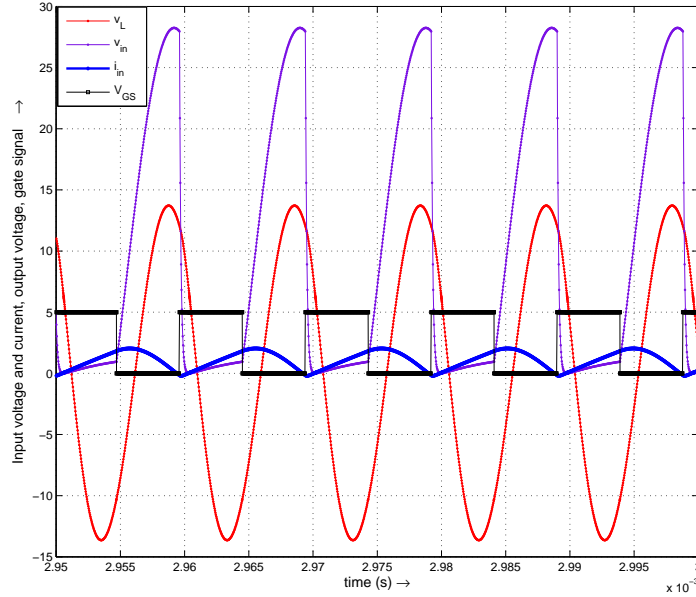


Figure 4.13: Simulation results of PT based class E converter

E converter was built by using the equivalent circuit parameters of the PT#1, the duty cycle of the gate control signal is 50%, the DC bus voltage $V_{DCbus} = 10V$. In figure 4.13, the violet and blue line are input voltage and current of PT, the black and red line are the gate control signal and voltage on the resistive load, respectively. The simulation result in figure 4.13 confirms that, when operation with the class E topology, not only

the PT but also the switch will be suffered by a high voltage stress leading to low transferred energy, higher loss and hence, the ZVS operation range will be narrowed [7, 16]. In order to verify the simulation result and prove the estimation above, a PT based class E inverter was built. The PT#1 was chosen for measurement. The experiment was carried out with following parameters:

- Input inductor $L_f = 42\mu\text{H}$
- Operating frequency in range $\sim 92\text{kHz}$
- Resistive load: $R_L = 65\text{k}\Omega$
- DC bus voltage $V_{DCbus} = 10\text{V}$

The experimental results are represented in figure 4.14 below: In the experimental results

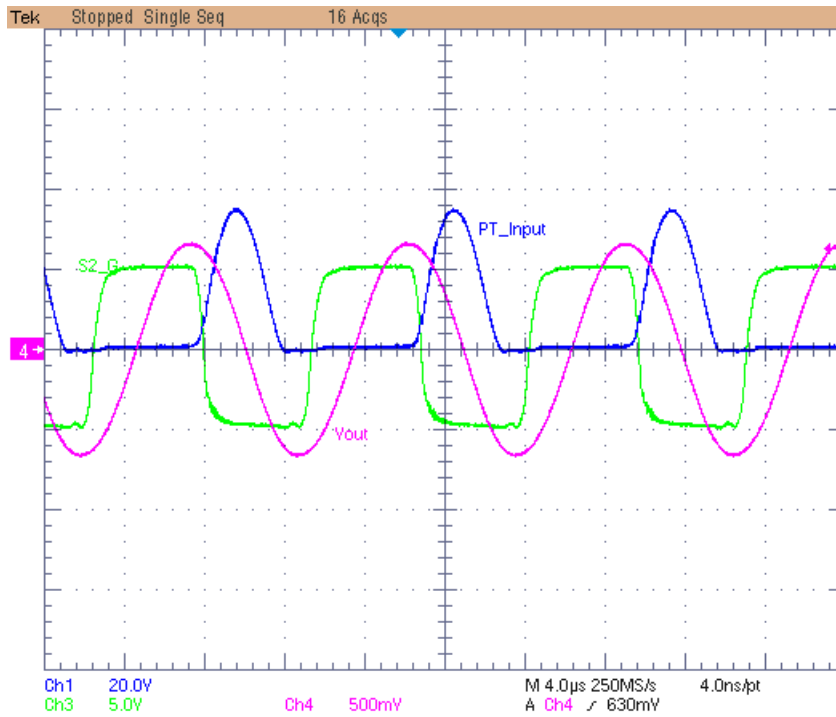


Figure 4.14: Experimental results of PT based class E converter

above, the yellow line, green line and pink line are PT's input voltage (20 volt/div), voltage on the load (500 volt/div), which is measured via a high voltage probe with scale: 1:1000, and the drive signal at the gate of the switch, a power MOSFET IRF 740. During the measurement, the temperature is also monitored continuously. The temperature evolution of PT#1 with different DC bus voltage is shown in figure 4.15.

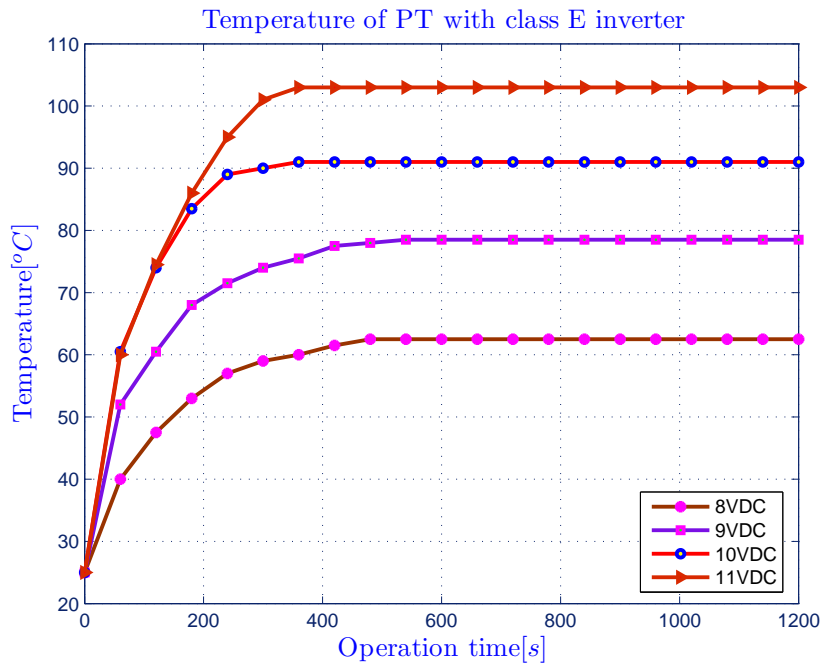


Figure 4.15: Temperature rising of PT based class E converter

The temperature of PT reached its limit when the DC bus voltage was 11V. The result is then compared to the PT's temperature in the previous parts (4.2.2 and 4.2.3).

4.4 Resonant Frequency Tracking

4.4.1 Purpose of Frequency Tracking for PT

When working with resonant devices, including PT, it often requires resonant frequency tracking. Resonant frequency tracking should be applied for PT because of the following reasons:

- When the maximum output to input voltage boost ratio is needed. This occurs only at one of the series resonant frequencies of PT
- When a load change leads to a change of operating frequency range of PT, in order to be able to continue operating PT within its bandwidth, a frequency correction must be used.

- As mentioned in the chapter three, the effect of operating environment conditions like temperature, operating time ... on the material properties of PT leads to a change of resonant frequency. These effects can be eliminated or diminished by using a resonant frequency tracking method.

Most piezoelectric devices are operated based on resonant principle, that means, their operation point is at a resonant frequency or in the vicinity of that one. It means that frequency tracking is indispensable to some applications using piezoelectric devices including PT. There are several methods to track the frequency, among them, self oscillators [4, 74] and phased-locked-loop (PLL) [28, 99, 119] are most popular. Both of these methods use as a criterion of control the fact that when resonance exists, all the reactive components of the input impedance are mutually compensated. Hence, under the conditions of resonance, the phase-shift between the input current and the input voltage is zero. The difference between the two mentioned methods above is that the first one includes a resonant system as part of itself, whereas the latter is driven by means of an external oscillator, controlled in a closed loop by a special device called a phase detector. In practical applications using PT, the PLL is preferred to the self oscillator method [8, 53, 58].

4.4.2 Series and Parallel Resonant Frequency of a PT

When studying the operation of piezoelectric transformer based on its equivalent circuit, it can be seen clearly that in specific vibration mode (full wave or λ mode for instance), a PT has two kinds of resonance: parallel and series. At the series resonant frequency, PT shows the lowest input impedance. In contrast, at the parallel resonant frequency, PT's input impedance is at its highest value. These concepts are derived from the analogy between piezoelectric devices and a resonant circuit [73]. It is important to note that series resonance occurs as a result of coincidence between the frequency of the input signal and the mechanical self-resonant frequency of the PT's body. Parallel resonance, in turn, occurs not at the frequency of mechanical resonance, but is rather an imaginary resonance whose frequency depends not only on the mass and elasticity of the material, but also on the value of the input capacitor created by the input electrodes, which is an unavoidable element of all piezoelectric devices.

Resonant frequency tracking may be needed for either parallel or series resonance, depending on the requirements of the product. Parallel resonance is often used in operating piezocrystallic or piezoceramic one-port systems (resembling a PT without output electrodes) in order to build self-oscillators. The criterion of resonance in this case is zero

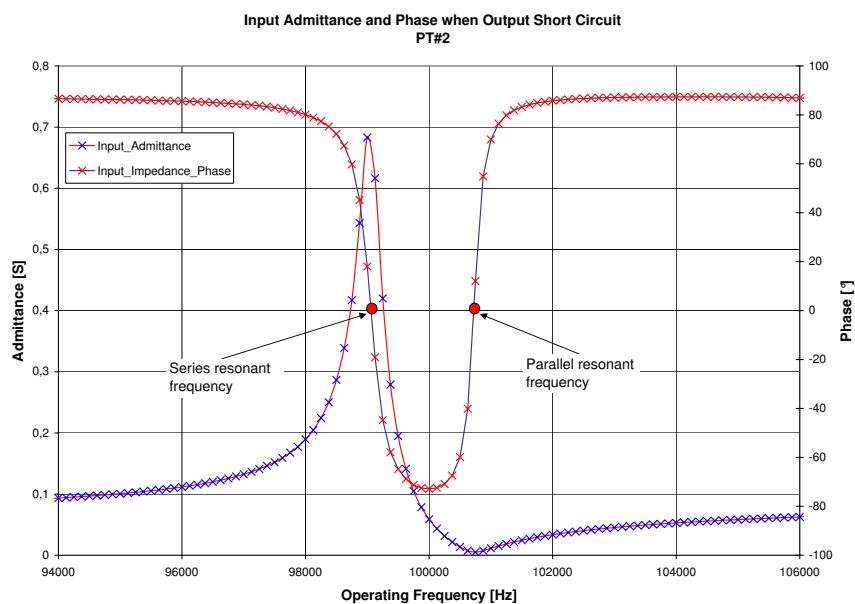


Figure 4.16: Series and parallel resonant frequency of PT#2 when output short circuit

phase-shift between the input voltage and input current. Parallel resonance frequency tracking can be used also when working with PTs [90], but in this case there arise certain complications. Figure 4.16 demonstrates the input admittance and the phase shift of PT#2 when its output was short circuited. While the excitation frequency varies from 90kHz to 105kHz leading to the phase shift of the input's admittance is changing from $+90^\circ$ to nearly -90° then back to 90° again and meets the zero line twice corresponding to series and parallel frequency, but at the series resonant frequency, the admittance reaches maximum value. From an energy transfer point of view, only at the series resonant frequency a PT is able to transfer the maximum energy into a load with a specific input voltage. For this reason, the frequency tracking is referred to as series resonant frequency.

4.5 Discontinuous Working Mode of PT

In the previous parts of this chapter, the operation of PT with two typical amplifier topologies was introduced and their valid work area, from a power transfer point of view, is always limited by temperature rise. If their temperature can be released as fast

as possible, the throughput power of PT will be improved significantly. The PT's heat will be transferred and radiated to the ambient environment during the operating period and reduced faster when PT stops working. This becomes an innovation to increase the power density P_D of PT by operating PT at a high power level in the discontinuous mode where PT will be fed by high power level within period as long as its temperature rise is still less than the critical point (smaller than half the Curie temperature!). The theory of discontinuous working mode of PT [75, 76, 113] can be expressed by diagram in figure 4.17.

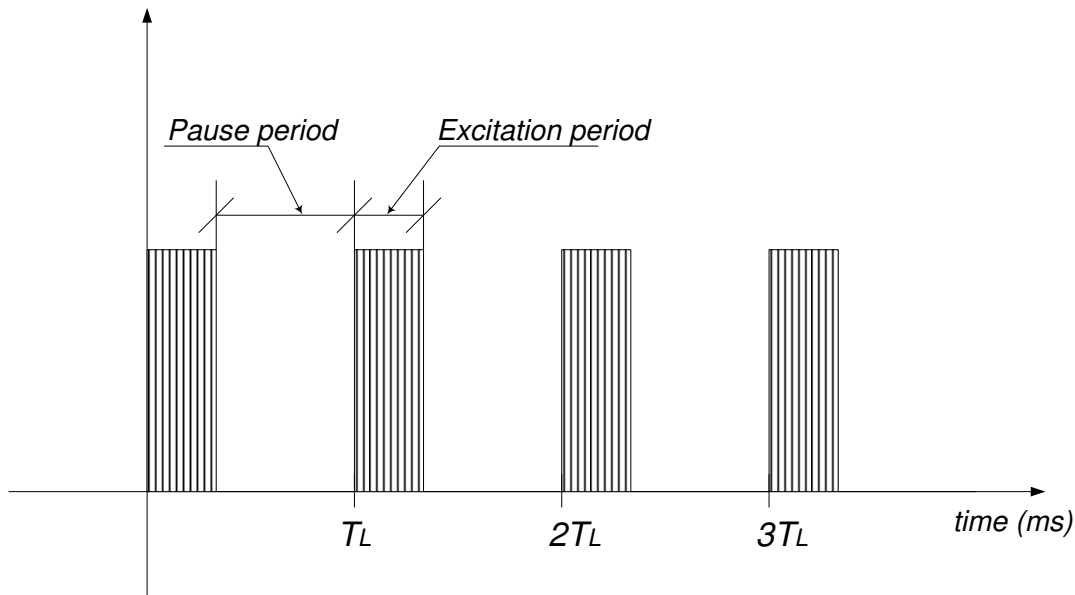


Figure 4.17: Excitation scheme for PT in discontinuous working mode

The operation of PT in both the time domain and the temperature domain can be regarded as an overloaded - repeatedly mode. Within this working mode, there are three important parameters that should be taken into consideration to guarantee the safe operation of PT and higher transferred power to load:

1. Excitation period t_x
2. Cycle time of excitation T_L
3. Amplitude of excitation which is represented by DC bus voltage V_{DCbus}

The excitation period must be chosen to be large enough to guarantee the output voltage reaches the desired value. Because of the combination between PT's output capacitor C_o and the output load (with or without output rectifier), it can be considered as a first order delay unit. In figure 4.18, the behavior of the output voltage of PT#3 is expressed

by the yellow line. As shown in figure 4.18, during t_x , in order to get the high output voltage, PT must be excited with a frequency range close to the resonant frequency, so the t_x must be:

$$t_x \geq t_{trans} \gg \frac{1}{f_r} \quad (4.8)$$

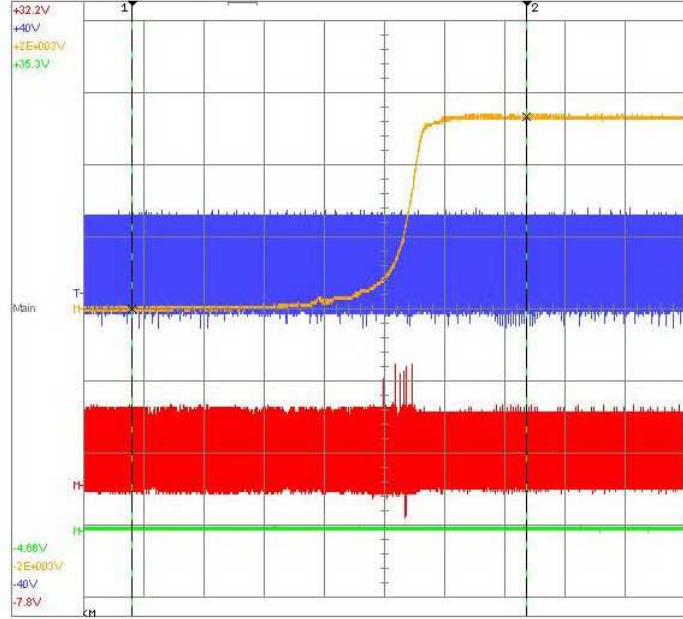


Figure 4.18: Dynamic response of PT's output voltage

where t_{trans} is the transient time - the minimum time for PT's oscillation reaches to steady state. Following [113, 114], the transient time t_{trans} is defined as:

$$t_{trans} = \frac{Q_{eff}}{f_r} \quad (4.9)$$

where Q_{eff} is the effective factor and depends on both PT's parameters and load. Based on the results in [113], while operating at a frequency in the range of 100kHz (λ mode), the excitation time is around 2.5 ms.

The next parameter is cycle time of excitation expressed as T_L . With the excitation time t_x was chosen 2.5ms, the T_L must be long enough to allow the heat within PT, which arises during the excitation phase, to be transferred to ambient environment within the period $T_L - t_x$. The value of T_L depends on the material quality, structure of the PT and in the measurement of the research work $T_L = 10ms$, that means the break time for PT is triple the excitation time before it is excited again.

The last parameter is the limit of the DC bus voltage V_{DCbus} . Based on the maximum stress S_{max} and the information of the dimension, to operate PTs safely, the limit of V_{DCbus} must be smaller than the maximum voltage. In the experiment, the limit of V_{DCbus} for PT#1, PT#2 and PT#3 are 60V, 70V and 110V respectively.

The experiment setup for discontinuous operation of PT are depicted in figure 4.19.

The FG1 and FG2 are two function generators, DRV is the half-bridge driver, the PWR-AMP is a class D power amplifier. The FG1 generates the low frequency (in this experiment $f_{FG1} = 100Hz$, duty cycle = 25%) and its output signal is connected to the gate input of FG2 which is operated in gating mode and creates the high frequency closed to PT's resonant frequency. Then the output of FG2 is connected to half-bridge driver IC.

The experiments were implemented on all the PT sample. In figure 4.20 introduces one

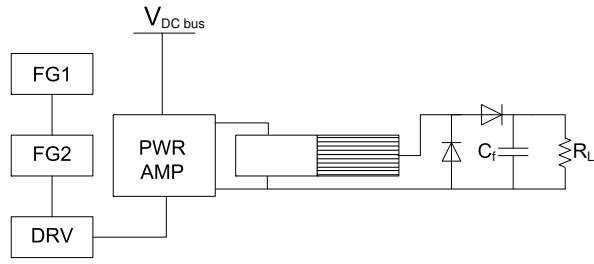


Figure 4.19: Experiment setup for PT in discontinuous working mode

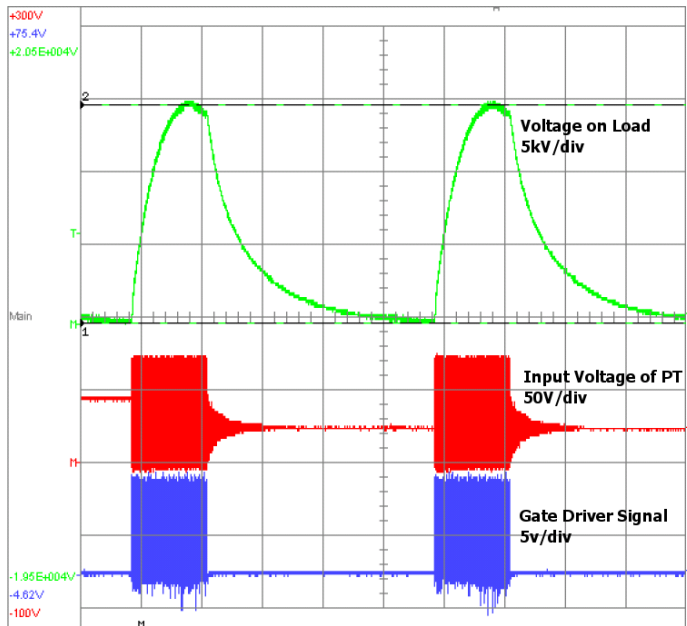


Figure 4.20: Performance of discontinuous operation mode PT

of measurement results carried out with PT#3, DC bus $V_{DCbus} = 110VDC$, excitation period $t_x = 2.5ms$, cycle period $T_L = 10ms$, the load $R_L = 7.8M\Omega$, $C_f = 220pF$.

For other PT samples and operation with different DC bus voltage V_{DCbus} , their output voltage are demonstrated in diagram 4.21. Derivation from the experimental results and the model shown in figure 4.19 the throughput power, and then the power density P_D will be calculated. The dissipated energy on the load following the setup in figure 4.19

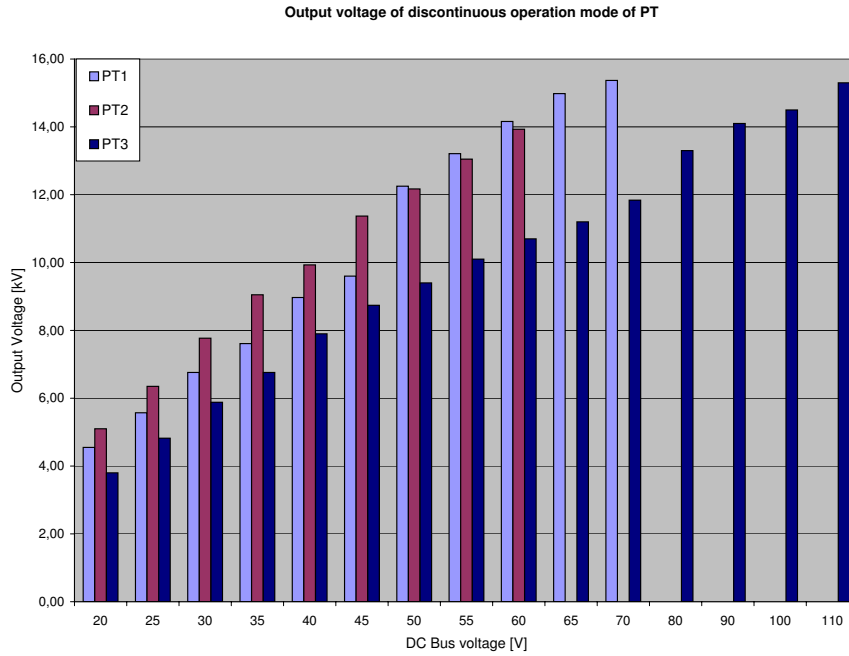


Figure 4.21: Output voltage of discontinuous operation mode PT with different V_{DCbus}

includes 2 part:

- Dissipated power on the output load:

$$P_{RL} = \frac{V_{out}^2}{R_L} \quad (4.10)$$

- Energy to load the filter capacitor C_f :

$$W_{Cf} = \frac{C_f V_{out}^2}{2} \quad (4.11)$$

With the voltage doubler setup in this experiment, to load the capacitor C_f , PT has to transfer an amount of energy twice of W_{Cf} , that is: $W_{Cf}^* = 2W_{Cf}$. From a power transfer point of view, this amount energy was delivered to C_f within the excitation time, hence the power to load the capacitor C_f can be calculated as in equation 4.12:

$$P_{Cf} = \frac{W_{Cf}^*}{t_x} \quad (4.12)$$

So the total transferred power of PT in each excitation is:

$$P_{PT} = P_{RL} + P_{Cf} \quad (4.13)$$

From the measurement results shown in figure 4.21, the maximum transferred power is correlative with the critical DC bus voltage. The maximum output voltage for PT#1, PT#2 and PT#3 are 15.37kV, 13.93kV and 15.3kV respectively. These results are applied to equations from 4.10 to 4.13 to determine the maximum throughput power. Finally, the maximum transferred power of PT#1, PT#2 and PT#3 are 51W, 42W and 49W. The results show that the throughput power of PT in the discontinuous working mode were stepped up nearly ten times than the nominal power in continuous mode.

4.6 Summary and Discussion

The operation of PT with two common power amplifier topologies was investigated from a power transfer point of view. With the first topology - a class D amplifier - the operation of a PT based class D converter was studied in two cases: without and with an input matching network. With the inductor-less class D amplifier, PT's excitation contains high order harmonic components. They are the causes to make PT's temperature increase, hence limits the throughput power of PT. The high order harmonic elements of PT's excitation can be removed by adding a low-pass filter which provides an input impedance matching. Among the low-pass filter topologies for PT, an inductor in series connected with PT's input was chosen because of its simplicity.

The second topology that was investigated for PT was a class E amplifier. In comparison with a class D amplifier topology, a class E requires less active components than those of a class D amplifier. However, the PT's excitation from class E amplifier contains very high peak voltage. This is the main reason that prevents the DC bus voltage from being increased leading to limiting the throughput power of PT.

First of all, the operational characteristics of PT with amplifier models were simulated in the Matlab-Simulink environment with embedded PLECS. Finally, the simulation results were verified by experiments performed on three different types of PT samples. The measurements were also matched with analysis and simulation. From a power transfer point of view, among the mentioned power amplifiers, PT performs the best with series inductor class D topology, then the class E and the worst case is the inductor-less class D amplifier topology.

The contents of this part focused not only on the amplifier topologies but also on the control method to track the optimum operation point for PT while operating conditions change. Following the analysis, at a specific vibration mode, a PT has two resonant points: series resonant point and parallel resonant point. In order to achieve the maximum output power, the operation of PT must be tracked to its series resonant point, in another word, PT is in series resonant oriented operation mode.

Finally, a new working mode of PT was introduced - discontinuous working mode in which, PT is excited by a series of high amplitude voltage pulses. With this working mode, a PT can transfer a much greater amount of power than the nominal power level in continuous mode because it has a long pause period in each operation cycle. In the pause period, the heat derived from the electrotechnical losses would be transferred and radiated almost completely. Experiment and calculation have confirmed that, in discontinuous mode, a PT is able to transfer an amount of power nearly ten time of what is can transfer in continuous operation. The discontinuous working mode of PT opened a new method to increase its power density approaching to ideal power density of piezoelectric material mentioned in the previous chapter. Some applications using PT are introduced in the next chapter as the illustrations for integration possibility of PT in practice.

Chapter 5

High Power Density Applications

5.1 Introduction

In this chapter, some prototypes of electronics devices using PT will be introduced to illustrate the integration possibility of PT in practice. These applications are:

- Igniter for high intensity discharge lamps
- High output voltage DC/DC converters
- Electronic ballasts for light emitting diode lamps
- Stand alone ionizer for food sterilizers

5.2 Igniter for HID Lamp

5.2.1 Ignition Concepts for HID Lamp

Nowadays, in some specific applications concerning to lighting technology, the high intensity discharge (HID) lamp is the best choice because of its advantages over incandescent lamps such as higher brightness, higher efficiency, longer life time. They have been widely used for various applications in outdoor and large scale indoor spaces. Some of them, the small HID lamps with low power range have been developed for spotlighting, liquid crystal projector, headlights in automobile, and so on... In the HID lamp family, metal halide (MH) lamps return the best color rendering, they also offer much higher efficiency than mercury vapor lamps, better light quality than either mercury or sodium lamps [10, 43, 110]. Metal halide lamps, however, have had some limitations and most of them that must be mentioned are:

- High ignition voltage, in the range of several kilovolt in order to start the lamp, even much higher in the case of hot - re-ignition, more than ten kilovolt.

- MH lamp's impedance changes over operation time.
- Difficult to operate the MH lamp with a high frequency after ignition phase. [10, 107]

Figure 5.1 depicts the dependence of the MH lamp's impedance¹ on the operating time. These lamps, as all gas discharge lamps, are an open circuit load if not ignited yet. Due to the strong heat development of the lamp during operation, the glass bulb becomes a high electrical load. If the lamp has to be reignited after a short interruption of its operation, this has to be considered when designing the igniter [76]. In [107], many ignition concepts for HID lamp were discussed and compared and a series of high DC pulses is an approach to apply to the igniter. Derivation from this feature, a high voltage pulses generator based on discontinuous working mode of PT was developed to ignite the HID lamps.

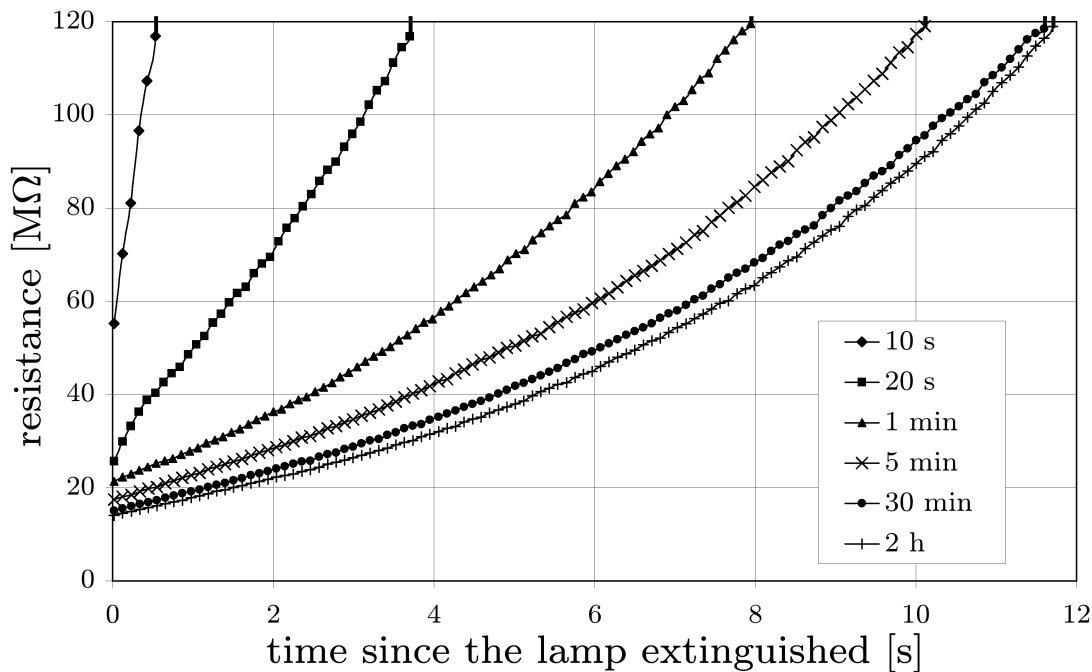


Figure 5.1: Resistance of metal halide lamp with different operating period

5.2.2 PT based Igniter for HID Lamp

Because of operational characteristics of both the HID lamp and the PT, the igniter was designed with following requirements:

¹This diagram is supplied by Dr.Siesegger - OSRAM GmbH, Munich,Germany

- Due to the variation of the HID lamp's impedance requiring a frequency control circuit, it is necessary to operate PT at its maximum output to input voltage boost ratio n_{21max} .
- The output rectifier should be chosen to match the high load and high voltage.
- The simplicity and minimized EMI are highly emphasized.

Based on these requirements, the HID lamp igniter using discontinuous working mode of PT was designed and introduced in figure 5.2: The igniter includes a class D power

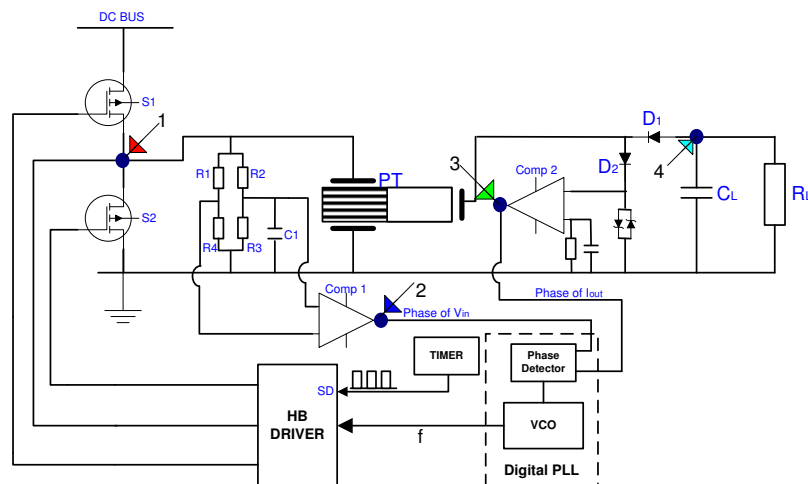


Figure 5.2: Design of HID lamp igniter using discontinuous working mode of PT

amplifier with a frequency control as the main control loop. The voltage on load was twice multiplied by applying a voltage doubler rectifier at the output stage. The design of the circuit, especially the signal conditioning for the feedback, had to be done very carefully here. Due to the close arrangement of the high voltage PT and sensitive circuit elements, unwanted noise in the feedback path prevented the PLL from working correctly. The input voltage probing network was finally changed from a diode based one [8] to a voltage divider/filter based ($R_1 \div R_4/C_1$). Also the output probing network had to be changed to guarantee proper operation. So, the diode voltage is not compared against ground but against an offset. A timer is added in the model in order to regulate the period of excitation - T_L , and the excitation period - t_x .

To verify the design for the igniter mentioned above, a prototype of the igniter was fabricated as depicted in figure 5.3 where the PT#3 was applied and a HEF 4046 IC was used as frequency controller. The igniter was tested with the HID lamp D1S and D2S series of Osram, in the worse case operation the impedance of these lamps is around

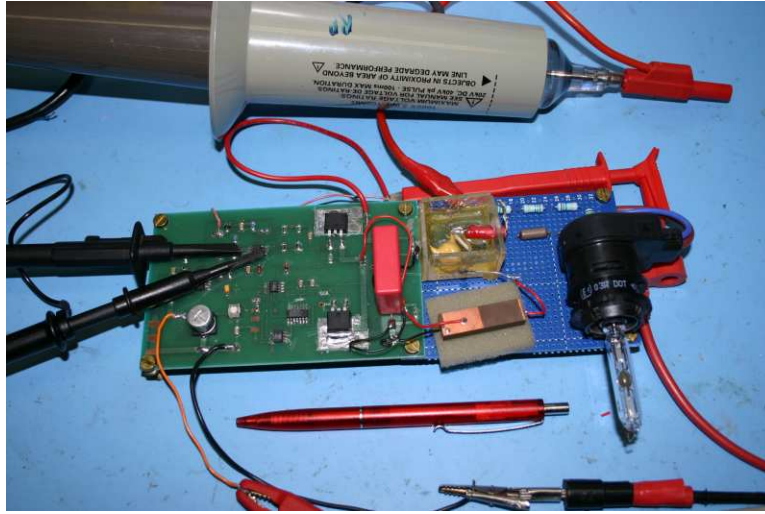
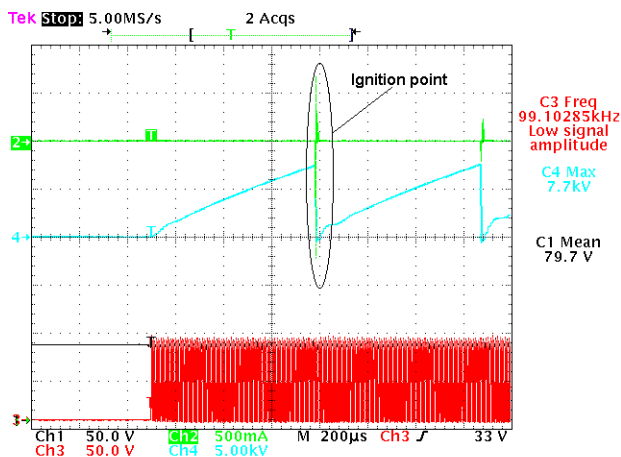
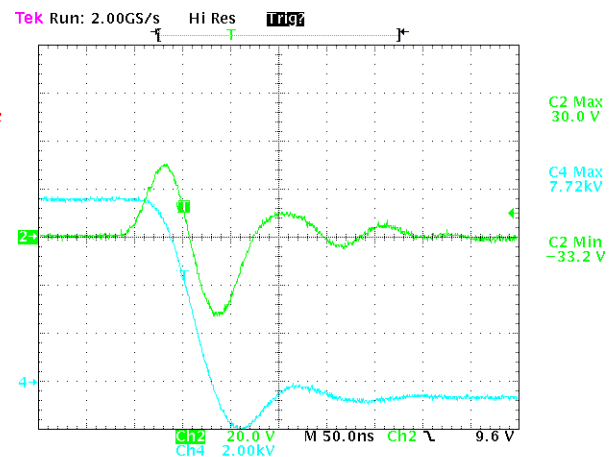


Figure 5.3: Prototype of HID lamp igniter using discontinuous working mode of PT

$7.8M\Omega$ and the voltage in hot re-ignition condition is in the range of $15kV^2$. These requirements were verified by experiment in the previous section which is expressed in figure 4.20. In this section, the operation of the igniter for the HID lamp was tested in cold ignition condition. The ignition process are depicted in figure 5.4. The overview of the ignition process is shown in figure 5.4a where the red-line (channel 3) and the black-line (channel 1) are PT's excitation and it's RMS respectively. The blue and green lines are HID lamp's voltage and current during ignition. The ignition's voltage and current are detailed in figure 5.4b.



(a) Ignition process



(b) Voltage and current of HID lamp at ignition point

Figure 5.4: Behavior of igniter for HID lam using discontinuous working mode PT

²following the discussion via email with Dr. Siessegger - HID lamp developer from Osram

In comparison with other ignition concepts based on the magnetic transformer discussed in [107], the igniter for HID lamp using PT can be operated separately from the rest of electronic ballasts. It means that, after the ignition and running up phase, the igniter can be switched off and does not give any side-effects to the performance of the ballasts in the steady state. This has the following advantages:

- Reduction of the losses of the electronic ballasts in permanent operation.
- Opening a chance to drive the electronic ballasts in a higher level of operating frequency (more than 1MHz).

5.3 High Output Voltage DC/DC Converter

In practice, some specific applications require a high output DC voltage, for example in flash lamp, electric shocker or other hand-held devices. Usually, these device are powered from low DC voltage source like battery, and then the voltage will be boosted to high level by a high ratio magnetic transformer. To illustrate the feasibility of integrating PT into the applications, in this section, a very simple high DC voltage power supply using HVPT is introduced. The design of the power supply based on PT is illustrated in figure 5.5. In figure 5.5, the PT based power supply uses the class E topology with

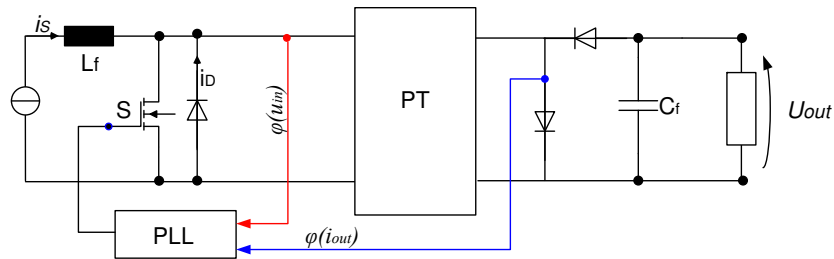


Figure 5.5: Design of high DC voltage power supply

a frequency closed loop using PLL to track the optimal frequency. The phase of PT's input voltage $\varphi(u_{in})$ was measured via a voltage divider and the phase resonant current $\varphi(i_{rL})$ was indirectly sensed via the diode. At the steady state, the difference between angle $\varphi(u_{in})$ and $\varphi(i_{rL})$ should be so small, theoretically it is zero, to guarantee that the PT is always driven at its optimum frequency.

The prototype of high output voltage power supply was built and shown in figure 5.6 where the PT and output rectifier stage were placed in the bottom layer. In the prototype, the PT#2 was chosen for measurement.

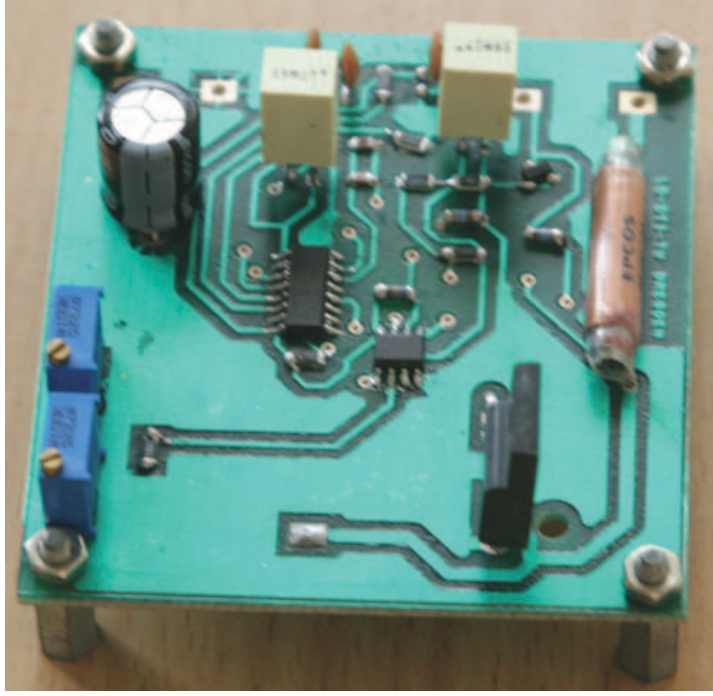


Figure 5.6: Prototype of high DC voltage power supply

With the parameters of the equivalent circuit described in appendix B.2, the important element is the input inductor which will be calculated to guarantee the ZVS operation of the switch. Following the suggestion in [16, 73], L_f should be:

$$L_f = \frac{1}{C_{in} \left(\frac{\omega_{rs}^2}{\omega^{*2}} + \frac{1}{4R_{opt}^2 C_{in}^2} \right)} \quad (5.1)$$

where input capacitor $C_{in} = 96nF$; series resonant frequency $f_{rs} = 105kHz$; optimum load R_{opt} - the load is chosen following equation 2.20, and the normalized frequency $\omega^* = 1/\sqrt{2}$.

Equation 5.1 can be rewritten as the inequality 5.2:

$$L_f \leq \frac{\omega^* R_{opt}}{\omega_{rs}} \quad (5.2)$$

The operational characteristics of the high output DC converter are represented in figure 5.7 and 5.8. In figure 5.7, the red line is the gate signal of the MOSFET, the blue line is the input wave form of the PT and the green line is the voltage on the load. Figure 5.8 expresses the control signal at the feedback path. The blue and red line introduce the input voltage of PT and the offset compared value. The input voltage of PT was captured directly via a voltage divider and then compared to an offset value instead of the ground. This is a "tactic" to prevent the comparator from being compensated due

to the variation of the DC bus. The green and yellow lines are the captured images of the input voltage phase and current phase, respectively. The measurement results inform that the converter was being operated in the ZVS condition.

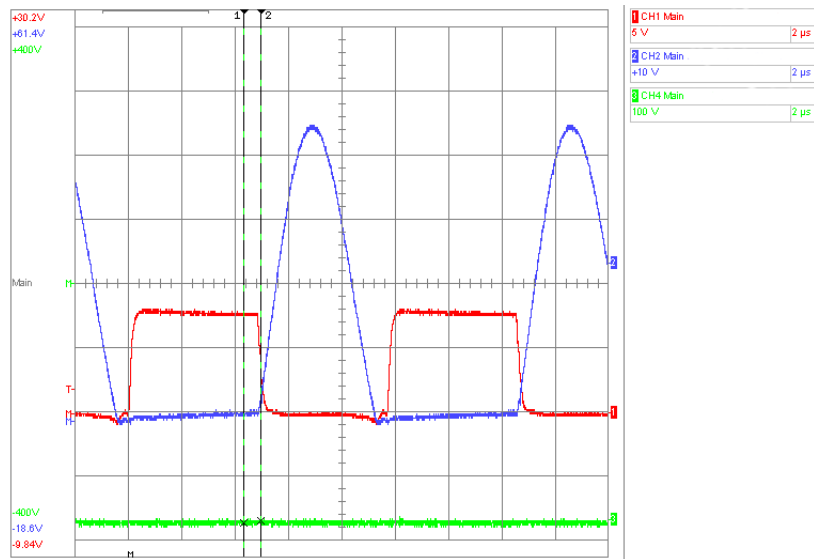


Figure 5.7: Measurement results of high output voltage power supply

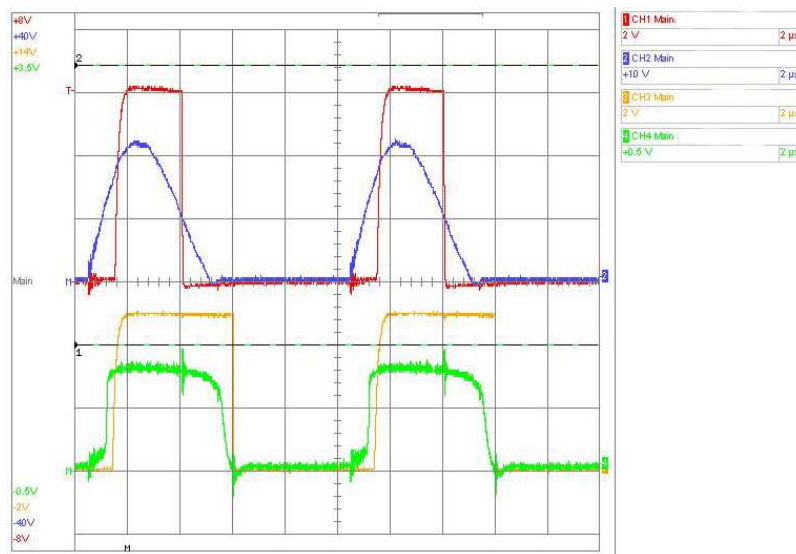


Figure 5.8: Feedback signals: voltage and current phase

5.4 PT based Electronics Ballasts for LED

Nowadays, advanced lighting technology like the LED is paid attention to from the point of view in energy saving, improvement in the lifetime and stability of the product. In comparison with some other lighting sources such as CCFL and HID, etc an individual LED is a very small lighting source, but an LED system containing arrays of LEDs will be re-markable lighting source with some advantages such as: small power consumption, low heat generation, small current, color changeable, etc and they have been used more and more in various lighting systems illustrated in figure



Figure 5.9: A single LED: 3W - 350 mA

5.10 - lighting system in tram and bus is an example. Similar to other types of lamps, the illumination power of the LED is proportional to its forward current and a single LED, shown in figure 5.9 for example, requires from 2 to 4 VDC and current level is in range up to 1A (normally, some hundreds of mA, typical: 350 - 750 mA). These characteristics of LED match those of PT.



Figure 5.10: Applications of light emitting diode

Within the content of this work, a simple electronic ballasts for LED using PT is introduced; the concept of the ballasts is expressed in figure 5.11 where PT is driven with a quasi square wave pulse from a class D power amplifier. The output stage, the combination of power rectifier and LC filter are used to ensure that LEDs will be operated with a "truly" DC source. At the control part, it contains two closed loops, the inner is a frequency control loop to ensure that PT is always driven in its optimum area, the outer is a current control loop operating as the over current protector and LED dimmer.

To verify the approach mentioned above, a very simple prototype of electronic ballasts for LED using PT was built (figure 5.12) to power up an array of 4 to 6 LEDs in series with total power consumption around 12 to 15 watts. Because the conducting resistance of each LED is unchangeable during operation, that means the PT is working at a fixed operating point. To simplify the ballasts, the frequency control loop (inner loop in figure 5.11) is ignored. The prototype of electronic ballasts for LEDs using PT is shown in

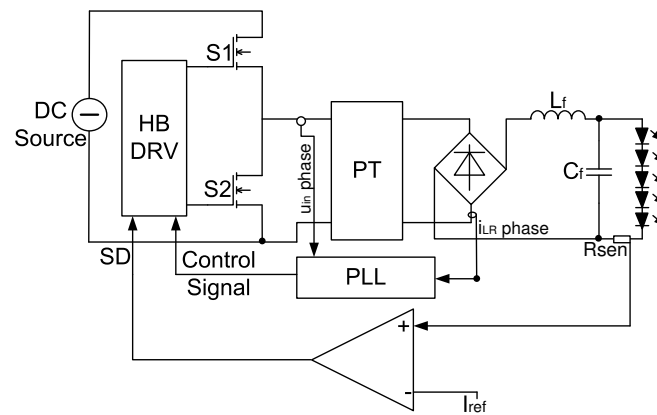


Figure 5.11: Proposal design for LED ballasts using PT

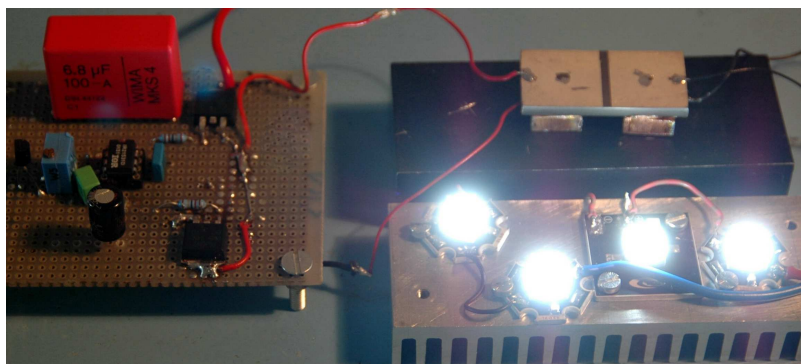


Figure 5.12: Prototype of LED ballasts using PT

figure 5.12 using a class D amplifier created by two power MOSFETs (IRF640) and

driven by a self oscillating half-bridge driver IC which is fed by an external oscillator R-C network. The operating frequency of the PT's excitation is determined:

$$f = \frac{1}{2\pi\sqrt{RC}} \quad (5.3)$$

where R and C are chosen following the operational characteristics of half-bridge driver IC. In the prototype circuit, the resistor R was replaced by variable resistor so the operation frequency of the ballasts can be changed manually. The prototype of LED ballasts using PT was tested with 4 LEDs connected in series (figure 5.12), the nominal current is 350mA. The operational wave-form of the ballasts for LED is shown in figure 5.13 where the blue line is the input excitation of PT, the red line is the gate signal of low-side power MOSFET and the yellow line is the LED's current.

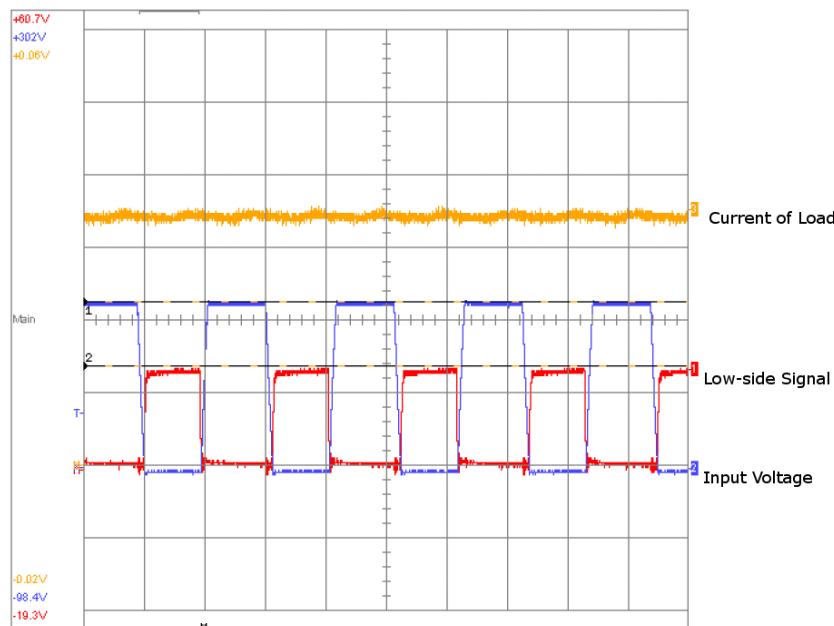


Figure 5.13: Wave-form of ballasts for LEDs

5.5 Stand Alone Ionizer for Food Sterilizer

The ozone food sterilizer is a fast and effective way to sterilize water, fruits and vegetables as well as meat and seafood products and now the home use sterilizers are being marketed to consumers as a safe and cheap method of sterilizing a product. The market volume for food sterilizer is millions of units per year³ and it have been an indispensable household

³Source: Internet

device.

Recently, the use of pulsed electric field (PEF) in food sterilization has attracted a lot of attention [24, 41, 96]. The main part of a sterilizer is an ionizer where a high voltage pulsed power supply generates a high voltage pulsed field [27, 108]. The high voltage pulses can be generated via a high voltage transformer, and the output pulse's amplitude is from a few to some tens of kilovolt depending on the specific application. With the advantage of a high voltage step up ratio, a Rosen-type PT can replace the magnetic transformer in a home-use sterilizer. Within this section, the proposal of a very simple ionizer using PT in discontinuous working mode is introduced, the circuit of the ionizer is shown in figure 5.14 where load (ozone membrane) is in series connected to a spark-gap which guarantees the required high voltage pulses transferred to the load. For a home use sterilizer, the required voltage is in the range from 6kV to 10kV.

As depicted in figure 5.14, in this case the PT will be operated in discontinuous open

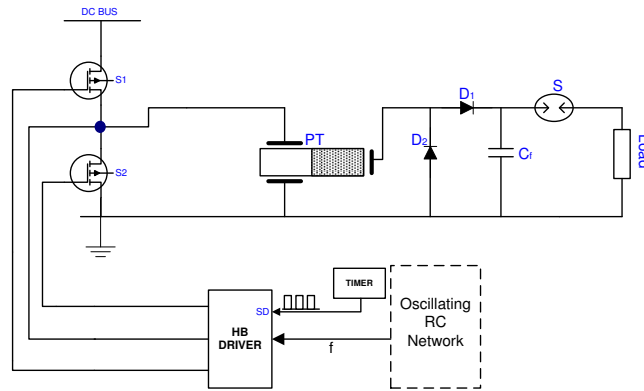


Figure 5.14: Principle circuit of stand alone ionizer for food sterilizer

circuit mode with a non series connected class D amplifier driven by a self oscillating half-bridge driver IC. The operational duration of the ionizer is specified by an additional timer. The prototype of the ionizer is represented in figure 5.15, where the PT#1 was chosen to generate the high output voltage. With the proposal shown in figure 5.14, PT will operate in an output open circuit condition. From the parameters of the equivalent circuit of PT#1 in table B.1 in Appendix B, the operating parameters of the ionizer are defined as follows:

- Operating frequency: Derivation from equation 2.9, the operating frequency of class D amplifier should be:

$$\omega_{r0} = \sqrt{\frac{C'_o + C_r}{L_r C_r C'_o}} = \sqrt{\frac{n^2 C_o + C_r}{L_r C_r n^2 C_o}} = 102kH z \quad (5.4)$$

- The requirements for the ionized voltage is from 6kV to 10kV after being increased via a voltage doubler. Derivation from the equations, the effective value of PT#1 output voltage should be from 3kV to 5kV (part 3.4.1).
- The output to input voltage boost ratio n_{21} : applying the equations 2.15 and 2.16 when $R_L \rightarrow \infty$, the voltage boost ratio $n_{21} \simeq 200$. So the DC bus can be set in the range $V_{bus} = 15V \div 20V$.

Figure 5.15 expresses the prototype of ionizer at its operation period.

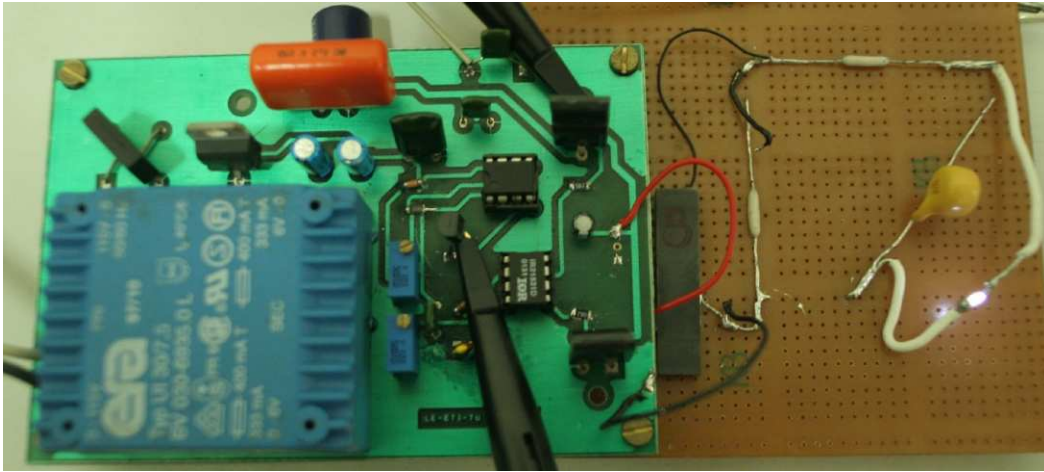


Figure 5.15: Stand alone ionizer

Chapter 6

Conclusions and Future Work

The target of the research is to study the feasibility of piezoelectric transformers to replace the traditional magnetic transformers, which is the most bulky and expensive element, in power electronic devices. The study has mentioned and dealt with some of the following issues:

The fundamentals of the piezoelectric transformer from material, structure and electrical engineering point of views. The operational characteristics of a piezoelectric transformer depend on its material properties, and structure. To realize the capability of integrating the piezoelectric transformer into power electronic systems, the transferred power of this component must be larger than that of a traditional magnetic transformer which has the same volume at the same operational conditions. This capability is expressed by the term: power density P_D , which is the ratio of output power to volume of the component.

When applied to power electronic systems, a piezoelectric transformer is regarded as a series parallel resonant element. The electrical characteristics of a piezoelectric transformer are based on its equivalent circuit having a set of parameters correlating with specific vibration modes. These parameters can be defined by using the admittance circle method. The main facts that limit the transferred energy through a piezoelectric transformer are then mentioned. There are three main reasons: the effect of temperature rising during operation, the limitations regarding the critical electro-mechanical limits defined directly by material properties and other operational conditions like output rectifier stages.

With in three main limitations mentioned above, the effect of temperature is the most important issue to not only the stable operation but also the lifetime of the piezo-

electric transformer. The critical point of temperature is half of the Curie point. The temperature of piezoelectric transformer is rising up in during operation due to the losses leading to the change of material properties and operational characteristics. The effect of temperature is then confirmed by measurements and calculations on three different piezoelectric transformer samples. The next issue is the limitations in the field of electro-mechanic. The power is transferred from electrical form (at input) to electrical form (at output) via electromechanical coupling described by linear relationships, so the limitation can be seen either from an electrical or mechanical point of view. Not losing the generality, the transferred energy of piezoelectric transformer is investigated within an operating cycle. The calculations on PT samples shown that the maximum transferred energy based on the mechanical boundary would be taken as the restriction. Following the calculation results, the power density of piezoelectric transformer is very persuasive, $P_D \simeq 350W/cm^3$!

Finally, the effect of the rectifier stage at the output was taken into consideration. The comparison between two common rectifier topologies for piezoelectric transformers were carried out: voltage doubler and current doubler. On one hand, a voltage doubler is suitable for applications require high voltage and high resistive load, on the other hand, the current doubler matches applications where high current and low resistive load is required. But the power lost in the former case is higher than the one in the latter case. The interaction between the power amplifier and piezoelectric transformer is the next content of the study. Because it is used in low power range applications, the topology of the amplifier is the important role in reduction of the profile of the whole system. The amplifier topology was chosen based on its simplicity. Two common topologies were taken into consideration: class D and class E. The operation of piezoelectric transformer with these amplifiers is simulated by Matlab - Simulink with embedded PLECS, then verified by experiment.

Class D amplifier is considered as a square wave voltage source. The power density of a piezoelectric transformer driven by class D amplifier was studied with the variations: without and with an input series connected inductor. In the first case, the input waveform fed to piezoelectric transformer contains high order harmonic components leading to high temperature stress due to higher losses. In the second case, a small inductor is connected in series with the piezoelectric transformer to remove the high order harmonic components. The input waveform is sinusoidal and this helps to reduce the temperature rise, resulting in a higher power density level compared to the first case.

The class E can feed piezoelectric transformers with a sinusoidal waveform but under

high voltage stress. For this reason, the DC bus voltage was limited and usually much smaller than the one of class D topology.

The control method to operate the piezoelectric transformer to achieve optimum output power was also discussed. The phase locked loop (PLL) was used for tracking the optimum operating frequency of the element. Then, the discontinuous working mode of the piezoelectric transformer was proposed as a significant way to improve the power density of the device to overcome the temperature and electromechanical limitations. The proposal of the circuit to operate piezoelectric transformers in discontinuous mode is introduced. In this working mode, the power density P_D of a given PT can be increased around ten times in comparison to nominal working mode.

Last but not least, prototypes of four different applications:

- Igniter for HID lamps.
- High output DC voltage power supplies.
- Electronic ballasts for LED lamps.
- Stand alone ionizer for food sterilizer machine.

using piezoelectric transformer were developed in order to improve the integration of this element into low profile power electronic devices.

With the subjects mentioned and dealt with are listed above, this research also opens some issues relating to piezoelectric transformers and their applications:

- Effect of aging process to materials properties leading to the changes of operational characteristics of piezoelectric transformers.
- Because the relationships between transferred power of a piezoelectric transformer with its materials and structure are not linear, hence, approaches in design (materials improvement, new geometry) and driving technics in order to increase the transferred power of piezoelectric transformers to satisfy the practical incessantly requirements
- Operations of piezoelectric transformers either in parallel or in series connection are the effective ways to increase the output power, but the methods to minimize the influence of non-equality of parameters among them to remain their advantages are still open.

Appendix A

Specifications of PT samples

A.1 Sample PT#1: MPT3608A70L0

The fundamental materials characteristics of the Piezoelectric Transformer are issued in the Table A.1 below:

Item	Mark	Unit	Values
Density	ρ	g/cm^3	8
Electromechanical coupling coefficient	K_{33}	%	68
	K_{31}		35
	K_r		60
Specific inductive capacity	$\varepsilon_{33}^T/\varepsilon_0$	-	1200
Piezoelectric strain coefficient	d_{33}	$10^{-12}m/V$	280
	d_{31}		122
Elastic coefficient	S_{11}^E	$10^{-12}m^2/N$	10.8
	S_{12}^E		-4.437
Frequency Constant	N_r	$Hz.m$	2270
Temperature characteristics	T_{fr}	$P_{pm}/^{\circ}C$	100
	T_{Cf}	$(-40 \sim 20^{\circ}C)$	3000
	T_{fr}	$P_{pm}/^{\circ}C$	50
	T_{fr}	$(20 \sim 80^{\circ}C)$	2500
Poisson's ratio	σ	-	0.409
Mechanical quality factor	Q_m	-	1700
Curie point	T_C	$^{\circ}C$	320
Dielectric loss factor	$\tan\delta$	%	0.65

Table A.1: Fundamental materials characteristics of sample PT#1

The outlook of PT#1 is shown in figure A.1:

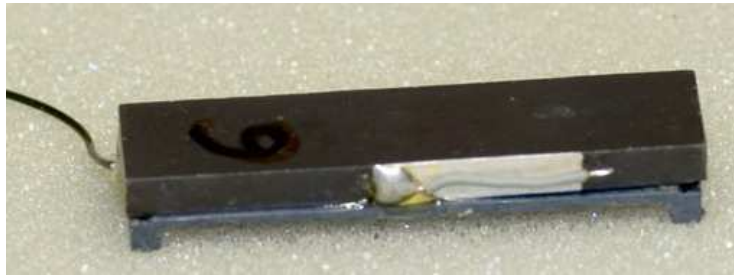


Figure A.1: The outlook of PT sample #1

A.2 Sample PT#2: ELM610

The fundamental materials characteristics of the Piezoelectric Transformer are issued in the Table A.2 below:

Item	Mark	Unit	Values
Density	ρ	g/cm^3	7.9
Electromechanical coupling coefficient	K_{33}	%	70
	K_{31}		37
	K_r		62
Specific inductive capacity	$\varepsilon_{33}^T/\varepsilon_0$	-	1300
Piezoelectric strain coefficient	d_{33}	$10^{-12}m/V$	290
	d_{31}		140
	g_{33}	$10^{-3}Vm/N$	24.3
	g_{31}		-11.5
Elastic coefficient	S_{33}^E	$10^{-12}m^2/N$	14.28
	S_{11}^E		-11.9
Frequency Constant	N_r	$Hz.m$	2200
	N_{33}		1500
	N_{31}		1700
Poisson's ratio	σ	-	0.27
Mechanical quality factor	Q_m	-	2000
Curie point	T_C	$^{\circ}C$	290
Dielectric loss factor	$tan\delta$	%	0.5

Table A.2: Fundamental materials characteristics of sample PT#2

The outlook of PT#2 is shown in figure A.2:



Figure A.2: The outlook of PT sample #2

A.3 Sample PT#3

The fundamental materials characteristics of the Piezoelectric Transformer are issued in the Table A.3 below:

Item	Mark	Unit	Values
Density	ρ	g/cm^3	7.9
Electromechanical coupling coefficient	K_{33}	%	70
	K_{31}		37
	K_r		62
Specific inductive capacity	$\varepsilon_{33}^T/\varepsilon_0$	-	1300
Piezoelectric strain coefficient	d_{33}	$10^{-12}m/V$	290
	d_{31}		140
	g_{33}	$10^{-3}Vm/N$	24.3
	g_{31}		-11.5
Elastic coefficient	S_{33}^E	$10^{-12}m^2/N$	14.28
	S_{11}^E		-11.9
Frequency Constant	N_r	$Hz.m$	2200
	N_{33}		1500
	N_{31}		1700
Poisson's ratio	σ	-	0.27
Mechanical quality factor	Q_m	-	2000
Curie point	T_C	$^{\circ}C$	290
Dielectric loss factor	$\tan\delta$	%	0.5

Table A.3: Fundamental materials characteristics of sample PT#3

The outlook of PT#3 is shown in figure A.3:

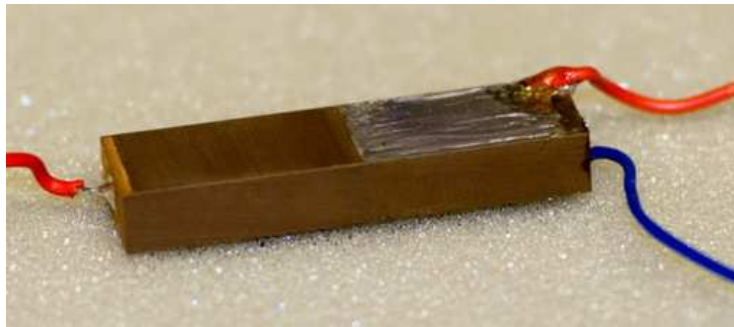


Figure A.3: The outlook of PT sample #3

Appendix B

Determination of Parameters of Equivalent Circuit

B.1 Introduction to Admittance Circle Method

The lumped parameters of PT's equivalent circuit shown in figure B.1 when operating in the frequency range close to one of its resonant circuits can be determined by a method so-called admittance circle [16]. If the secondary side of PT is short circuited, the complex input admittance values can be express as the relation B.1:

$$Y_{in}(\omega) = i_{in}(\omega)/u_{in}(\omega) = G(\omega) + jB(\omega) \quad (\text{B.1})$$

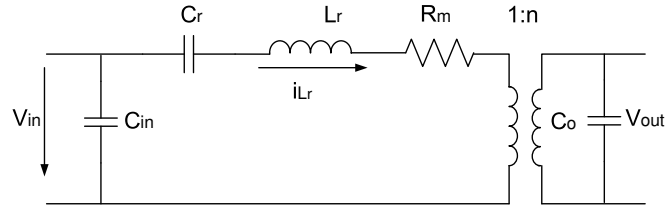


Figure B.1: Equivalent circuit of PT operating closed to resonant frequency

In case the output is short circuit and the operating frequency varies in the range $0 < \omega < \infty$, the input admittance will be:

$$Y_{in}(\omega) = j\omega C_{in} + \frac{j\omega C_r (1 - \omega^2 L_r C_r) + \omega^2 R_m C_r^2}{(1 - \omega^2 L_r C_r)^2 + (\omega R_m C_r)^2} \quad (\text{B.2})$$

when $\omega = \omega_r$, and $\omega_r = 1/\sqrt{(L_r C_r)}$, the equation B.2 will be:

$$Y_{in}(\omega_r) = \frac{1}{R_m} + j\omega_r C_{in} \quad (\text{B.3})$$

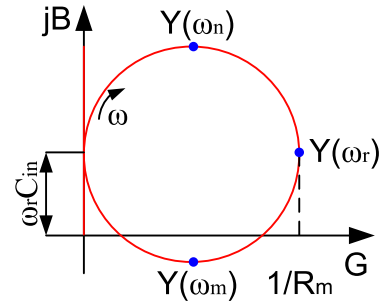


Figure B.2: Admittance circle

From the measured real and imaginary parts of admittance $Y(\omega_r)$ in fig B.2 then the value of R_m and C_{in} would be determined. Further more, from the frequencies which are correlative to the maximum f_m and minimum f_n imaginary point of the admittance circle, the value of L_r and C_r can be defined:

$$C_r = \frac{1}{R_m} \frac{(\omega_m - \omega_n)}{\omega_m \omega_n} \quad (\text{B.4})$$

$$L_r = R_m \frac{1}{(\omega_m - \omega_n)} \quad (\text{B.5})$$

Repeat the same admittance measurement with the input short circuit, with the same procedure mentioned above to calculate the value of output capacitance C_o and the output to input voltage step ratio:

$$n = \sqrt{\frac{R_m}{R_m''}} \quad (\text{B.6})$$

where R_m'' is the real part of the admittance circle from the output side when input is short circuited. In another method, the value of input capacitor C_{in} and output capacitor C_o can be measured directly by multi-meter. The parameters of equivalent circuit in λ mode of PT samples are shown in table B.1

Parameters	C_{in} (nF)	L_r (mH)	C_r (nF)	R_m (Ω)	n	C_o (pF)
PT Sample					-	
PT#1	230	0.41	6.7	0.221	107	20
PT#2	105	0.66	3.925	1.33	32	20
PT#3	40	0.72	4.2	0.9	30	12

Table B.1: Parameters of equivalent circuit of PT samples

B.2 Parameters of Equivalent Circuit of PT

B.2.1 Admittance circle of PT#1

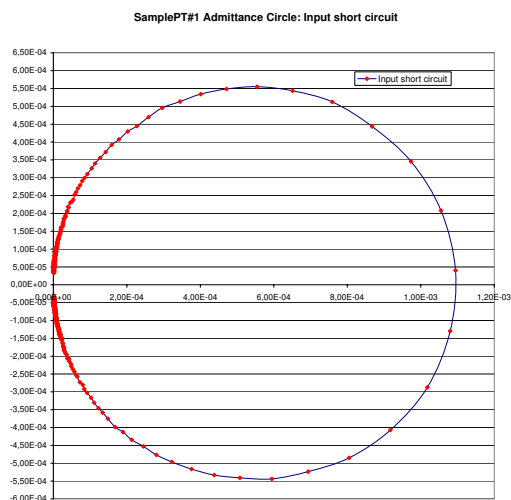


Figure B.3: PT#1: Admittance Circle - Input short circuit

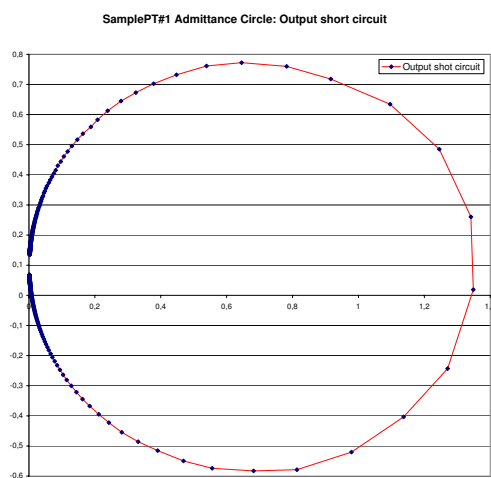
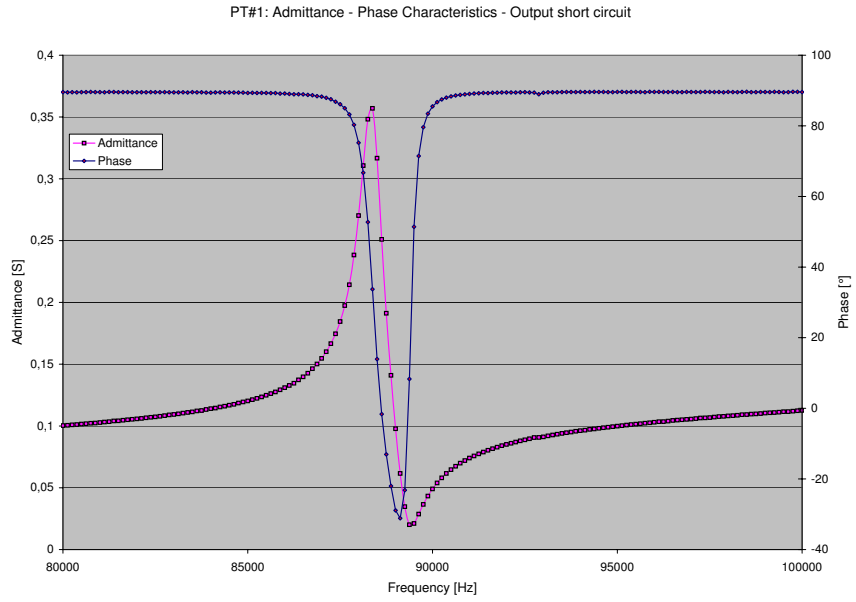
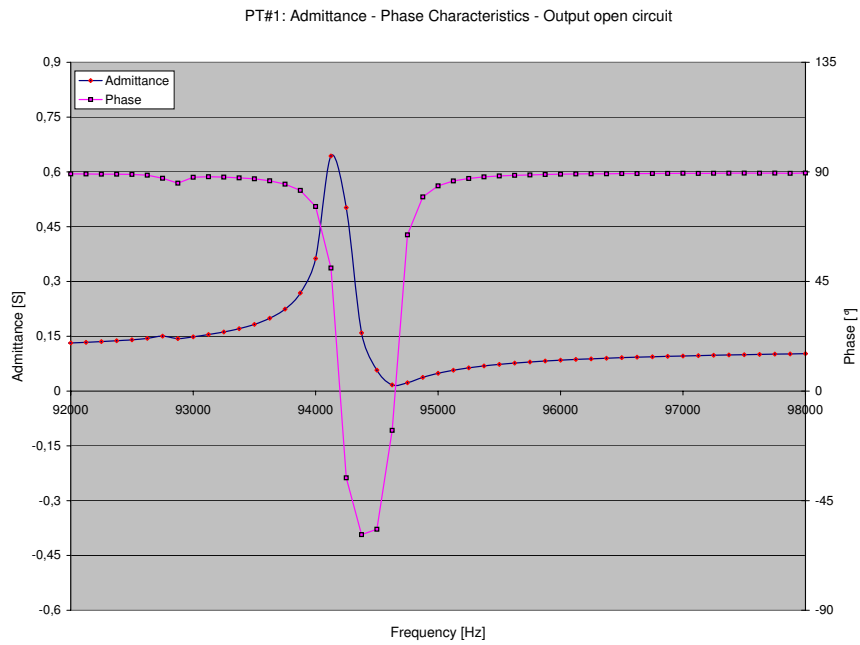


Figure B.4: PT#1: Admittance Circle - Output short circuit



(a) Output short circuit



(b) Output open circuit

Figure B.5: PT#1: Admittance and phase characteristics

B.2.2 Admittance circle of PT#2

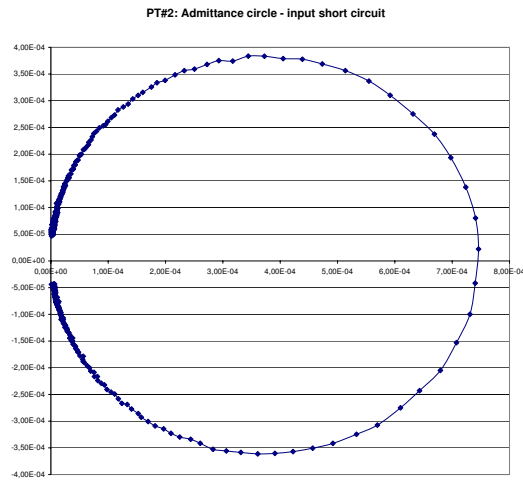


Figure B.6: PT#2: Admittance Circle - Input short circuit

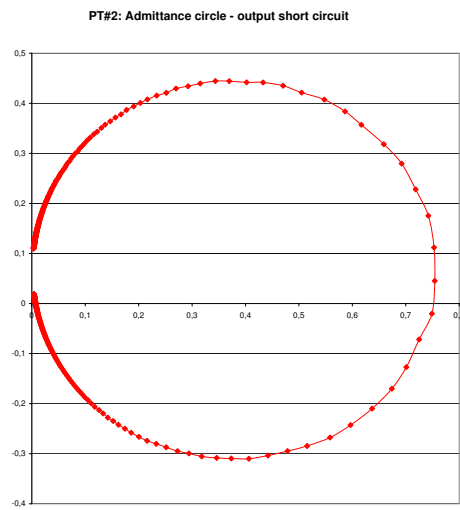
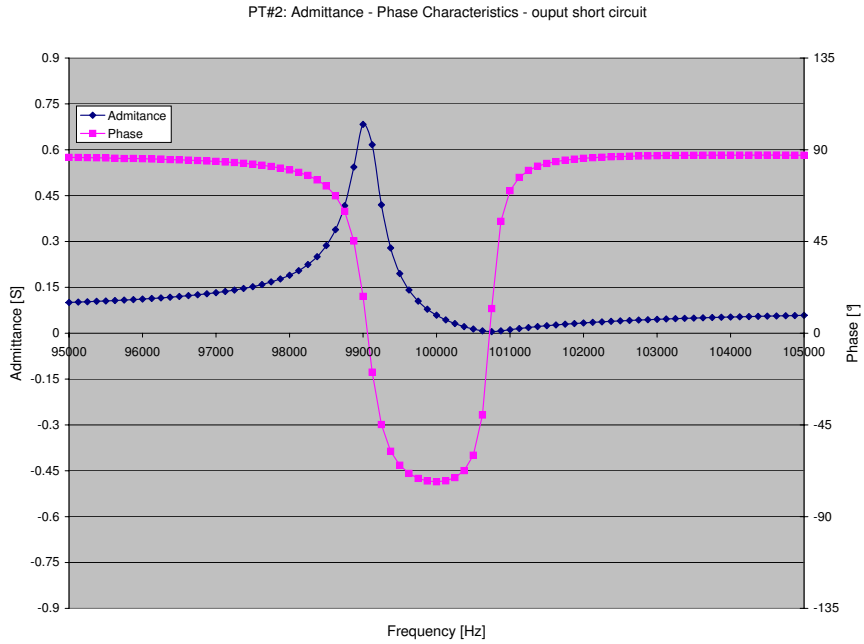
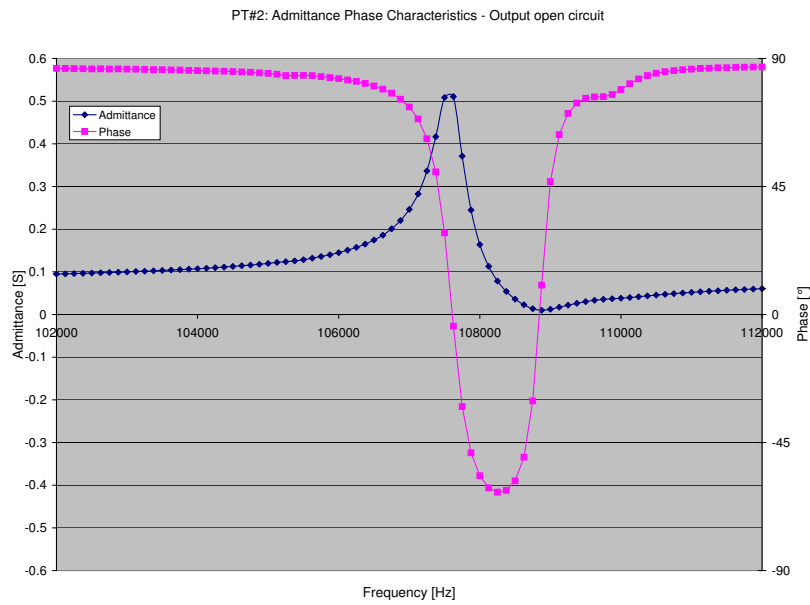


Figure B.7: PT#2: Admittance Circle - Output short circuit



(a) Output short circuit



(b) Output open circuit

Figure B.8: PT#2: Admittance and phase characteristics

B.2.3 Admittance circle of PT#3

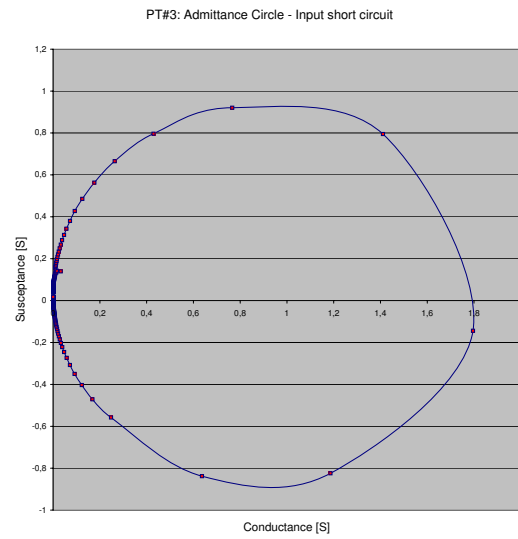


Figure B.9: PT#3: Admittance Circle: Input short circuit

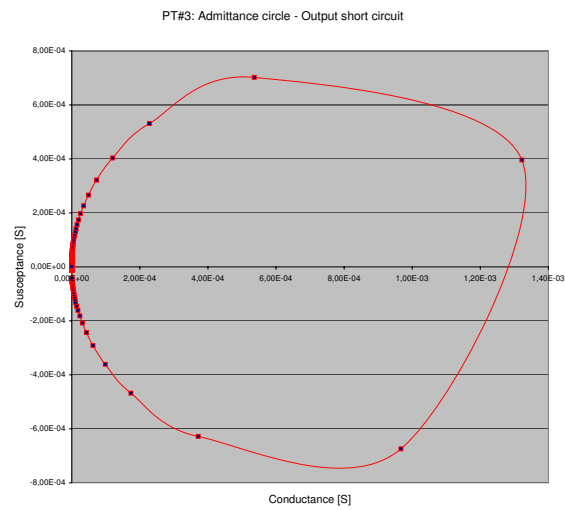
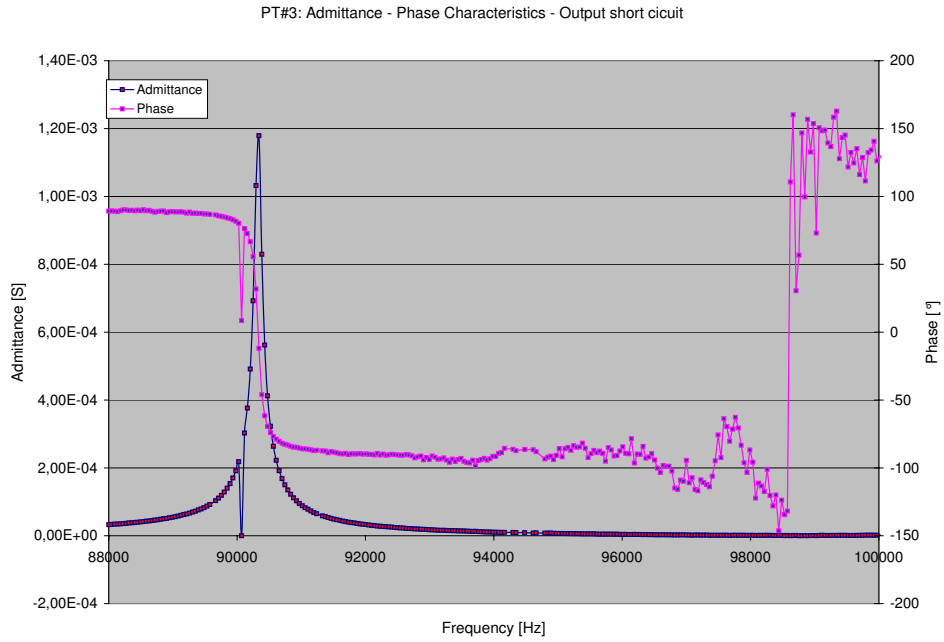
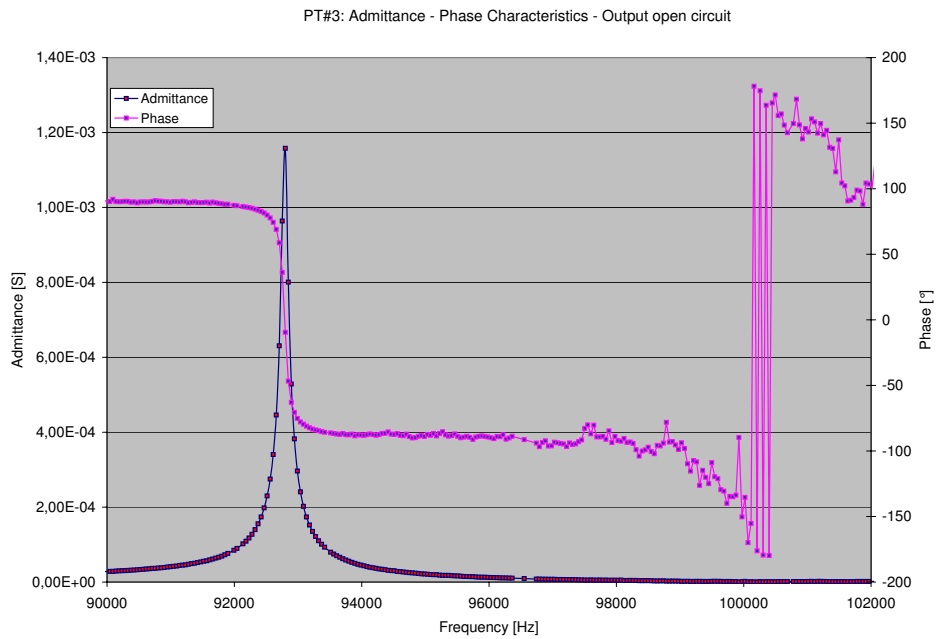


Figure B.10: PT#3: Admittance Circle: Output short circuit



(a) Output short circuit



(b) Output open circuit

Figure B.11: PT#3: Admittance and phase characteristics

Appendix C

Program to Determine the Operational Characteristics of PT

***** Input Voltage Related Output Power Calculation *****

```
Vin=2; % Input Voltage of PT
R0=0.221; % Mechanical losses
%RLk=1000;
Lr=0.821e-3; % Series inductor
Cr=13.46e-9; % Series capacitance
n=107; % Ideal transformer ratio
Cin=230e-9; % Input Capacitance of PT
Cout=20e-12; % Output Capacitance of PT
f=[43000:100:53000]; % Operating frequency range
fr=1/(2*pi*sqrt(Lr*Cr)); % Mechanical resonant frequency
omega_rs=1/(sqrt(Lr*Cr)); % Angle resonant frequency of PT
Coeq=n*n*Cout; % Output to input converted of Output capacitance
c=Coeq/Cr; % Ratio of capacitances
Qm=sqrt(Lr*Cr)/Cr*R0; % Mechanical quality factor
RLk=175e3; % Load resistance
f1=f/fr; omega=2*pi.*f;
RLoptm=1./(omega*Cout);
RLk1=RLk/(n*n);
Q=(1/sqrt(Lr*Cr))*Cout.*RLk;
RC=(Coeq*omega.*RLk1).*(Coeq*omega.*RLk1); RLk2=RLk1./(1+RC);
Coeq1=Coeq./((1+RC)./RC);
%theta=RLk2./(RLk2+R0);
```



```

Y=((1-c*(f1.*f1-1)+R0./RLk).*(1-c*(f1.*f1-1)+R0./RLk)+((c./Q).*(
(fr./f).*(f1.*f1-1)+(f/fr).*(c/Qm)).*((c./Q).*(fr./f).*(f1.*f1-1)+(f/fr).*(c/Qm)));
N21=n./sqrt(Y);
for i = 1:9
Vin = Vin + 1;
Pout=(N21.*N21.*Vin.*Vin)/RLk;
plot(f,Pout);
hold on;
end

```

***** Generic operational characteristics of PT *****

Main function

```

function pt_exact
hold off;
clear all;
syms Q;
% Parameter PT
C0 = 23*10e(-12);
n = 30;
Rm = 0.52;
Lr = 1.118*10e(-3);
Cr = 7.4*10e(-9);
% Calculation of equivalent and nominal parameters
w_rs = 1/sqrt(Lr*Cr);
C0_rf = n*n*C0;
c = C0_rf/Cr;
Q_m = 1/(w_rs*Cr*Rm);
% Call sub function
io_e = io_exact(c,Q_m);
pow_e = pow_exact(io_e,c,Q_m);
eff = efficiency(c,Q_m);
% Label and scale the axes
xmark = solve(eff-0.5,Q);
mark1 = xmark(1,1);
mark2 = xmark(2,1);
mark3 = subs(eff,Q,1/sqrt(1+1/(2*c)));

```

```

xm1 = double(mark1);
xm2 = double(mark2);
if xm1>xm2
i=xm1; j=xm2;
xm1=j; xm2=i;
end
xm3 = double(mark3);
ymark1 = subs(eff,Q,xm1);
ymark2 = subs(eff,Q,xm3);
ym1 = double(ymark1);
ym2 = double(ymark2);
pow_max = subs(pow_e,Q,xm1);
pmax = double(pow_max);
% Calculation the critical value for graphical visualizing
range = solve(eff-0.2,Q);
lo = range(1,1);
up = range(2,1);
lower = double(lo); upper = double(up);
% graphical output
Q_range = logspace(-4,4,1000);
io_ = subs(io_e,Q,Q_range); % io = abs(io_);
pow_ = subs(pow_e,Q,Q_range); % pow = abs(pow_);
e_ = subs(eff,Q,Q_range); % e = abs(e_);
semilogx(Q_range,io_,'b-'); hold on;
semilogx(Q_range,pow_,'b-'); hold on;
semilogx(Q_range,50*e_,'b-'); hold on;
axis([10e(-4) 10e4 0 pmax+10]);
set(gca,'XTick',[xm1 xm3 xm2]);
set(gca,'XTickLabel','c/Qm', '1/sqrt(1+1/2c)', 'Qm/c+1');
set(gca,'YTick',[ym1*50 ym2*50 pmax]);
set(gca,'YTickLabel','n = 0.5', 'n_max', 'Pmax');
title('output power P_0, input to output voltage ratio k_21, efficiency \eta \newline as a
function of the electrical quality factor Q');
xlabel('electrical quality factor Q (Q=\omega_{rs}C_0R_0)');
ylabel('P_0, k_21, \eta \rightarrow');
%legend('k_21exact(Q)', 'P_0exact(Q)', '\eta_exact(Q) *50', 'Location', 'NorthEastOutside');
% Qup = Q_m/(c+1);

```

```
% Qdown = c/Q_m;
% Rup = Qup/(w_rs*C0);
% Rdown = Qdown/(w_rs*C0);
```

Sub function: Power calculation

```
function pow_e = pow_exact(i,j,k)
% i = io_app
% j = c = C0_rf/Cr
% k = Q_m = w_rs*Cr*Rm
syms Q Q_m c x;
P0_e = c*(i)^2/Q;
P0_ex = subs(P0_e,c,j);
P0_ex = subs(P0_ex,Q_m,k);
pow_e = P0_ex;
```

Sub function: Voltage step up ratio

```
function io_e = io_exact(a,b)
% a = c
% b = Q_m
syms Q Q_m c x;
Y = (1-c*(x-1)+c/(Q*Q_m))^2+(c/sqrt(x)/Q*(x-1)+sqrt(x)*c/Q_m)^2;
dY = x^3+(1/(2*Q_m^2)+1/(2*Q^2)-1/c-1)*x^2-1/(2*Q^2);
y=solve(dY);
y1_e=y(1,1);
Vmax=subs(Y,x,y1_e);
Vmax=subs(Vmax,c,a);
Vmax=subs(Vmax,Q_m,b);
io_e=(sqrt((Vmax)))^(1/2);
```

Sub function: Efficiency

```
function eff = efficiency(a,b)
syms Q Q_m c x; % approximate result y1_a = sqrt(0.5*(1+1/c-1/Q^2)+sqrt(0.25*(1+1/c-1/Q^2)^2+1/Q^2));
n = 1/(1+c/Q_m*(1/Q+x^2*Q)); nu = subs(n,x,y1_a);
num = subs(nu,c,a);
num = subs(num,Q_m,b);
eff = num;
```

Bibliography

- [1] High temperature piezoceramics. Tech. rep., TRS Technologies, Inc., TRS Technologies, Inc. 2820 E. College Avenue, Suite J State College, PA 16801 USA, 2006.
- [2] A.J.MOULSON, AND J.M.HERBERT. "*Electroceramics: Materials, Properties, Applications - second edition*". John Wiley & Sons, 2002.
- [3] A.M.SANCHAZ, M.SANZ, P.ALOU, R.PRIETO, AND J.R.COBO. "*Experimental Validation of an Optimized Piezoelectric Transformer Design with Interleaving of Electrodes*". *Proceeding of IEEE Power Electronics Specialist Conference PESC'04 Aachen, Germany* (2004).
- [4] A.SEDRA, AND K.SMITH. "*Microelectronic Circuits*". Oxford University press, 1998.
- [5] A.V.TURIK, V.YU.TOPOLOV, AND V.I.ALESHIN. "*On a Correlation Between Remanent Polarization and Piezoelectric Coefficients of Perovskite-Type Ferroelectric Ceramics*". *J. Phys. D: Appl. Phys.* (October 2000), 738–743.
- [6] B.BONA, E.BRUSA, P.CANESTREUI, G.GENTA, AND A.TONOLI. "*Finite Element Modeling and Experiment a1 Validation of an Elastic Beam with Surface Bonded Piezoelectric Devices*". *1050-4729/94 \$03.00 0 1994 IEEE* (1994).
- [7] BEN-YAAKOV, S., AND IVENSKY, G. *Drivers and Rectifiers for Piezoelectric Elements*. Power Electronics Laboratory, Ben-Gurion University of the Negev, 2005.
- [8] BEN-YAAKOV, S., AND LINEYKIN, S. "*Frequency Tracking to Maximum Power of Piezoelectric Transformer HV Converters under Load Variations*". *0-7803-7262-X/02/ \$10.00 @ 2002 IEEE* (2002).
- [9] BEN-YAAKOV, S., AND PERETZ, M. M. "*A Self-Adjusting Sinusoidal Power Source Suitable for Driving Capacitive Loads*". *IEEE Transaction on power electronics* (February 2004).

- [10] BERNHARD SIESSEGGER. "Beitrag zur physikalischen Beschreibung von Hochdruckgasentladungslampen und deren elektronische Ansteuerung". PhD thesis, Technische Universität Dresden, Germany, February 2006.
- [11] BIGGA, A. "Entwicklung einer universellen Testpallform für Piezoelectrische Transformatoren". Master's thesis, Technische Universität Dresden, Deutschland, Diplomarbeit, 2001.
- [12] BRONSTEIN, S., AND BEN-YAAKOV, S. "Design Considerations for Achieving ZVS in a Half Bridge Inverter that Drives a Piezoelectric Transformer with No Series Inductor". Internet Source: www.ee.bgu.ac.il/~pel/pdf-files/conf87.pdf.
- [13] BRONSTEIN, S., AND BEN-YAAKOV, S. "Design Considerations for Achieving ZVS in a Half Bridge Inverter that Drives a Piezoelectric Transformer with No Series Inductor". 0-7803-4340-9/98/\$10.00 © 1998 IEEE. (1998).
- [14] C.A.ROSEN. "Ceramic Transformers and Filters". *Proceeding of Electronic Component Symp* (1956), 205–11.
- [15] "C.A.ROSEN". "Electrical conversion apparatus". *United States Patent - Free Patent Online*, "No. 2975354" ("Nov." "1956").
- [16] CHIH-YI LIN. "Design and Analysis of Piezoelectric Transformer Converters". PhD thesis, Virginia Polytechnic University, USA, July 1997.
- [17] CHOI, S.-J., LEE, K.-C., AND H.CHO, B. "Design of Fluorescent Lamp Ballast with PFC using a Power Piezoelectric Transformer". 0-7803-4340-9/98/IEEE *Transaction on Power Electronics* (1998).
- [18] CHUNG, J. H., LEE, S.-M., LEE, M. M.-O., AND MOON, Y. H. "HIGH POWER 30W AND HIGH EFFICIENCY 80% PIEZOELECTRIC TRANSFORMER FOR ELECTRONICS BALLAST". 0-7803-5728-0/99 \$4.00 © 1999 IEEE 33, 2 (April 1999).
- [19] C.KEAWBOONCHUAY, AND T.G.ENGEL. "Factors Affecting Maximum Power Generation in a Piezoelectric Pulse Generator". 0-7803-7915-2/03 ©2003 IEEE (2003).
- [20] C.S.MOO, W.M.CHEN, AND H.K.HSIEH. "Electronic Ballast with Piezoelectric Transformer for Cold Cathode Fluorescent Lamps". *Proceeding of IEEE Power Electronics Specialist Conference PESC'98* (May 1998).

- [21] C.Y.LIN, AND F.C.LEE. "*Design of a Piezoelectric Transformer Converter and Its Matching Networks*". *Proceeding of IEEE Power Electronics Specialist Conference PESC'94* (1994), 607 – 612.
- [22] D.BERLINCOURT, M.-E.-C., AND REVISED BY C.NEAR, H. Properties of morgan electro ceramic ceramics. Tech. rep., Morgan Electro Ceramics, Website:www.morgan-electroceramics.com.
- [23] DU, J., HU, J., AND TSENG, K. J. "*High-Power, Multioutput Piezoelectric Transformers Operating at the Thickness-Shear Vibration Mode*". *IEEE transactions on ultrasonics, ferroelectrics, and frequency control* 51, 5 (May 2004).
- [24] E.DUNN, J., AND S.PEARLMAN, J. *Methods and apparatus for extending the shelf life of fluid food products*. *United States Patent - Free Patent Online*, 4695472 (Sep. 1987).
- [25] FÁBIO ECKE BISOGNO. "*Advanced High-Frequency Electronic Ballasting Techniques for Gas Discharge Lamps*". PhD thesis, Technische Universität Chemnitz, Germany, June 2006.
- [26] F.E.BISOGNO, M.RABDECKER, AND A.KMOLL. "*Comparison of Resonant Topologies for Step-down Applications Using Piezoelectric Transformers*". *Proceeding of IEEE Power Electronics Specialist Conference PESC'04 - Aachen, Germany* (2004).
- [27] F.ESPINO-CORTES, A.H.EL-HAG, O.ADEDAYO, S.JAYARAM, AND W.ANDERSON. "*Water Processing by High Intensity Pulsed Electric Fields*". *2006 Annual Report Conference on Electrical Insulation and Dielectric Phenomena* (2006).
- [28] F.GARDNER. "*Phaselock Techniques*". John Wiley & Sons, 1979.
- [29] FURUTANI, K., AND IIDA, K. "*A Driving Method of Piezoelectric Actuator by Using Current Pulses*". *INSTITUTE OF PHYSICS PUBLISHING* (July 2006), 2387–2394.
- [30] FURUTANI, K., AND IIDA, K. "*Exact Analysis of Multi-Layer Piezoelectric/Composite Cantilevers*". *INSTITUTE OF PHYSICS PUBLISHING* (September 2006), 1447–1458.
- [31] G.IVENSKY, S.BRONSTEIN, AND S.BEN-YAAKOV. "*A Comparison of AC/DC Piezoelectric Transformer Converters with Current Doubler and Voltage Doubler*".

- Rectifiers*". *Proceeding of IEEE Power Electronics Specialist Conference PESC'03* (2003).
- [32] G.SPIAZZI, AND S.BUSO. "Analysis of Instabilities in Piezoelectric Transformers Driving Cold Cathode Fluorescent Lamps". *Proceeding of IEEE Power Electronics Specialist Conference PESC'04 - Aachen, Germany* (2004).
- [33] G.SPIAZZI, AND S.BUSO. "Cold Cathode Fluorescent Lamp Power Supply based on Piezoelectric Transformers". *Proceeding of IEEE Power Electronics Specialist Conference PESC'04 - Aachen, Germany* (2004).
- [34] GUYOMAR, D., MAGNET, C., LEFEUVRE, E., AND RICHARD, C. "Nonlinear Processing of the Output Voltage of a Piezoelectric Transformer". *IEEE transactions on ultrasonics, ferroelectrics, and frequency control* 53, 7 (July 2006).
- [35] GUYOMAR, D., MAGNET, C., LEFEUVRE, E., AND RICHARD, C. "Power Capability Enhancement of a Piezoelectric Transformer". *INSTITUTE OF PHYSICS PUBLISHING* (Jan 2006), 571–580.
- [36] HAMAMURA, S., NINOMIYA, T., YAMAMOTO, M., AND KATSUNO, M. "Combined PWM and PFM Control for Universal Line Voltage of a Piezoelectric Transformer Off-Line Converter". *Proceeding of IEEE Power Electronics Specialist Conference PESC'04 - Aachen, Germany* (2004).
- [37] HAMAMURA, S., ZAITZU, T., NINOMIYA, T., AND SHOYAMA, M. "Nose Characteristics of Piezoelectric Transformer DC-DC Converter". *Proceeding of IEEE Power Electronics Specialist Conference PESC'98* (1998).
- [38] H.FUKUNAGA, H.KAKEHASHI, AND Y.OHTA. "Effect of Dimension on Characteristics of Rosen-type Piezoelectric Transformer". *Proceeding of IEEE Power Electronics Specialist Conference PESC'98* (May 1998).
- [39] H.KAKEHASHI, T.HIDAKA, AND Y.OHTA. "Electronic Ballast Using Piezoelectric Transformers for Fluorescent Lamps". *Proceeding of IEEE Power Electronics Specialist Conference PESC'98* (May 1998).
- [40] H.OHGUCHI, M.H.OHSATO, SHIMIZU, G.KIMURA, AND H.TAKAGI. "A High-Frequency Electronic Ballast for HID Lamps Based on a $\lambda/4$ Long Distributed Constant Line". *IEEE Transactions on Power Electronics* 13, 06 (November 1998).
- [41] H.SCHOENBACH, K., KATSUKI, S., H.STARK, R., BUESCHER, E., AND J.BEEBE, S. "Bioelectrics New Applications for Pulsed Power Technology". *IEEE TRANSACTIONS ON PLASMA SCIENCE* 30, 1 (Feb. 2002).

- [42] HU, J. "Analyses of the Temperature Field in a Bar-Shaped Piezoelectric Transformer Operating in Longitudinal Vibration Mode". *IEEE Transaction on ultrasonics* 50, 06 (2003).
- [43] HU, Y. "analysis and design of high-intensity-discharge lamp ballast for automotive headlamp". Master's thesis, Virginia Polytechnic University, USA, November 2001.
- [44] I.KARTASHEV, T.VONTZ, AND H.FLORIAN. "Regimes of Piezoelectric Transformer Operation". *INSTITUTE OF PHYSICS PUBLISHING* (July 2006), 2150–2158.
- [45] INTERNATIONAL-RECTIFIER. *IR21531D(S) & (PbF) SELF-OSCILLATING HALF-BRIDGE DRIVER*, 2004.
- [46] ISHIZUKA, Y., LEE, K.-W., OYAMA, T., AND KOGA, H. M. T. "Consideration of A Single-Switch Inverter for Piezo-Electric Transformer with A New Control Method". *0-7803-7754-0/03/\$17.00 02003 IEEE* (2003).
- [47] ITOH, H., TERANISHI, K., AND SUZUKI, S. "Glow Discharge Around Piezoelectric Transformer Operated Under Higher-Order Vibration Modes". *IEEE Transaction on plasm science* 33, 2 (April 2005).
- [48] IVENSKY, G., BRONSTEIN, S., AND BEN-YAAKOV, S. "Analysis and Design of a Piezoelectric Transformer AC/DC Converter in a Low Voltage Application". *IEEE Transaction on power electronics* (2002).
- [49] IVENSKY, G., BRONSTEIN, S., AND BEN-YAAKOV, S. "Analysis and Modeling of a Voltage Doubler Rectifier Fed by a Piezoelectric Transformer". *IEEE Transaction on power electronics* 19, 2 (March 2004).
- [50] IVENSKY, G., KATS, A., , AND BEN-YAAKOV, S. "An RC Load Model of Parallel and Series-Parallel Resonant DCDC Converters with Capacitive Output Filter". *IEEE Transaction on power electronics* 14, 3 (May 1999).
- [51] IVENSKY, G., ZAFRANY, I., AND BEN-YAAKOV, S. S. "Generic Operational Characteristics of Piezoelectric Transformers". *IEEE Transaction on power electronics* 17, 6 (Nov 2002).
- [52] J.A.OLIVER, R.PRIETO, M.SANZ, J.A.COBOS, AND J.UCEDA. "1D Modeling of Multi-layer Piezoelectric Transformers". *IEEE Transactions on Power Electronics* (2001).

- [53] JARROUSSE, J.-M., COSTA, F., VASIC, D., AND SARRAUTE, E. "Low-power high-voltage DC-DC converter based on a PZT transformer". *10th European Conference on Power Electronics and Applications EPE 2003 - Toulouse* (Jun. 2003).
- [54] J.DIAZ, F.NUFIO, M.A.PRIETO, AND J.A.MARTIN. "A New Full-Protected Control Mode To Drive Piezoelectric Transformers In DC/DC Converters". *IEEE Transaction on power electronics* (August 2001).
- [55] J.DIAZ, F.NUFIO, M.A.PRIETO, AND J.A.MARTIN. "A New Control Strategy for an AC/DC Converter Based on a Piezoelectric Transformer". *IEEE Transaction on industrial electronics* 51, 04 (August 2004).
- [56] J.DIAZ, J.A.MARTIN-RAMOS, M.J.PRIETO, AND F.NUNO. "A Double-Closed Loop DC/DC Converter Based On A Piezoelectric Transformer". *Proceeding of IEEE Applied Power Electronics Conference (APEC'04)-California, USA* (February 2004).
- [57] JIN, K. H., AND SOO", P. D. "High-efficiency piezoelectric transformer and ballast". *United States Patent - Free Patent Online*, "20040145279" ("July" "2004").
- [58] J.NAVAS, T.BOVE, J.A.COBOS, F.NUFIO, AND K.BREBOL. "Miniaturised Battery Charger Using Piezoelectric Transformers". 0-7803-6618-2/01/\$100.(c) 2001 *IEEE* (2001).
- [59] JOHN P. BUCHANAN. "Handbook of Piezoelectric Crystal for Radio Equipment Designers". Philco Corporation, 1954.
- [60] JOO, H. W., AND LEE, C. H. "Analysis of Piezoelectric Transformer by Using Finite Element Method and Equivalent-Circuit Considering Load Variation". *IEEE ultrasonics symposium* (2001).
- [61] J.S.KIM, K.CHOI, AND I.YU. "A New Method of Determining The Equivalent Circuit Parameters of Piezoelectric Resonators and Analysis of The Piezoelectric Loading Effect". *IEEE Transactions on Ultrasonics, Ferroelectrics, and Frequency Control* 40 (1993).
- [62] KALGAWA, Y., TSUCHIYA, T., AND KAWASHIMA, T. "Finite Element Simulation of Piezoelectric Vibrator Gyroscopes". *IEEE Transaction on ultrasonics, ferroelectrics, and frequency control* 43, 4 (July 1996).

- [63] LELAND, E. S., AND WRIGHT, P. K. "Resonance Tuning of Piezoelectric Vibration Energy Scavenging Generators Using Compressive Axial Preload". *INSTITUTE OF PHYSICS PUBLISHING* (July 2006), 1413–1420.
- [64] LI, H. L., HU, J. H., AND CHAN, H. L. "Finite Element Analysis on Piezoelectric Ring Transformer". *iee transactions on ultrasonics, ferroelectrics, and frequency control* 51, 10 (Oct. 2004).
- [65] LIN, C.-H., LU, Y., LO, Y.-K., PAI, K.-J., AND WANG, Y.-Y. "Control Strategy for Eliminating the Temperature Effect of Piezoelectric Transformer in the Backlight Module". *The 3Mh Annual Conference of the IEEE Industrial Electronics Society* (Nov. 2004).
- [66] LIN, R. L., LEE, F. C., M.BAKER, E., AND Y.CHEN, D. "Inductor-less Piezoelectric Transformer Electronic Ballast for Linear Fluorescent Lamp". 0-7803-6618-2/01/\$10.00 200 01 *IEEE* (2001).
- [67] LIN, Y.-C., AND CHEN, W. "AC/DC Converter with Worldwide Range Input Voltage by Series and Parallel Piezoelectric Transformer Connection". *Proceeding of IEEE Power Electronics Specialist Conference PESC'04 - Aachen, Germany* (2004).
- [68] LIN, Y.-C., AND MA, C.-C. "Experimental Measurement and Numerical Analysis on Resonant Characteristics of Piezoelectric Disks with Partial Electrode Designs". *IEEE Transactions on Ultrasonics, Ferroelectrics, and Frequency Control* 51, 08 (August-2004).
- [69] LINEYKIN, S., AND BEN-YAAKOV, S. "A Very Simple DC/DC Converter Using Piezoelectric Transformer". *IEEE Transaction on power electronics* (2001).
- [70] LINEYKIN, S., AND BEN-YAAKOV, S. "A Unified SPICE Compatible Model for Large and Small Signal Envelope Simulation of Linear Circuits Excited by Modulated Signals". *IEEE Transaction on power electronics* (2003).
- [71] LINEYKIN, S., AND BEN-YAAKOV, S. "Feedback Isolation by Piezoelectric Transformers Comparison of Amplitude to Frequency Modulation". *35th Annual PESC'04 Aachen, Germany, 2004* (2004).
- [72] L.Q.YAO, J.G.ZHANG, L.LU, AND M.O.LAI. "Nonlinear Dynamic Characteristics of Piezoelectric Bending Actuators Under Strong Applied Electric Field". *Journal of Microelectromechanical Systems* 13, 04 (August-2004).

- [73] MARIAN K.KAZIMIERCZUK, AND DATIUSZ CZARKOWSKI. "*Resonant Power Converters*". John Wiley & Son, Inc, New York, 1995.
- [74] MATTHYS, R. "*Crystal Oscillator Circuits*". John Wiley & Sons, 1983.
- [75] M.C.DO, TH.HANISCH, AND H.GÜLDNER. "*High Voltage Igniter Based on Discontinuous Working Mode of Piezoelectric Transformers*". 11th European Conference on Power Electronics and Applications EPE'05 (Sep. 2005).
- [76] M.C.DO, TH.HANISCH, AND H.GÜLDNER. "*Igniter for HID Lamp Based on Discontinuous Working Mode of Piezoelectric Transformers*". 6th International Conference on Power Electronics and Drive Systems PEDS'05 (Nov. 2005).
- [77] M.FLYNN, A., AND R.SANDERS, S. "*Fundamental Limits on Energy Transfer and Circuit Considerations for Piezoelectric Transformers*". *IEEE Transaction on power electronics* 17, 1 (Jan 2002).
- [78] M.J.PIETO, AND J.DIAZ. "*Design Considerations of Multi-Layer Piezoelectric Transformers*". *IEEE Transaction on Power Electronics* (2002).
- [79] M.J.PIETO, AND J.DIAZ. "*Closing a Second Feedback Loop in DC/DC Converters based on Piezoelectric Transformers*". *Proceeding of IEEE Power Electronics Specialist Conference PESC'04 - Aachen, Germany* (2004).
- [80] MORGAN-ELECTRO-CERAMICS. "piezo ceramics tutorial 11 of 15". Tech. rep., Morgan Electro Ceramics, Website: www.morgan-electroceramics.com.
- [81] M.SANZ, A.M.SANCHAZ, J.A.OLIVER, P.ALOU, R.PRIETO, J.R.COBO, AND J.UCEDA. "*FEA based Model of Multi-layer Piezoelectric Transformer Working in Thickness Mode*". *Proceeding of IEEE Power Electronics Specialist Conference PESC'04 Aachen, Germany* (2004).
- [82] M.SANZ, P.ALOU, A.SOTO, R.PRIETO, J.A.COBO, AND J.UCEDA. "*Magnetic-less converter based on Piezoelectric Transformers for Step-Down DC/DC and Low Power Application*". *IEEE Transaction on power electronics* (2003).
- [83] M.SANZ, P.ALOU, J.A.OLIVER, R.PRIETO, J.A.COBO, AND J.UCEDA. "*Interleaving of Electrodes in Piezoelectric Transformers*". 0-7803-7262-X/02/\$10.00 2002 IEEE. (2002).

- [84] M.SANZ, P.ALOU, R.PRIETO, J.A.COBO, AND J.UCEDA. "Comparison of Different Alternatives to Drive Piezoelectric Transformers". 0-7803-7404-5/02/\$17.00 ©2002 IEEE (2004).
- [85] M.SYED, E., AND P.DAWSON, F. "Analysis and Modeling of a Rosen Type Piezoelectric Transformer". 0-7803-7067-8/01/\$10.00 ©2001 IEEE (2001).
- [86] NELLYA N. ROGACHEVA. "The Theory of PIEZOELECTRIC SHELLS and PLATES". CRC Express, Florida-USA, 1994.
- [87] N.FERNANDO, J.A.MARTIN, J.DIAZ, M.J.PRIETO, AND F.M.FERNANDEZ-LINERA. "Quantum Mode Control for Piezoelectric Transformer in AC/DC Application". *Proceeding of IEEE International Power Electronics Congress CIEP 2002* (October 2002).
- [88] NITTAYARUMPHONG, S., BISOGNO, F., RADECKER, M., KNOLL, A., CARAZO, A. V., AND RIEDLHAMMER, A. "Dynamic Behaviour of PI Controlled Class-E Resonant Converter for Step- Down Applications Using Piezoelectric Transformers". *European Conference on Power Electronics and Applications EPE'05, Dresden, Germany* (2005).
- [89] NITTAYARUMPHONG, S., GUELDNER, H., BISOGNO, F., RADECKER, M., AND CARAZO, A. V. "Comparison of Control Concepts for Off-Line Power Supplies using Piezoelectric transformers in Class-E Topology". *37th IEEE Power Electronics Specialists Conference, Jeju, Korea* (2006).
- [90] N.VOLKERT. "DC-DC converter with very high insulation capability". *European Power Electronics And Drives Association - EPE'99* (1999).
- [91] OHGUCHI, H., OHSATO, M. H., SHIMIZU, T., KIMURA, G., AND TAKAGI, H. "A High-Frequency Electronic Ballast for HID Lamps Based on a $\lambda/4$ Long Distributed Constant Line". *IEEE Transaction on power electronics* 13, 6 (Nov. 1998).
- [92] "PARK, KI DUCK; HAN, J. M. "External electrode fluorescent lamp". *United States Patent - Free Patent Online*, "No. 20060197455" ("September" "2006").
- [93] PHILIPS-MAGNETIC-PRODUCTS. "piezoelectric transformer" - application note. Tech. rep., Philips Magnetic Products, Feb.
- [94] PHILIPS-SEMICONDUCTORS. *74HC HCT4046A Phase-locked-loop with VCO*, Nov 1997.

- [95] PRIYA, S. "High Power Universal Piezoelectric Transformer". *IEEE transactions on ultrasonics, ferroelectrics, and frequency control* 53, 1 (Jan. 2006).
- [96] QIU, X., TUHELA, L., AND ZHANG, Q. "Application of pulsed power technology in nonthermal foodprocessing and system optimization". *Pulsed Power Conference, 1997. Digest of Technical Papers. 1997 11th IEEE International* (Jul. 1997).
- [97] RADECKER, M., E.BISOGNO, F., KNOLL, A., AND V.CARAZO, A. "A Low-Size Multi-Power-Level Single-Transistor Ballast for Low Pressure Fluorescent Lamps, Using a Piezoelectric Transformer". *IAS 39th Annual Meeting* (Oct. 2004).
- [98] RAY.L.LIN, FRED.C.LEE, AND BAKER, E. "Characterization of Piezoelectric Transformer". *IEEE Transaction on power electronics* 13, 6 (Nov. 1998).
- [99] R.BEST. "Phase-Locked Loops". McGraw-Hill, 1997.
- [100] R.PRIETO, M.SANZ, J.A.COBOS, P.ALOU, O.GARCIA, AND J.UCEDA. "Design Considerations of Multi-Layer Piezoelectric Transformers". *IEEE Transaction on Power Electronics* (2002).
- [101] SASAKI, Y., UMEDA, M., TAKAHASHI, S., MITSURU YAMAMOTO, A. O., AND INOUE, T. "High-Power Characteristics of Multilayer Piezoelectric Ceramic Transducers". *Japanese Journal of Applied Physics* 40, 9B (Sep. 2001), 57435746.
- [102] S.H.FUNG, AND M.H.PONG. "A Microprocessor Controlled PT Converter".
- [103] S.H.FUNG, AND M.H.PONG. "An Improved Model for Rosen Type Piezoelectric Transformer for Power Converter". *Proceeding of IEEE Power Electronics Specialist Conference PESC'04 - Aachen, Germany* (2004).
- [104] S.H.FUNG, AND M.H.PONG. "Analysis of Parallel Connection of Rosen Type Piezoelectric Transformers". *Proceeding of IEEE Power Electronics Specialist Conference PESC'04 - Aachen, Germany* (2004).
- [105] SHIMIZU, T., JIN, Y., , AND KIMURA, G. "DC Ripple Current Reduction on a Single-Phase PWM Voltage-Source Rectifier". *IEEE Transaction on industrial applications* 36, 05 (September 2000).
- [106] S.HIROSE, N.TAKITA, AND S.TAKAHASHI. "New Design Method of Piezoelectric Transformer Considering High-Power Characteristics of Various Composition Ceramics". *1998 IEEE ultrasonics symposium* (1998).

- [107] SIEEGGER, B., GÜLDNER, H., AND HIRSCHMANN, G. "Ignition concepts for high frequency operated HID lamps". *Conference Record of IEEE Power Electronics Specialist Conference (PESC), Recife, Brasil* (Jun. 2005).
- [108] S.KABUKI, K.MOREIRA, F.DOBBS, R.P.JOSHI, AND K.H.SCHOENBACH. *Bacterial decontamination with nanosecond pulsed electric fields. Power Modulator Symposium, 2002 and 2002 High-Voltage Workshop. Conference Record of the Twenty-Fifth International*, 4695472 (June-July 2002).
- [109] TAKAHASHI, S., HIROSE, S., UCHINO, K., AND OH, K.-Y. "Electro-Mechanical Characteristics of Lead-Zirconate-Titanate Ceramics Under Vibration-Level Change". *Proceeding of IEEE 9th IEEE Int'l Symp. Appl.Ferroelectrics, Penn State, 1994* (1994).
- [110] TAO, F. "Energy-Related System Normalization and Decomposition targeting Sensitivity Consideration". PhD thesis, Virginia Polytechnic University, USA, June 2001.
- [111] TERANISHI, K., ITOH, H., AND SUZUKI, S. "Dynamic Behavior of Light Emissions Generated by Piezoelectric Transformers". *IEEE Transaction on plasma science* 30, 01 (February 2002).
- [112] TERANISHI, K., SUZUKI, S., AND ITOH, H. "Dielectric Barrier Discharge Generated by Piezoelectric Transformer in Atmospheric Pressure". *IEEE Transaction on plasma science* 33, 02 (April 2005).
- [113] TH.HANISCH, I.KARTASHEV, H.GÜLDNER, AND K.LEHNERT. "Non-permanent Excitation of Piezoelectric Transformer". *Proceeding of IEEE International Power Electronics Congress CIEP 2002* (October 2002).
- [114] THOMAS HANISCH. "Piezoelektrische Transformatoren in der Leistungselektronik". PhD thesis, Technische Universität Dresden, Germany, August 2004.
- [115] TOBA, A., SHIMIZU, KIMURA, G., SHIOYA, M., AND SANO, S. "Auxiliary Resonant Commutated Pole Inverter Using Two Internal Voltage-Points of DC Source". *IEEE Transaction on industrial electronics* 45, 02 (April 1998).
- [116] TSUCHIYA, T., KAGAWA, Y., WAKATSUKI, N., AND OKAMIIRA, H. "Finite Element Simulation of Piezoelectric Transformers". *IEEE Transaction on ultrasonics, ferroelectrics, and frequency control* 48, 4 (July 2001).

- [117] T.ZAITSU, T.SHIGEHISA, M.SHOYAMA, AND T.NINOMIYA. "*Piezoelectric Transformer Converter with PWM Control*". 0-7803-3044-7/96/\$5.00©1996 IEEE (July 1996).
- [118] VASIC, D., COSTA, F., AND SARRAUTE, E. "*New Method to Design Piezoelectric Transformer used in MOSFET and IGBT Gate Drive Circuits*". *IEEE Transaction on power electronics* (August 2001).
- [119] W.EGAN. "*Phase-Lock Basics*". John Wiley & Sons, 1998.
- [120] WEIXING HUANG. "Design of a Radial Mode Piezoelectric Transformer for a Charge Pump Electronic Ballast with High Power Factor and Zero Voltage Switching". Master's thesis, Virginia Polytechnic University, USA, April 2003.
- [121] WEY, C.-D., JONG, T.-L., AND PAN, C.-T. "*Design and Analysis of an SLPT-Based CCFL Driver*". *IEEE Transaction on industrial electronics* 50, 01 (February 2003).
- [122] W.ZHANG, D.ZHANG, AND Y.WANG. "*A Low Cost ZVS class E converter Using PT*". *Proceeding of IEEE Power Electronics Specialist Conference PESC'04 - Aachen, Germany* (2004).
- [123] YAMANE, T., AND HAMAMURA, S. "*Efficiency Improvement of Piezoelectric Transformer DC/DC Converter*". *Proceeding of IEEE Power Electronics Specialist Conference PESC'98* (May 1998).
- [124] ZUNFT, S. "Digitale Steuerung von Piezoelectrischen Transformatoren". Master's thesis, Technische Universität Dresden, Deutschland, Diplomarbeit, 2002.

Index

- class E converter, 61
- Curie point, 6
- current doubler, 41

- depolarization, 8
- direct piezoelectric effect, 5

- electric dipole moments, 7
- electrical depolarization, 8

- HID lamp, 75
- HVPT: High Voltage Piezoelectric Transformer, 12

- inverse piezoelectric effect, 5

- LVPT: Low Voltage Piezoelectric Transformer, 14

- maximum electrical energy: W_{Emax} , 37
- maximum mechanical energy: W_{Mmax} , 37
- mechanical depolarization, 8
- MH lamp, 75

- operating cycle, 35
- output equivalent capacitor: C_{Eq} , 44

- perovskite structure, 6
- piezoelectric ceramics, 1, 6
- piezoelectric effect, 1
- piezoelectric transformer; PT, 5
- polarizing process, 7
- Power density, P_D , 2
- pulsed electric field, 85

- Radial vibration mode PT, 14
- resonant mode, 15
- RMS: root mean square, 78
- Rosen-type PT, 12

- thermal depolarization, 9
- Thickness vibration mode PT, 13

- voltage doubler, 40

Curriculum Vitae

M. Sc. Manh Cuong Do

was born on 22 January 1977 in Phu tho - Viet Nam

From 1995 to 2000: Student at Chair of Industrial Manufacturing Automation, Faculty of Energy, Hanoi University of Technology - Ha Noi - Viet Nam, Engineer degree from 06.2000

From 2000 to 2002: Master of science (M. Sc) at Faculty of Energy, Hanoi University of Technology - Ha Noi - Viet Nam

From 2003 to 2008: PhD student at Chair of Power Electronics, Faculty of Electrical Engineering and Information Technology, Dresden University of Technology